

The Influence of the Electrode Material on the Sensor Characteristics of SnO₂ Thick Film Gas Sensors

Dissertation

der Mathematisch – Naturwissenschaftlichen Fakultät
der Eberhard Karls Universität Tübingen
zur Erlangung des Grades eines
Doktors der Naturwissenschaften
(Dr. rer. nat.)

vorgelegt von
Sven Rank
aus Bad Friedrichshall

Tübingen
2014

Tag der mündlichen Prüfung:

10.10.2014

Dekan:

Prof. Dr. Wolfgang Rosenstiel

1. Berichterstatter:

Prof. Dr. Udo Weimar

2. Berichterstatter:

Prof. Dr. Günter Gauglitz

Kurzfassung

Einfluss des Elektrodenmaterials auf die sensitiven Eigenschaften eines SnO₂ Dickschicht Gas Sensors

Obwohl SnO₂ das am besten untersuchte Material für chemoresistive Gassensoren darstellt, gibt es immer noch Lücken im grundlegenden Verständnis der Funktionsweise. Dies betrifft unter anderem die Wechselwirkung an der Dreiphasengrenze – Elektrode, sensitive Schicht & Atmosphäre. Die elektrische Charakterisierung von SnO₂ Dickschicht-Sensoren mit unterschiedlichen Elektrodenmaterialien (Gold (Au) & Platin (Pt)) zeigen je nach Typ charakteristische sensitive Eigenschaften in Abhängigkeit von der Temperatur. Unter Verwendung von Goldelektroden ist eine größere Änderung des zu messenden Widerstands (höheres Sensorsignal) gegenüber Exposition der reduzierenden Gase H₂ und CO bei niedrigeren Temperaturen zu erkennen. Bekanntermaßen ist adsorbierter Sauerstoff auf der Metalloxid-Oberfläche der Reaktionspartner für die Oxidation von CO & H₂. Demnach könnte eine erhöhte Oberflächenbeladung mit ionosorbierten Sauerstoff an SnO₂ mit Gold-Zugabe diese Effekte erklären.

Unter Verwendung eines Operando-Messaufbaus (kombinierte Messungen in realen Arbeitsbedingungen des Sensors) konnten phänomenologische und spektroskopische Erkenntnisse gekoppelt werden. So zeigen Widerstandsmessungen der mit Au Elektroden betriebenen Sensoren bei tieferen Temperaturen unter Erhöhung der O₂-Konzentration im Vergleich zu Sensoren mit Platinelektroden ein höheres Sensorsignal. Unter der Annahme, dass die Variation der Sauerstoffkonzentration - bei konstanter Temperatur der Probe - als einziger Faktor der Widerstandsänderung angenommen werden kann, liegt ein deutlicher Hinweis für eine Aktivierung der Sauerstoffadsorption an der Au/SnO₂ Grenzfläche (Spill-over Effekt) vor. Des Weiteren wurde mittels Umsatzmessungen an Pulvermischungen gezeigt, dass ein erhöhter Umsatz (Oxidation) von CO & H₂ auf der Platinelektrode den Anteil des zu detektierenden Gases signifikant verringern kann und somit nicht mehr für eine Reaktion auf der sensitiven Schicht zur Verfügung steht.

Um die Annahme der Aktivierung der Sauerstoffadsorption (Spillover Effekt) genauer zu untersuchen wurde mittels DRIFT-Spektroskopie in Isotopenaustausch-Experimenten die Bildung von OH/OD-Gruppen untersucht. In Abhängigkeit der Temperatur konnte in diesen Messungen ein quantitativer sowie qualitativer Unterschied in der Bildung von OH/OD Gruppen gezeigt werden; wobei bei Proben mit Goldanteil bei niedrigeren Temperaturen (200 °C) ein deutlich höherer Anteil an

gebildeten OH/OD-Gruppen, bedingt durch eine erhöhte Verfügbarkeit von preadsorbiertem Sauerstoff, nachzuweisen war. Proben mit Platinanteil hingegen zeigen bei diesen Temperaturen einen wesentlich geringeren Anteil an OH/OD-Gruppen. Mit steigender Temperatur relativieren sich diese Abweichungen, da anzunehmen ist, dass die direkte Adsorption von Sauerstoff auf SnO₂ dominiert und somit die Bedeutung des Spillover-Effekts nachlässt.

Contents

1 Introduction	1
1.1 Definition of Sensors	2
1.2 Historical development of gas sensors	4
1.3 Technical Development of SnO ₂ MOX sensors - a brief review	6
1.4 Current situation in research & How to meet the market demand	9
1.5 Future Prospects	14
2 General Aspects of SnO₂ Gas Sensors	17
2.1 Bulk properties of SnO ₂	18
2.1.1 Crystalline structure	18
2.1.2 Electrical bulk properties	18
2.1.3 Conductivity of the material	20
2.2 The reactive SnO ₂ surface [110]	21
2.2.1 Interaction with the surface	22
2.2.2 Oxygen	24
2.2.3 Water	25
2.2.4 Carbon monoxide	27
2.2.5 Hydrogen	28
2.3 Working principle	29
3 Motivation	33
3.1 Scientific point-of-view	35
3.2 The sensors investigated in this work	42
4 Experimental	45
4.1 Material preparation and sensor fabrication	46
4.1.1 SnO ₂ Synthesis	46

4.1.2	Sensor fabrication	48
4.1.3	SnO ₂ + Au / SnO ₂ + Pt powder mixtures	52
4.2	Measurement techniques	52
4.2.1	Gas mixing system	54
4.2.2	Electrical measurements	54
4.2.3	DRIFTS	55
4.2.4	Catalytic conversion	59
5	Results & Discussion	61
5.1	Sample overview	62
5.2	Electrical measurements I	63
5.2.1	Results	63
5.2.2	Discussion & Summary	68
5.3	Electrical measurements II	72
5.3.1	Results	72
5.3.2	Discussion & Summary	76
5.4	Electrical measurements III	78
5.4.1	Results	78
5.4.2	Discussion & Summary	81
5.5	Catalytic conversion measurements	82
5.5.1	Test conditions & Results	82
5.5.2	Discussion & Summary	84
5.6	DRIFTS measurements I	87
5.6.1	Results	89
5.6.2	Discussion & Summary	94
5.7	DRIFTS measurements II	96
5.7.1	Results	96
5.7.2	Discussion & Summary	106
6	Summary	111
7	Outlook	115
	Bibliography	119

Appendix	153
Publications	153
Curriculum Vitae	155

CHAPTER 1

Introduction

Despite the fact that there is a long history of gas sensor technologies, the first applicable commercially available chemical gas sensors were released just about 50 years ago. During this period a common understanding has been established and milestones have been achieved. However, modern day society demands the need for monitoring capabilities of the surrounding atmosphere. Increasingly intensified guidelines for protecting the public health and process controlling as well as smart monitoring of one's own lifestyle or detection of chemical, biological and toxin warfare agents are just some of the related fields of applications for chemical sensors. The challenge for understanding and improving gas sensors becomes increasingly important when the future demands are considered, as this will raise the requirements of a sensor like increased sensitivity, selectivity and stability.

Metal oxides, in particular SnO_2 , are widely used as the basis material for the preparation of gas sensing devices. In retrospect, tin oxide could well attract attention and curiosity by many researches over the world [Goe95; Iho94; Wat84; Wil99]. Due to these reasons, it can be considered the model of a metal oxide chemo-resistive gas sensor. Nevertheless, a full understanding of the ongoing processes on the surface and the interfaces (chemical interactions) together with the features in the bulk (physical properties) is still missing. Scientific findings up to now have demonstrated that especially the interface between the metal oxide and noble metals are giving an excellent contribution to the enhancement of the desired sensor characteristics [Wil91]. This area is of major interest since not only additives which are dispersed in the sensitive layer but also the electrode and the sensitive layer are forming an interface between a noble metal and the metal oxide.

1.1 Definition of Sensors

"A sensor is a converter that measures a physical quantity and converts it into a signal which can be read by an observer or by an (today mostly electronic) instrument" [Wikb]

Based on this simplified description a sensor gets stimulated by a specific input and converts it into a measurable electrical output signal Figure 1.1. The input can be either a physical measure like motion, temperature, acceleration or pressure or a certain supply of a chemical or biological agent. The output is generally a signal that is converted to human-readable display at the sensor location or transmitted electronically over a network for reading or further processing.

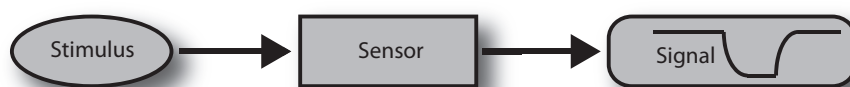


Figure 1.1: Sensing principle

One can usually allocate a sensor in different parts. (i) The sensitive element, basically the part of recognition of the variable to be measured, (ii) the transducer which converts this variable, respectively the interaction of the input with the sensitive element in an electrical signal and (iii) the data acquisition and data processing part, monitoring the status of the sensor it is connected to. Depending on the functionality, frame size, production technology and area of use one can distinguish between different kinds of sensors. Normally every condition of matter could be measured by one of the different types. However, since the sphere of interest is about finding a qualitative or quantitative measure of a certain gaseous atmosphere one carefully has to select a device which is fulfilling the requirements. Simply spoken, if the analyte to be measured is in a gaseous phase, a chemical gas sensor is the one to go back to. For the sake of completeness Table 1.1 represents an overview of the variety of chemical sensors.

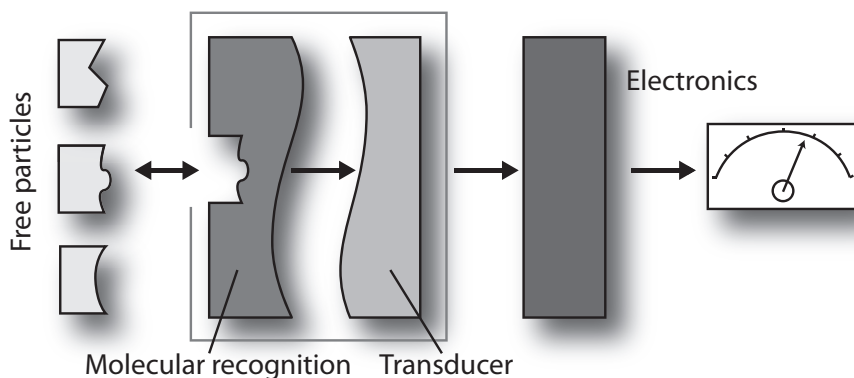
According to IUPAC, a chemical sensor itself is considered as "a device that transforms chemical information, ranging from the concentration of a specific sample component to total composition analysis, into an analytically useful signal. The chemical information mentioned above, may originate from a chemical reaction of the analyte or from a physical property of the system investigated" [Hul91]. As defined by Janata et al. in 1989, "chemical sensing is part of an information-acquisition process in which an insight is obtained about the chemical composition of the system

Table 1.1: Overview of different types of chemical sensors

Optical	Electrochemical	Electrical	Mass sensitive	Calorimetric
Chemi-luminescence	Ion-selective electrodes	Conductometric	SAW	Catalytic (Pellistors)
Photoacoustic	Conductometric	Work function	Cantilever	Thermal conductivity
Fiber-optic	Potentiometric	Capacitance	QMB	Thermoelectric
Spectro-photometric	Culonometric	FET		Pyroelectric
Surface Plasmon Flourescence	CHEMFET	Schottky diodes		

in real-time. In this process, an amplified electrical signal results from the interaction between some chemical species and the sensor" [Jan89]. Besides that, there are numerous other sources describing a chemical sensor [Mad89; Mos87; Ste03]. Göpel & Schierbaum got to the point simply by defining a chemical sensor as a device which converts a chemical state into an electrical signal [Goe91]. This definition may sound simple but describes the sensing process in a proper way.

As described above, a sensor in general can be decomposed into several parts. This also holds true for chemical sensors, a short description is outlined in the following. The chemical input reacts on the chemical active surface, which can be described as a (i) sensitive layer or receptor for the analyte particles. This reaction is presented graphically as a lock-and-key model (Figure 1.2). The interaction signifies a change

**Figure 1.2:** Sensing and Transduction of a chemical gas sensor. After [Mit98]

in the material properties of the receptor, which basically means an alteration of

the physical or chemical properties like temperature, conductivity or mass, to name but a few. The change will then be converted into an electrical output signal by the transducer (ii). Out of this variety of changeable parameters, the attention within this work is dedicated to the conductometric type of chemical gas sensors. Metal oxides, in that case SnO_2 , change its electrical properties when exposed to a certain reactive gas, which is finally measurable by a change in conductance.

1.2 Historical development of gas sensors

Sensing in a respective simplified prospectus is about finding a quantitative or/and qualitative measure. Gas sensing in particular is about distinguish different odors and identify the level of concentration. Biological systems and to a special degree humans with their senses and mind have developed a possibility to determine between hundreds of smells - however they fail if it comes to the detection of odorless toxic gases.

Centuries ago, people must have felt a special concern about the recognition of toxic gaseous components in the atmosphere after the effects of these on human health were discovered. To control this, it is essential to have a real-time monitoring of the gaseous atmosphere. In the early stages of industrialization, this aspect in particular was gaining in importance considerably as more technological processes were confronted with the threats of hazardous substances. For example, the high health risks associated with coal-mines encouraged scientists to develop a method to detect possible dangers at an early stage. One of the first measures taken were canaries in cages brought into the mines. A canary is more susceptible than humans to carbon monoxide, methane and low oxygen concentration; in fact, the dangers the miners had to deal with. A passed out canary would indicate a dangerous gas situation, whereby commonly two canaries has been used to ascertain a false alarm. In 1815 Sir Humphry Davy, an English chemist, invented the first technical gas detector [Eri]. The Davy lamp is basically an oil lamp which indicates high rates of flammable gases or low levels of the partial oxygen pressure through the intensity of the flame. Soon after the first technical solutions were found to detect gases and made their way into the mining, other industrial sectors followed suit. Given that the technology was not applicable to all manufacturing branches a new solution had to be found, which led to the development of the catalytic diffusion sensor. A device which was able to give a reading of the concentration of a gas burnt inside the apparatus. The problem here was the inability of an online-monitoring. Each

measurement of the concentration had to be started manually.

The discovery by Brattain and Bardeen in 1953, that the semiconducting properties of germanium changes as soon as a change in oxygen concentration occurs was an important preceding breakthrough in the direction of developing gas sensors [Bra53]. While Heiland et al. and Bielanski et al. already in the 1950s stated the change in conductivity of semiconducting oxide catalysts - in detail ZnO - upon exposure to different gases [Bie57; Hei57], it was Seyiama et al. in 1962 reporting the associated potential for gas sensing in particular [Sei62]. Similar properties have been discovered on SnO₂. A few years later, Taguchi was the one to bring the metal oxide gas sensor to the market [Nao72], subsequently founding the company FIGARO Engineering Inc. in 1969, which is still one of the biggest sensor manufacturers in the world. In fact, with the conductometric gas sensors on metal oxide basis, a way was found to have a reliable, user-friendly, robust and cheap-in-production product on the market which was of course just the beginning of the success story. This success was clouded by some unwelcome attendant circumstances such as high cross-sensitivity, sensitivity to humidity, long-term signal drift and slow sensor response. Despite these obstacles, research and industry have devoted significant resources to increase the performance and capabilities of metal-oxide based gas sensors.

Metal oxides are composed of special properties such as their stability in a wide range of temperature in relatively harsh environments combined with the large variety of materials. This makes metal oxides suitable for detecting a wide range of gases. Table 1.2 gives an overview of different kinds of materials respective to the detecting gases.

Table 1.2: Metal oxide materials for gas detection

gas to be detected	Suitable metal-oxide material	References
Oxidizing gases (O ₃ , NO _x , Cl ₂)	In ₂ O ₃ , WO ₃ , ZnO, TiO ₂	[Gal02; Mar04; Tam02; Yam94]
Reducing gases (CO, H ₂ , CH ₄)	SnO ₂ , CTO, Ga ₂ O ₃ , In ₂ O ₃	[Elo12; Hoe01; Nak12; WÖ3]
H ₂ S, SO ₂	SnO ₂ /CuO	[Jia00; Rum97; Vas98]
NH ₃	WO ₃ , MoO ₃ , In ₂ O ₃	[Jim04; Pra03]
CO ₂	Nd(OH) ₃	[Dje09]
Formaldehyde	In ₄ Sn ₃ O ₁₂	[Kem12]

1.3 Technical Development of SnO₂ MOX sensors - a brief review

A certain time after the first reports about the gas sensitive properties of SnO₂ were released, it became the most conceived material of metal-oxide based gas sensor. Whereas in the past, research was conducted empirically by trial to understand and improve the sensor characteristics, recently systematic studies and developments are taking on increased importance and significance.

The ongoing survey made it possible to acquire important information about the modifiable parameters to gain better sensor characteristics, for example the preparation technology, working temperature, layer morphology, additives, transducer design etc. For all the improvements the parameters of tuning the sensing material itself are of particular interest, but not exclusively. Apart from the basic sampling and transducing on a chemical sensor there may be other identifiable intermediate steps in the sensing process which can be modified in order to obtain a more specific output. Especially filtering and preconditioning or pre-converting of analytes has been further developed in the past years. The general approach is to implement a filter material in the packaging or housing of the sensor, being used in commercially available gas sensors. Recent developments offer to that purpose an interesting alternative of combining a filter or membrane directly with the sensitive layer [Gen84; Hug00; Pra10].

While the interaction of gas molecules is the first step and further the transition to a readable signal brings the relevant data, also the data processing part cannot be underestimated. With a well selected and applied model-based or data-based algorithm it is possible to increase the selectivity and predict the measured concentration of gases more precisely (Figure 1.3). In the meantime the topic of feature extraction and pattern recognition is far advanced. Major innovative results have been achieved by Göpel et al. and Gardner et al. [Gar91; Gar92; Wei90]. There have been numerous publications in the field of gas sensing which has of course improved the understanding of this material making it a very appealing technology. In particular, working with "additives" holds a leading position in research during the last few years. Noble metals are well known for their catalytic activity. The reaction of gases on the metal oxide surface could be improved simply by adding small quantities of finely dispersed noble metals into the material. The advances in improving selectivity and sensitivity by noble-metal additives like Palladium or

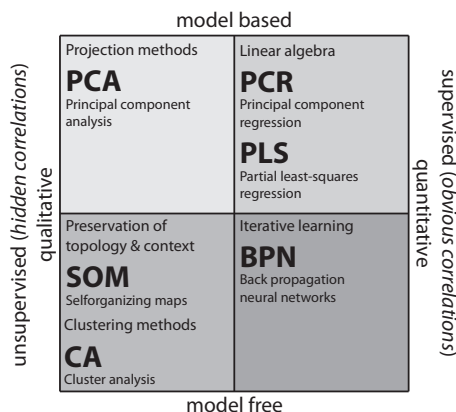


Figure 1.3: Models for feature extraction and pattern recognition [Mit07]

Platinum were one of the most striking developments in the short history of metal oxide gas sensors. Whereas these effects were already known in the early stages of MOX gas sensing [Sei72] and reviewed by Yamazoe et al. [Yam83] and Kohl [Koh90], a more complete understanding has come to light in the past few years [Hue11b; Koz09].

As the sensor performance and function principle also depends very much on the preparation method and the morphology of the sensing material, the most common preparation methods - in connection with the subsequent structure - can be divided into two classes:

- Thick film technology (characterized by rather thick layer - up to several hundred micrometers)
- Thin film technology (typical thickness of several hundred nanometers)

Other approaches which reflect the recent developments are nano-based structures and FSP layers and will be discussed in Section 1.5. The first proto-types of chemical gas sensors went into the direction of ceramic sensors and were achieved quite simply by pressing powder into pellets with integrated electrode wire and heater coil [Chi92]. The so called Taguchi Sensors [Nao72], which were basically the first reproducible sensor devices on the market, were fabricated by applying the sensitive material as a paste on an alumina tube with a heater structure separated from the sensing layer. The characteristic thick-film layers obtained therefrom are rather thick and having a highly porous sensitive layer, thus leading to a high surface area in contact with the gas phase. In order to fabricate the first SnO₂ thick film layer, only commercial available SnO₂ was needed. Meanwhile also synthesis starting from tin, tin salts (mostly SnCl₄) or organo-tin compounds (mostly tin alkoxides) have become widely

accepted [Pin80; Wei01]. Based on the synthesized material, the sensitive layer is obtained via painting, dipping, printing or pouring of a paste or even spray-coating of a sprayable solution. Due to a robust level of reproducibility, the sophisticated method of screen-printing the sensitive layer on heatable substrates provided with electrodes has been enforced in many laboratories, but include also large sensor manufacturer like Figaro.

The ongoing development in the semiconductor industry in the 1980s provided in-depth knowledge and expertise for the preparation of the first thin films. The following table summarizes some typical preparation methods such as for thin film sensors (Table 1.3). In 1988 Demarne and Grisel patented the first metal oxide

Table 1.3: Deposition techniques for the preparation of MOX gas sensors. After [Bar99]

Chemical vapor deposition (CVD)	Powder preparation	Physical vapor deposition (PVD)	
		Sputtering	Evaporation
Thermal CVD	Sol-gel from precursors	Sputtering	Molecular beam epitaxy
Plasma activated CVD	Precipitation of precursors	Reactive sputtering	Thermal evaporation
Laser induced CVD	Laser pyrolysis	Cathode sputtering with bias voltage	Reactive evaporation
Electroless plating		Ion beam deposition	Ion plating
Spray pyrolysis		Ionized cluster beam (reactive)	Reactive ion plating
Melt dipping		Plasma decomposition	Arc evaporation
Liquid quenching			Laser evaporation
Deposition of organic polymers			
Deposition of emulsions			

based thin film gas sensor on a micro machined silicon substrate by means of chemical vapor deposition [Dem88]. By licensing this technology, Motorola has been trying to break into the sensor market for several years. After a short trip through the field of applied gas sensing, MicroChemical Systems SA in Switzerland was taking

over the technology from Motorola and begun to accept and implement the current development trends of that time to be aligned with the actual research and market situation [Bri13]. After several years of development of micro machined metal oxide gas sensors, creative, mature ideas capable of making efficient and effective thin film gas sensors on micro hotplates were gained, mainly in view of lowering the power consumption of the sensor [Cav95; Fag99; Sem01]. Typical power consumption of various micro-hotplate designs lie between 10 and 100 mW [Bri13].

Even if this innovative technology certainly is very versatile, several difficulties remain such as the stability and reproducibility of thin film layers. These issues drew attention back to the thick film based metal oxide sensors and the potential for deposition on micro machined substrates. Barsan was the first to succeed in the attempt of combining a thick film sensing layer with a micro hotplate [Gar95]. Subsequently research efforts in this field were intensified, increasing the prolific output [Bar99; Hei97], which finally resulted in the commercialization of the miniaturized metal oxide thick film sensors in 2006 [Bla06; Sen].

Additionally, the temperature modulation of the working gas sensor is another important objective which was given a lot of research activities. While the constant temperature mode of sensors was commonplace for several decades, the new miniaturized technology made it possible to bring the sensors in a steady state even with short heating pulses, thereby resulting in lower power consumption [Cou12]. Besides that, many other authors additionally reported an improvement in sensor performance [Fag99; Llo02].

Simon et al. reviewed the opportunities to improve the sensor performance in thick-film as well as thin film sensors and concluded that the main benefits of the miniaturized sensor technology are the reduced power consumption, the possibility to integrate the sensitive layer with control and signal evaluation electronic on one chip and the easy integration of sensor arrays [Sim01].

1.4 Current situation in research & How to meet the market demand

Based on the high success rate in the field of metal oxide gas sensors, it is extremely important to study the trends and to observe some basic rules that lead to this success in order to ensure continued development of this field in the future. Understanding what has to be done and what are the key aspects that will lead to the development

of efficient novel sensors in the future. According to Taylor et al. an examination of the core characteristics of a new device could be summarized as follows [Tay96]:

- How specific & sensitive is the sensor? Can it match competing other devices? Can it meet the market demand?
- How about the reliability accuracy and the reproducibility in manufacturing the sensor?
- How stable and durable is it?
- Are there any restrictions for its usage?
- What are the estimated costs for this device?
- Are there already similar technologies on the market? Patents?
- What is its target market?

Specific market knowledge particularly with regards to the capacity to convert interdisciplinary knowledge and new findings directly into marketable solutions, are the key requirements to design a new sensor. Regarding the large number of gas sensors and measurement systems available on the market, identification of the market demand and the selection criteria for designing a new gas sensing application is a challenging task. Nevertheless, the global market for gas analyzers¹ in terms of revenue was estimated to be worth \$2.2 billion in 2012 and is expected to reach \$3.2 billion by 2018, growing at a CAGR (compound annual growth rate) of 5.5 % from 2013 to 2018 [Onl]. If a new market has been recognized in an early stage, designers have to define basic parameters for the purpose of examining the level of development [Kor11].

- High sensitivity, high selectivity or a broad range of detection? What are the demands and requirement of the application?
- Necessity of combining different technologies in order to fulfill all requirements, or it is sufficient to optimize the parameters of the sensing device carefully?
- What kind of other demands have to be met - e.g. special materials or fabrication procedures because of specific requirements of the application environment?

¹ gas analyzers in general; not specifically metal oxide gas sensor

As previously described there are many essential parameters in the development of gas sensing applications in order to optimize and continuously improve the characteristics of a final product. For the development of chemical sensors, a wide range of knowledge is necessary. Among the critical appraisal of the most effective technology, it is necessary to find the appropriate choice in terms of material and surface functionalization/modification and production technologies as well as having constant understanding of the processes, in respect of the sensor function. It is therefore necessary to combine expertise across different discipline like chemical science, material science, physical science and engineering.

In a time of rapid change in the industrial world, changing technologies and growing standards demand the need for easily implemented ready solutions. Therefore, developing an accomplished sensor device which is able to measure in any reasonable environment even under harsh conditions is a very difficult and serious task. Expected interferences and interactions as well as the required sensor parameters like response time, resolution and reliability should be all the time considered. Table 1.4 summarizes the current market demands to get an insight into the potential applications for chemical sensors.

Table 1.4: Market demands & potential fields of application for gas sensors. After [Kor11].

Market	Applications	Competitive advantages
Medical/clinical	Diagnostics; point-of-care patient monitoring; drug monitoring; artificial organs and prostheses; new drug discovery	(A) Real-time analysis, immediate/continuous monitoring, high specificity and selectivity (B) Diverse applications, taste, smell, and other sensory capabilities, ease of use
Processing/industrial	Process monitoring and control; quality control; workplace monitoring; waste stream monitoring; leakage alarms	(C) Portability, cost effectiveness, designed to be smart sensors, low energy demands and low heat generation, analog/digital computing capabilities
Environmental	Detection /monitoring of pollutants, toxic chemicals, waste water and waste streams	

Environmental safety, decreasing indoor and outdoor air pollution and maintaining the standards and norms given by environmental organizations (e.g. the World

Health Organization (WHO), the U.S. Environmental Protection Agency (EPA) and the Bundesministerium für Umwelt, Naturschutz und Reaktorsicherheit (BMU)) have recently been the main concerns. The World Health Organisation summarizes the main critical points as follows: "Air pollution is a major environment-related health threat to children and a risk factor for both acute and chronic respiratory disease. Outdoor air pollution is large and increasing a consequence of the inefficient combustion of fuels for transport, power generation and other human activities like home heating and cooking. Combustion processes produce a complex mixture of pollutants that comprises of both primary emissions, such as diesel soot particles and lead, and the products of atmospheric transformation, such as ozone and sulfate particles. Urban outdoor air pollution is estimated to cause 1.3 million deaths worldwide per year. Children are particularly at risk due to the immaturity of their respiratory organ systems. Those living in middle-income countries disproportionately experience this burden. Exposure to air pollutants is largely beyond the control of individuals and requires action by public authorities at the national, regional and even international levels" [WHO]. The U.S. Environmental Protection Agency has set National Ambient Air Quality Standards (NAAQS) for six principal pollutants, which are called "criteria" pollutants. They are in Table 1.5 according to [EPA]. Units of measure for the standards are parts per million (ppm) by volume, parts per billion (ppb) by volume, and micrograms per cubic meter of air ($\mu\text{g}/\text{m}^3$). The World Health Organization (WHO) is setting the standards in 2005 as summarized in Table 1.6 according to [WHOa]. On the other hand, it is not surprising that there is such great interest in indoor air quality measurements: In western societies, approximately 80-90 % of people spend the day indoors. Each day an adult of average size breathes about 20 m³ of air. This conforms to a mass of about 20 kg and far exceeds the mass of daily drinking water and food. High amounts of indoor smoke with a certain level of harmful pollutants are generated by indoor cooking and heating with biomass fuels or coal. There is a danger of acute lower respiratory infections especially for younger children, and lung cancer and chronic obstructive pulmonary disease for adults. Indoor air pollution is responsible for 2 million deaths annually [WHOb]. In addition to monitoring the indoor and outdoor air quality, production monitoring is another essential field of application. Many manufacturing processes are producing unwanted by-products such as explosive or toxic gases. Nuclear power plants are always subject to the risk of unsafe levels of hydrogen; biogas plants have to face the fact of toxic sulfur containing gas contaminations. Therefore it is essential to have

Table 1.5: National Ambient Air Quality Standards (NAAQS) for six principal pollutants [EPA]

Pollutant [final rule cite]	Primary/ Secondary	Averaging Time	Level	Form	
Carbon Monoxide [76 FR 54294, Aug 31, 2011]	primary	8-hour	9 ppm	Not to be exceeded more than once per year	
		1-hour	35 ppm		
Lead [73 FR 66964, Nov 12, 2008]	primary and sec- ondary	Rolling 3 month average	0.2 $\mu\text{g}/\text{m}^3$	Not to be exceeded	
Nitrogen Dioxide [75 FR 6474, Feb 9, 2010] [61 FR 52852, Oct 8, 1996]	primary and sec- ondary	1-hour	100 ppb	98th percentile, aver- aged over 3 years	
		Annual	53 ppb	Annual mean	
Ozone [73 FR 16436, Mar 27, 2008]	primary and sec- ondary	8-hour	0.075 ppm	Annual fourth-highest daily maximum 8-hr concentration, averaged over 3 years	
Particle Pollution Dec 14, 2012	PM _{2.5}	primary	Annual	12 $\mu\text{g}/\text{m}^3$	annual mean, averaged over 3 years
		secondary	Annual	15 $\mu\text{g}/\text{m}^3$	annual mean, averaged over 3 years
		primary and sec- ondary	24-hour	35 $\mu\text{g}/\text{m}^3$	98th percentile, aver- aged over 3 years
	PM ₁₀	primary and sec- ondary	24-hour	150 $\mu\text{g}/\text{m}^3$	Not to be exceeded more than once per year on average over 3 years
Sulfur Dioxide [75 FR 35520, Jun 22, 2010] [38 FR 25678, Sept 14, 1973]	primary	1-hour	75 ppb	99th percentile of 1-hour daily maxi- mum concentrations, averaged over 3 years	
		secondary	3-hour	0.5 ppm	Not to be exceeded more than once per year

Table 1.6: World Health Organization (WHO) principal pollution standards (2005) [WHOa]

Pollutant	Level & Averaging Time
Particulate matter	PM _{2.5} 25 µg/m ³ 24-hour mean
	PM _{2.5} 10 µg/m ³ annual mean
	PM ₁₀ 20 µg/m ³ 24-hour mean
	PM ₁₀ 50 µg/m ³ annual mean
Ozone	100 µg/m ³ 8-hour mean
NO ₂	40 µg/m ³ annual mean
	200 µg/m ³ 1-hour mean
SO ₂	20 µg/m ³ 24-hour mean
	500 µg/m ³ 10-minute mean

an efficient analysis to be able to react not belatedly to such risks. Analysis of the exhaled breath shows significant levels of certain gases like acetone or NO₂ depending on the personal circumstances. Hence, breath analysis can help recognizing diseases early and providing medical treatment in time. Maintaining health and monitoring physical and medical conditions in an automatic and sophisticated way by the means of sensors, is critical if one considers the demographic change. Important efforts are being made to develop full integrated solution to assist elder people [Wei09]. The detection of potential hazards is of course the highest priority; even so other application areas play a complementary role. Smart cities, smart homes, smart cars - people are trying to make everyday life simpler. The ability to facilitate everyday operations like intelligent air conditioning in enclosed rooms or efficient traffic management depending on air pollution in cities are just some of the applicable fields. Of course a straight forward development and use of innovative technologies is necessary to fulfill the requirements and go beyond the current state of the art.

1.5 Future Prospects

Thanks to the endless possibilities offered by semiconductor gas sensors, they will become increasingly important in the future. The challenges for the upcoming decades are first and foremost reduced costs and lower power consumption and size, followed by increased performance and robustness, to make them applicable in currently not foreseen fields.

The already arrived development of miniaturization technologies such as micro-electromechanical systems (MEMS) allowed a significant reduction in size and the associated savings in power consumption. However, regarding the rapid developments in chip technology a further decrease in size and power consumption is quite conceivable and is at least as important. An autonomous energy supply, for example through motion of the sensor device, would be the ultimate highlight for a freely usable instrument. While the improvement of the transducer design and the composition of a metal oxide gas sensor is relatively straight forward and viable in terms of application, the scheme of improvement related to the sensing material itself is by far the most complex issue.

In the last years, the interest in nanotechnologies has increased exponentially. Auspicious results in laboratories worldwide not only showed very interesting electronic properties and great possibilities to control the material structure by special experimental techniques, also sensing characteristics as well as size and power consumption interests are showing clear signs of improvement. It is assumed to have different behavior in selectivity and sensitivity depending on the morphology of the nanomaterial [Com06], while a controlled growth of nanostructures allows gaining meticulous heterostructures with the characteristics of high selectivity for certain gases [Kim11]. Another discernible trend is the development of self-heated, single nanowire gas sensors [HR09]. Although these novel approaches are giving perspectives and presenting broader views what might be possible, the realization concept seems not to be easy to implement.

Others base their innovation on existing technologies. Flame spray pyrolysis is a well-known process to obtain reproducible large quantities of nano-sized sensing material [Kem13a]. While the direct deposition on substrates has the disadvantage of low mechanical stability, new approaches of printing the material on a substrate or deposit the material via a sheet-to-sheet process increase those properties significantly [Kem13b].

Overall, it can be concluded that the challenge lies not only to fulfill the requirements in ideal environments in the laboratory, but also guarantee the feasibility towards practical and technical aspects.

CHAPTER 2

General Aspects of SnO₂ Gas Sensors

The following chapter offers an overview of the general aspects of tin oxide gas sensors. The first part focuses towards details involving the basic properties of SnO₂, such as the structural properties, bulk properties and the electrical properties of the considered intrinsic semiconductor. A detailed description of essentially the bulk properties provides a comprehensive knowledge about the base material; however it won't cover the most relevant aspects of gas sensing. Hence, in the following section the attention is drawn firstly to the surface of SnO₂. After a brief discussion about the basic aspects of adsorption theories, a comprehensive discourse about the reaction and influence - mostly on electrical properties - of the most common (oxygen, gaseous water) or studied (carbon monoxide, hydrogen) gaseous species is given. After this preliminary introduction of the general aspects, the final section of this chapter will condense this knowledge in an explanation of the working principle of a SnO₂ based gas sensor. It is noteworthy to mention that parts of this chapter are adopted from the habilitation dissertation of U. Weimar [[Wei01](#)].

2.1 Bulk properties of SnO₂

Tin dioxide, also known by its specific name tin (IV) oxide - abbreviated as tin oxide within this work - is an inorganic compound with the formula SnO₂. Tin oxide is a wide band gap semiconductor with different specific and unique properties, making it particularly suitable for various applications such as ceramic glazes, glass coatings, and resistors - in its insulating form - as well as transparent electrodes, transparent heating elements, transistors or other parts in which transparency is required - in its conducting form. A detailed description of all the surveys which have been made on SnO₂ would be far beyond the scope of this chapter; hence, the focus is essentially on the electrical properties and everything around, which may have an impact on these properties.

2.1.1 Crystalline structure

SnO₂ crystallizes with a tetragonal rutile structure (D_{4h} [P4₂/mnm]) and is an anisotropic polar crystal [Jar76]. The mineral form of SnO₂ is called cassiterite, and this is the main ore of tin. Within the unit cell two molecular units can be placed, i.e., six atoms, two tin and four oxygen atoms as depicted in Figure 2.1. In the SnO₂ matrix, tin atoms are sixfold coordinated to threefold coordinated oxygen atoms. The lattice parameters are $a = b = 4.74 \text{ \AA}$ and $c = 3.19 \text{ \AA}$. The c/a ratio is 0.673. The ionic radii for O²⁻ and Sn⁴⁺ are 1.40 and 0.71 \AA , respectively. The tin cations Sn⁴⁺ are located at (0,0,0) and ($\frac{1}{2}, \frac{1}{2}, \frac{1}{2}$) in the unit cell. The oxygen anions O²⁻ are located at $\pm(u, u, 0)$ and $\pm(\frac{1}{2}+u, \frac{1}{2}-u, \frac{1}{2})$ with $u = 0.307$. Each cation has two anions at a distance of $\sqrt{2}ua$ (2.053 \AA) and four anions at $[2(\frac{1}{2}-u)^2 + (c/2a)^2]^{1/2} a$ (2.597 \AA).

2.1.2 Electrical bulk properties

Because of its inherent non-stoichiometry caused by oxygen vacancies, SnO₂ is an n-type, wide-band gap semiconductor. While at the Γ point in the Brillouin zone (90 % tin *s*-like state) the minimum of the conduction band can be found, the maximum of the valence band, which in turn is a set of three bands (2⁺, 3⁺ and 5⁺) is a Γ_3^+ state. As a consequence, SnO₂ has a direct band gap of $E_{dir}(\Gamma_{3v}^+ - \Gamma_{1c}^+) = 3.596 \text{ eV}$ for E_{\perp} and 3.99 eV for E_{\parallel} (at 4 K). All of that is depicted in Figure 2.2. Further Figure 2.2 shows the projection of the density of states (DOS) for the 1-states of Sn and O. Between -7 and -5 eV the Sn(*s*)-states have the largest share, while further the Sn(*p*)-states contribution is decreasing up to the top of the valence band, as the

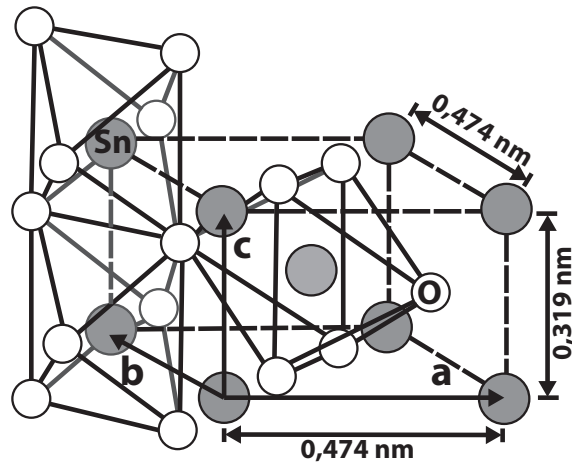


Figure 2.1: Unit cell of SnO₂ (rutile crystalline structure) with four O²⁻ anions and two Sn⁴⁺ cations. Each tin atom is sixfold coordinated, placed approximately at the corners of a regular slightly deformed octahedron, to threefold coordinated oxygen atoms.

Sn(*d*)-states are occupying these states. However, in the valence band an extended contribution of the O(*p*)-states is found. The bonding between Sn- and O-atoms can be classified by a planar-trigonal configuration, in a way that the oxygen *p* orbitals are incorporated in the four-atom plane - the *p_x* and *p_y* orbitals, define the bonding plane. Consequently, the oxygen *p* orbitals perpendicular to the bonding plane, i.e., *p_z* orbitals, have a non-bonding character and are expected to form the upper valence levels [The92]. The conduction band shows a large contribution of Sn(*s*) states up to 9 eV. For energies larger than 9 eV an equal contribution of Sn- and O-states is found in the conduction band. For a detailed description of the valence band properties see [De 94; K95; The92] and references therein.

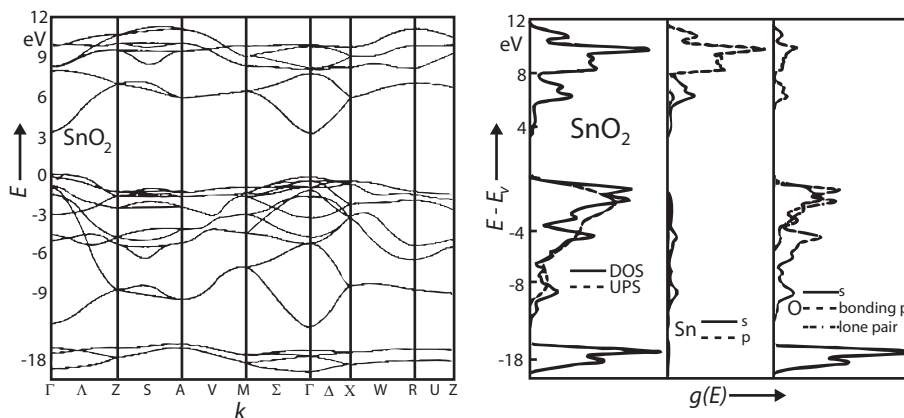


Figure 2.2: Band diagram of SnO₂ (left) and projection of the density of states (DOS) for the 1s states of SnO₂, Sn and O (right) [Jol86].

2.1.3 Conductivity of the material

With the consideration of an independent conduction process, the conductivity σ_{tot} of a semiconductor crystal can be described according to Equation (2.1).

$$\sigma_{tot} = \sigma_e + \sigma_p + \Sigma\sigma_{ion,i} \approx \sigma_e + \sigma_p \quad (2.1)$$

with electronic (σ_e and σ_p) and ionic conductivity (σ_{ion}). In the temperature range of a working sensor (200 - 400 °C), the ionic contribution can be neglected. The resistance of bulk material can be calculated according to Equation (2.2):

$$R_b = \frac{l}{\sigma_b \cdot b \cdot d} = \frac{l}{\sigma_b \cdot A} \text{ with } \sigma_b = \sigma_e + \sigma_p = n \cdot \mu_e \cdot e + p \cdot \mu_p \cdot e \quad (2.2)$$

with bulk conductivity σ_b , mobility μ , length l and cross section A and with the charge carrier concentrations n and p . For an intrinsic semiconductor, n and p can be calculated according to Equation (2.3):

$$n = \int_{E_C}^{\infty} D(E)f(E)dE ; p = \int_{\infty}^{E_V} D(E)(1 - f(E))dE \quad (2.3)$$

The Fermi-Dirac distribution $f(E)$ and the density of states $D(E)$ is given by Equation (2.4):

$$D(E) = \frac{1}{2\pi^2} \left(\frac{2m_e}{\hbar^2} \right)^{\frac{3}{2}} (E - E_C)^{\frac{1}{2}} ; f(E) = \frac{1}{1 + e^{\frac{E-E_F}{kT}}} \quad (2.4)$$

For $E_C - E_F \geq 4kT$, the charge carrier concentrations n and p can be approximated by Equation (2.5) & Equation (2.6):

$$n = N_C \cdot e^{\frac{E_F - E_C}{kT}} ; N_C = 2 \left(\frac{2\pi \cdot m_e \cdot kT}{h^2} \right)^{\frac{3}{2}} \quad (2.5)$$

$$p = N_V \cdot e^{\frac{E_V - E_F}{kT}} ; N_V = 2 \left(\frac{2\pi \cdot m_p \cdot kT}{h^2} \right)^{\frac{3}{2}} \quad (2.6)$$

In its stoichiometric form, SnO₂ is an isolator with a wide energy band gap of around 3.6 eV [Mun83]. In Section 4.1.1 the formation of oxygen vacancies is described in

relation to the synthesis and fabrication of SnO₂ respectively the sensor layer. Due to the low formation energy of the oxygen vacancies a natural nonstoichiometric situation is given for SnO₂ which results in its n-type semiconducting properties. The discussed oxygen vacancies are singly- and doubly ionized and therefore form donor levels E_1 and E_2 , which are located around 34 *meV* and 140 *meV* below the conduction band (see Figure 2.3) [Sam73]. With the assumed multi-step donors, the bulk conductivity of SnO₂ is dependent of the number of electrons in the conduction band and on the upper and lower donor levels. A comprehensive statistical discussion about divalent centers in SnO₂ can be found in the dissertation thesis of M. Hübner [Hue11a]. Therefore, the main conclusion is the full ionization of the donor levels in the typical working temperature range of SnO₂ gas sensors (200 - 400 °C).

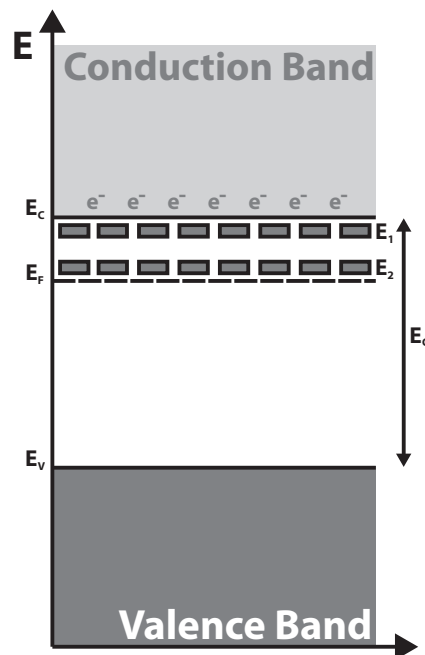


Figure 2.3: Band diagram (schematic) of SnO₂ with a band gap (E_g) of 3.6 *eV*. Two donor levels (E_1 & E_2), which results out of the oxygen vacancies, are located 0.03 and 0.15 *eV* below the conduction band.

2.2 The reactive SnO₂ surface [110]

Within the previous theoretical discussion about the basic properties of tin oxide, the surface and its reactivity towards ambient gas atmosphere has been neglected. While the properties of the bulk of a crystal can be adequately described because of its periodicity, the properties of the surface are somewhat harder to comprehend because the periodicity of the lattice is interrupted. The distortion in periodicity

of the lattice - the non-uniformly surrounded atoms and the perturbation of the overlapping orbitals - makes it much more difficult to understand such a system. It is well known that the SnO₂ [110] is the thermodynamically most stable surface [Cox83]. The rows of bridging oxygen ions can be removed easily to create a reduced surface with Sn²⁺ ions (see Figure 2.4).

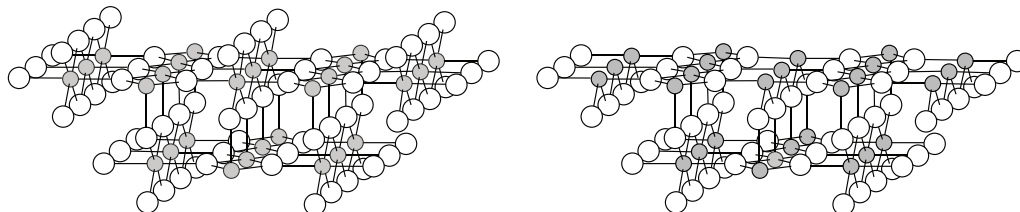


Figure 2.4: Ideal SnO₂ [110] surface (left) & reduced SnO₂ [110] surface (right)

However, the removal of those bridging oxygen rows does not provide additional donor levels in the band gap [Mun83], but additional surface states or energy states in the band gap - the so called Tamm states [Mor77b] - are introduced, because of the periodicity distortion.

2.2.1 Interaction with the surface

As long as a solid crystal phase is not enclosed by vacuum or doesn't come into direct contact with another solid substance, a surrounding atmosphere will cause a certain affectation of the surface. The molecules of the ambient atmosphere possibly interact with the surface, which in turn lead to a generation of surface states. Depending on the type and nature of the metal oxide and the gaseous reactant, a distinction is made between donor states and acceptor states, which may affect the electronic structure of the semiconductor. It is therefore easy to imagine that the adsorption, that is to say the reaction between a gas and a solid surface, plays a crucial part and is ultimately the reason why a gas sensor is sensitive to a change in the ambient atmosphere. There are mainly two different kinds of adsorption to be distinguished, which are basically discriminable by the strength of the formed bond and the influence on the electrical structure of the material.

Physisorption - The physisorption, which is the weaker type of bonding, is generally based on Van-der-Waals forces - a physical interaction - which originate from electrostatic interaction of induced fluctuating dipoles [Our03]. The physisorption process already can take place even at longer distances from the solid surface and is characterized by small binding energies of less than 50 *kJ/mol* [Goe94]. Due to

its low adsorption enthalpies the adsorbate will not dissociate. Moreover, there is no charge transfer between the interacting molecules and the solid phase, but still physisorption is the first step in the interaction between a gaseous species and the surface of a solid.

Chemisorption - The adsorption of a certain species with a covalent bonding characteristic is referred to as chemisorption. Due to a profound modification of the charge distribution of the adsorbed molecule the adsorption enthalpies are much higher in the case of chemisorption and the bonding situation is energetically comparable to chemical bonds. The values of the adsorption enthalpy are typically around 200 to 400 *kJ/mol*, depending on the surface and the adsorbing species. In contrast to the physisorption, a chemisorbed molecule can dissociate, which is the basis of heterogeneous catalytic processes in most of the cases [Atk06]. One can distinguish between neutral chemisorption and ionosorption, which constitutes a specific case of the chemisorption process and will be discussed separately for the case of oxygen adsorption below.

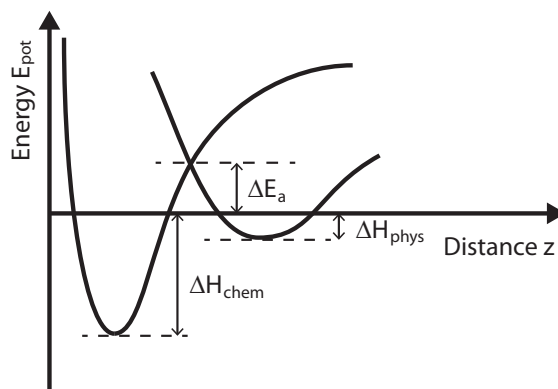


Figure 2.5: Energetic representation of Physisorption and Chemisorption

Figure 2.5 illustrates the potential energies in the case of physisorption (E_{phys}) and chemisorption (E_{chem}) as a function of the distance r from the solid surface. The interaction of a gaseous molecule with the solid surface can be described as follows: If a gaseous molecule approaches the surface it will first be physisorbed, gaining ΔE equal to E_{phys} . Approaching further to the surface the molecule encounters a growing energy barrier, tending towards an infinite energy for a finite distance r . By spending the activation energy E_a a dissociation of the molecule takes place, which allows a further rapprochement to the surface, which enables a stronger interaction respectively a higher energy gain ΔE equal to E_{chem} .

2.2.2 Oxygen

With the introduction and explanation of all adsorption processes of general interest, further debate will have to address the adsorption of specific molecules which are of particular importance in the field of metal oxide gas sensors.

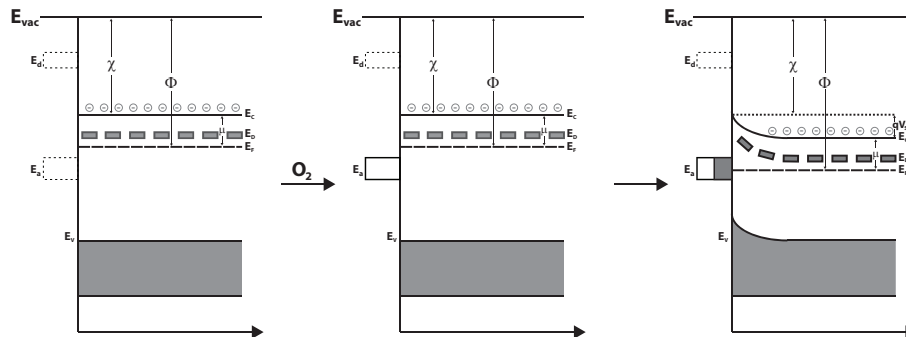


Figure 2.6: Schematic energy band representation of oxygen interaction with the SnO₂ surface. Acceptor levels are created in a first step, which are then filled with electrons from the conduction band. The resulting band bending (qVs) leads to a formation of a potential barrier at the grain-grain boundaries and thus to an increase in resistance.

The adsorption of oxygen is one of the cases that is of particular importance, for the simple reason that one has to consider a special case of chemisorption, namely the ionosorption. This process can be divided into two parts: a chemical and an electronic one. As illustrated in Figure 2.6, one can consider a flat band situation of the metal oxide in the absence of oxygen. In the presence of oxygen, adsorption occurs according to the mechanism explained in the previous section forming an acceptor level, whereas the limiting factor is the activation energy for adsorption and dissociation (chemical). From there on, changes in the electronic properties of the semiconductor are induced by a charge transfer of an electron from the conduction band which has enough energy to reach the surface. Consequently, the surface is negatively charged due to the trapped electrons in the acceptor level. This negative charge has to be compensated by a positive countercharge in the solid. According to the Schottky approximation, this region is characterized by a total depletion of the charge carriers and is therefore called depletion layer. Due to the electrostatic repulsion of the negative surface layer, the potential energy of an electron near the surface is increased, which can be explained as a band bending and a formation of a surface barrier qVs . This can be seen then as the second limiting factor - the electronic one. The reaction of oxygen including the charge transfer can be described

by the following equation [Mos87]:



These considerations are followed by a more detailed discussion in [Bar01]. From a chemical point of view, the adsorption of oxygen depends on many parameters, such as crystal structure, surface dopants and temperature, where a variety of possible species are suspected. An insight into the many facets of the adsorption process and the different adsorbed oxygen species is represented in Figure 2.7. A more detailed discussion will be given in a further chapter and is also reviewed in [Bat05; Gur06].

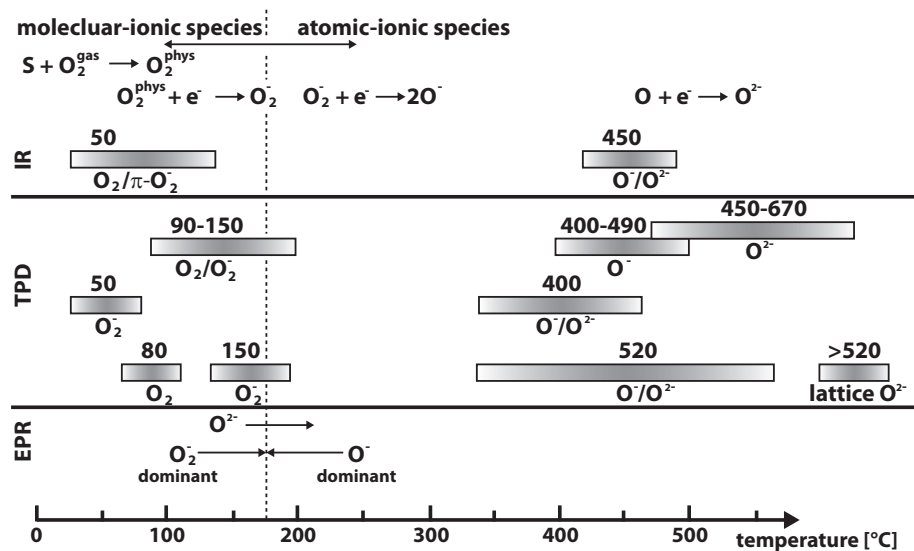


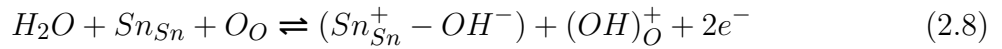
Figure 2.7: Literature review of oxygen species at the SnO₂ surface dependent on the temperature detected by the means of IR (Infrared) - spectroscopy, TPD (Temperature Programmed Desorption) and EPR (Electron Paramagnetic Resonance) after [Bar01]. For details see [Cha80; Gil76; Jol86; Len95; Vol81; Yam79]

2.2.3 Water

Humidity plays an integral part of the atmosphere in which an application oriented metal oxide gas sensor is put into service. It is quite well known that water - in its gaseous phase - has a profound impact on the sensing characteristics, especially on metal oxides in its pure form (e.g. undoped SnO₂). In some other cases, depending on the target gas and sensing material characteristics, water can even enhance the sensing properties. Even if an unfavorable impact of humidity on the detection of several gases can be generally minimized by the introduction of noble metal additives (e.g. Pd) [Har03], or exactly because of that, a crucial understanding of the water

adsorption processes is indispensable. Electrical measurements which provide, first and foremost, an insight into the characteristics, reveals an increase in conductance, whereas it is a reversible effect. In order to gain a deeper understanding of exactly what gives rise to conduction, the adsorption of water molecules and their chemical properties have to be examined more closely. However, in the specific case of tin oxide, as a result of numerous surveys, there are various proposed mechanisms describing the surface reaction of gaseous water, as well as the related species which are formed:

- dissociation of water and reaction with lattice oxygen resulting in the formation of a terminal hydroxyl group and a rooted hydroxyl group [Hei88]



- dissociation of water and reaction with adsorbed oxygen resulting in the formation of two terminal hydroxyl group [Hen94]



A third mechanism, according to which the water reacts with lattice oxygen and creates an ionized oxygen vacancy, has been recently disproved for undoped SnO₂ systems by Großman et al. [Gro12a]. Irrespective of the proposed mechanism, the formed hydroxyl groups can be generally regarded as:

- terminal hydroxyl groups (OH group attached to a Sn atom - Sn_L-OH)
- rooted hydroxyl groups (lattice oxygen integrated in the OH group - O_L-H)

Since the terminal OH group forms a dipole and therefore changes the electron affinity of the material, but the change in conductance, respectively resistance, must be explained by the withdrawal of the pre-adsorbed oxygen and the consequential release of an electron in the conduction band. This interpretation indicates that the pre-adsorbed oxygen ions play a key role as partner for the reaction of water on tin oxide surfaces [Koz06]. In the case of the rooted hydroxyl group, the decrease in resistance is based on the assumption of a lower electron affinity of the formed hydroxyl group, which implies ionization as denoted in Equation (2.9). In addition, it can be assumed that neighboring hydroxyl species can form hydrogen bonds. Further, water can adsorb in its molecular form (physisorption) at lower temperatures.

All these parameters are derived from different spectroscopic methods such as infrared spectroscopy and temperature programmed desorption measurements (TPD) and are summarized in Figure 2.8. Infrared spectroscopy is a very useful technique for the detection of water related species on the metal oxide surface. Comprehensive IR data is given in several books and articles such as [Dav03]. With regard to the present context, the corresponding IR bands for the relevant terminal and rooted hydroxyl groups appear as discrete absorption bands between 3740 - 3555 cm⁻¹ [Koz06]. The formation of hydrogen bonds is found to diminish the frequency of the OH stretching vibration and hence the bands ascribed to these OH groups are broadened and shifted towards lower wavenumbers [Dav03].

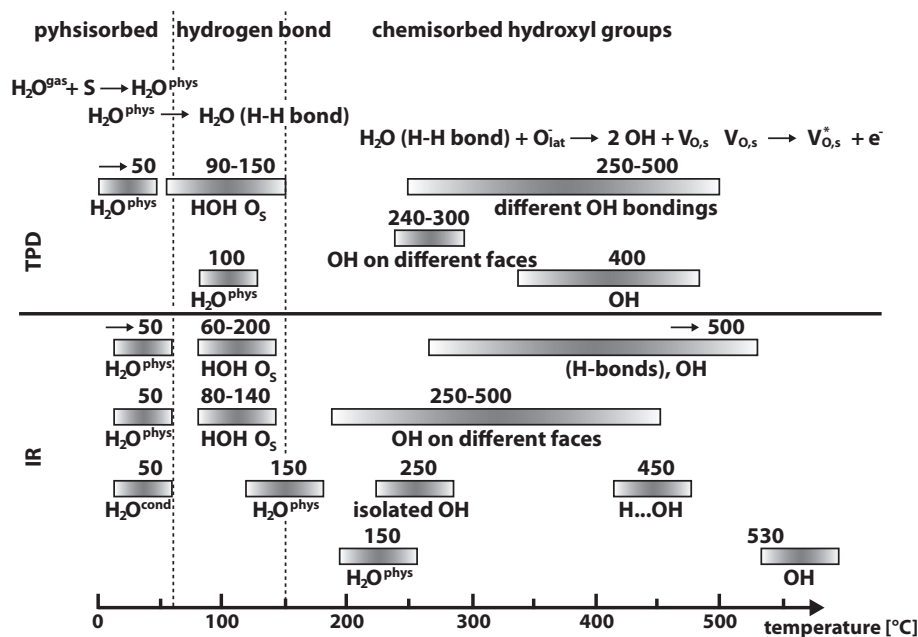
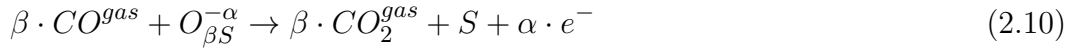


Figure 2.8: Literature review of hydroxyl species at the SnO₂ surface dependent on the temperature detected by the means of IR (Infrared) - spectroscopy and TPD (Temperature Programmed Desorption) after [Bar99]. For details see [Ber96; Ega81; Gue85; Koh92; Len95; Mor80; Tho75]

2.2.4 Carbon monoxide

Carbon monoxide is a colorless, odorless, and tasteless gas that is slightly less dense than air and toxic to humans and animals [Wika]. This certainly gives reason for its presence on the list of the six principal pollutants, which are called "criteria" pollutants, as specified in the introduction. Thus, there is a considerable interest for detecting carbon monoxide in low concentrations and therefore also for a general scientific understanding of the reaction of carbon monoxide on the metal oxide surface.

On account of the experience and expertise which is gained also in other fields of surface science (e.g. heterogeneous catalysis), the reaction of carbon monoxide on the sensor surface is the basis for numerous basic research studies [Bar02; Hah03; Har03; Sah05]. It is widely accepted that carbon monoxide reacts with pre-adsorbed or lattice oxygen [Hen94]. In the quasi-chemical formalism, the reaction is described by:



Where α is equal 1 for single and 2 for double ionized form of adsorbed oxygen, and β is equal 1 for atomic and 2 for molecular form of oxygen respectively. Barsan et al. derived the dependence of the conductance on the partial pressure of carbon monoxide [Bar01]. Keeping in mind that pre-adsorbed oxygen is considered to be the

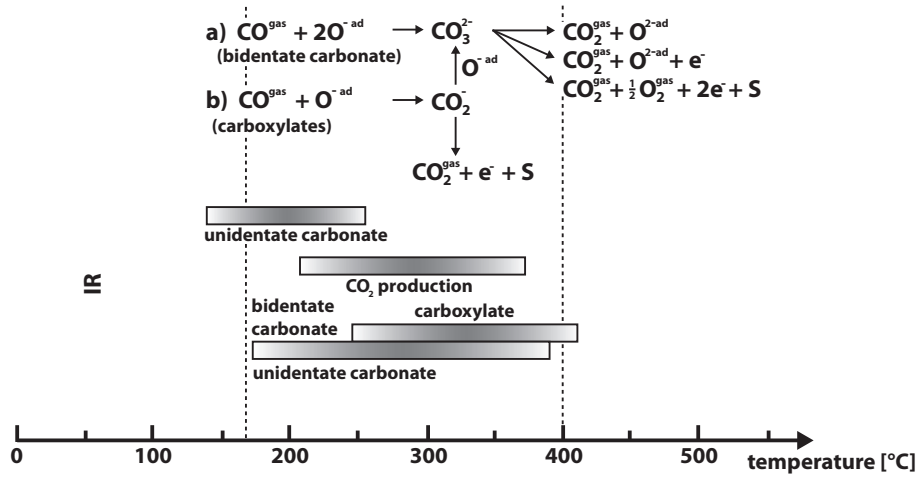


Figure 2.9: Literature review of CO reaction intermediates at the SnO₂ surface dependent on the temperature detected by the means of IR (Infrared) - spectroscopy [Bar99]. For details see [Boy77; Gen86; J. 98; Len95; Tho75; Win79]

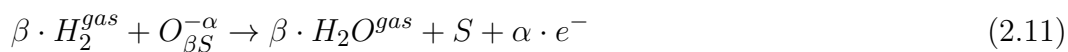
reaction partner of carbon monoxide, it is therefore logical that the aforementioned chemical equation is over-simplistic and does not accurately reflect the whole reaction process on the surface. Different intermediate species as well as the formation of carbon dioxide as reaction product could be identified by means of IR studies. A summary of the related literature data is given in Figure 2.9.

2.2.5 Hydrogen

Hydrogen is a colorless, odorless, tasteless and non-toxic gas. Despite of all these rather unspectacular characteristics, there is a major interest of sensing hydrogen because of its high combustibility. Furthermore, comparable to carbon monoxide,

hydrogen and its surface reactions are well researched and can be easily modeled. Therefore, the examination of hydrogen detection with metal oxide gas sensors is still in the focus in terms of ensuring safety guidelines (e.g. explosion protection in industry) or in basic research as developer model.

The reaction of hydrogen itself can partly be drained from the previously described situations on the tin oxide surface. Hydrogen reacts in all probability with the same adsorbed oxygen species as it is described for carbon monoxide and that, in consequence, is leading to an oxidation of hydrogen to molecular water. Therefore, the reaction can be described by the following equation:



There is no significant difference regarding the intermediates compared to the intermediates describes in Section 2.2.3 for the water adsorption. But of course, such as in most of the cases, the reaction, the reaction rate and the intermediates are heavily driven by the properties of the material (e.g. morphology, doping, etc). A comprehensive overview about different materials and the reaction of hydrogen respectively deuterium is given in [Gro12a].

2.3 Working principle

The previous sections have described the adsorption of some specific gases as well as their contribution to the change in free charge carrier concentration. At a usual working temperature of a metal oxide gas sensor (200 - 400 °C), the chemisorption of oxygen has an essential contribution to the sensing properties of such layers, most importantly facilitating the reaction or detection of other gaseous species like carbon monoxide or hydrogen [Bar01]. First and foremost, the ionosorption of oxygen on the SnO₂ surface generates a depletion layer with an upward band bending. With increasing the potential barrier, less and less electrons are available which have sufficient energy to pass this barrier. On the other hand, the reaction of reducing gases like carbon monoxide and hydrogen, which are oxidized by the latter formed oxygen - as discussed previously, will detach the trapped electrons out of the acceptor level, from where they'll return to the conduction band. This, naturally results in a lowering of the band bending.

In a porous thick film layer, which fits very well with the system under examination (c.f. Section 3.2), crystalline SnO₂ grains are loosely connected. In general, with

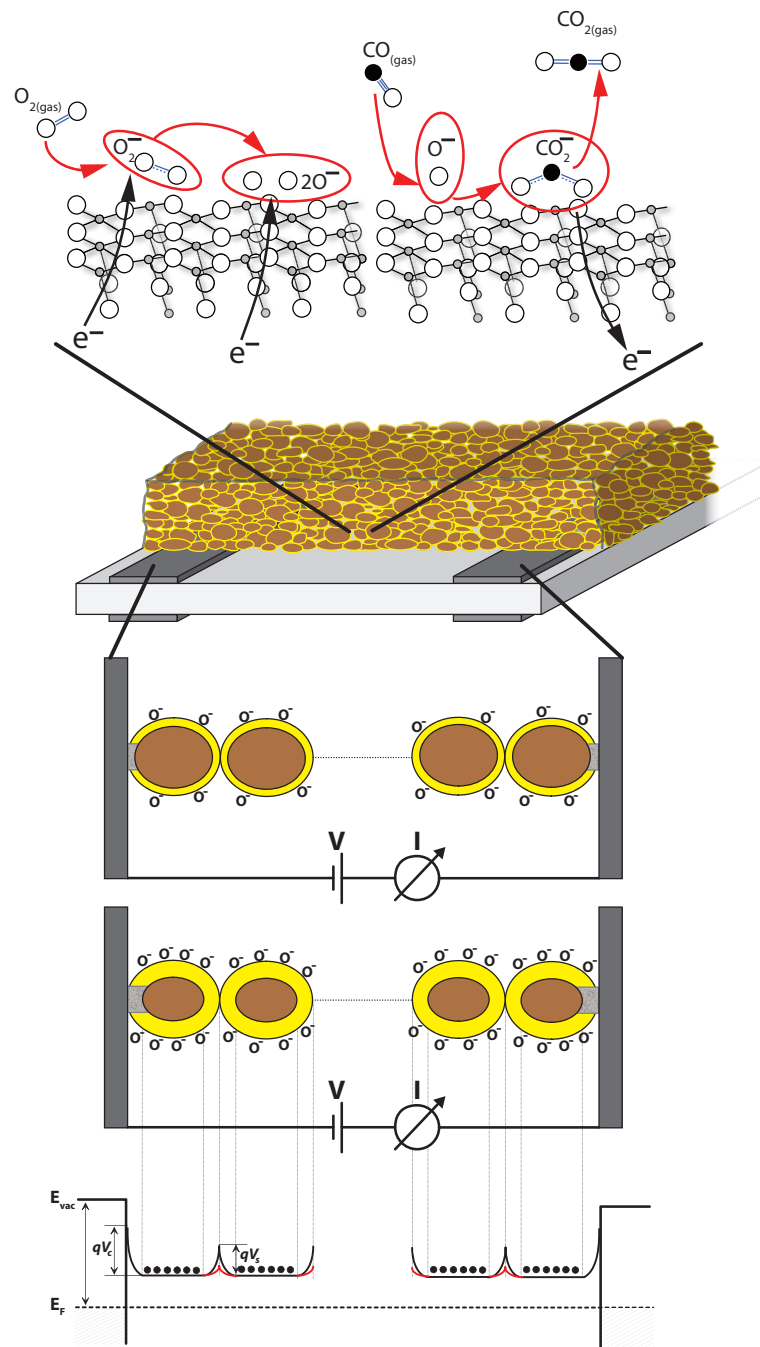


Figure 2.10: From the reaction of a gaseous species on the surface to the electrical signal - Schematic representation of the working principle of a n-type metal oxide gas sensor. Depending on the amount of chemisorbed oxygen a depletion layer is formed at the surface of each SnO₂ grain. A reducing gas (e.g. carbon monoxide) use up the pre-adsorbed oxygen and thus the depletion layer or the potential barrier respectively is decreased, which finally results in a decrease in resistance.

a rather large grain size of approximately 100 nm, the former described depletion layer will not affect the whole grain ($d \gg L_D$). The affected area or range of such a depletion layer is given by the Debye length, which is defined in the Schottky approximation as:

$$L_D = \sqrt{\frac{kT\varepsilon\varepsilon_0}{q^2n_b}} \quad (2.12)$$

It was recently demonstrated by Hübner et al. that the values of L_D found for the type of tin oxide which is also investigated within this work, are much lower than the grain size. In the case of smaller grains a full depleted layer is considerable. As a result, a single SnO₂ grain ($d \gg L_D$) can be partitioned in a section which can be directly influenced by gas exposure forming a depletion region around the grain and an inner part - the bulk - which is unaffected by any surface reactions and therefore more conductive. When one considers now the conduction as a pathway from one contact through a numerous number of grains to the other contact, only the electrons having enough energy to overcome the potential barriers are able to contribute to the conduction process. Denoting the band bending as qV_s and the electrons with enough energy to reach the surface as n_s , one can describe the relation between those variables by the following equation:

$$n_s = n_B e^{\left(-\frac{qV_s}{kT}\right)} \quad (2.13)$$

The validity of this relation is only given if:

- bulk diffusion of oxygen can be excluded, which can be ensured by moderate working temperatures
- full ionization of the donor levels related to the oxygen vacancies - recently demonstrated by Hübner et al. [Hue11a]
- no contribution from the holes to the conduction

The resulting corresponding relation between the band bending and the conduction is therefore as follows:

$$G_n \propto e^{\left(-\frac{qV_s}{kT}\right)} \quad (2.14)$$

When thus relating the relative change in conductance to the change in band

bending upon exposure to oxygen yields to the following equation:

$$q\delta V = -kT \ln \left(\frac{G_{O_2}}{G_0} \right) \quad (2.15)$$

The whole working principle of the conduction process and how it is influenced by surface reactions is depicted schematically in Figure 2.10.

CHAPTER 3

Motivation

Every chemoresistive gas sensor operates on the same basic principle. The interaction of a gas on the metal oxide surface causes a change in the physical properties which influences the conductance of the semi-conductor. In its basic form, two electrode contacts are allowing the readout of the changes in resistance of the semiconducting metal oxide material. This applies regardless of the used production method respectively the obtained structure of the receptor, such as thick film sensors or thin film sensors. Noble metals, such as gold or platinum, are the most commonly used materials for the electrode contacts. Not only the fact that these type of materials are excellent conductors, but also their chemical and mechanical stability makes them fully viable. The electrode material and geometry have been modified repeatedly in the last decades. With the "classical" probe setup of Taguchi, which we have today left behind us, the two-electrode configuration was used in the first types of chemoresistive gas sensors contacting the sensitive material on each face [Chi92].

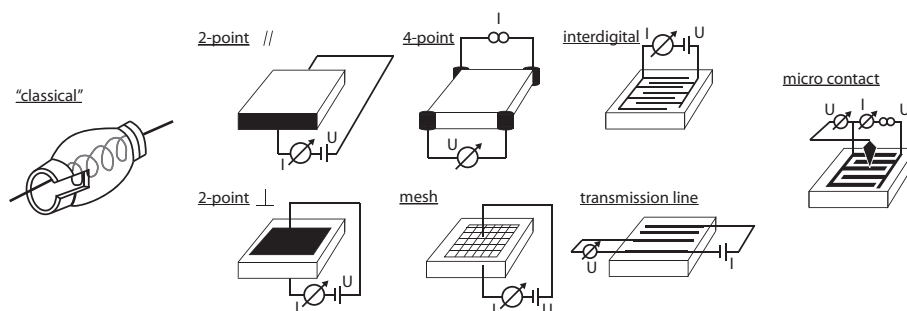


Figure 3.1: Overview of typical electrode geometries. From the "classical" Taguchi type gas sensor to the "modern approach" of micro contacts. After [Goe95].

An interdigitated geometry of the electrode provides the decisive advantage of a large electrode-sensing layer contact area within a small footprint. Consequently,

further improvements could have been made in terms of a miniaturization of gas sensing devices. Figure 3.1 is representing a non-exhaustive overview of the different approaches in electrode geometries [Goe95].

It is conceivable that such differences in the nature of the electrode in terms of material and geometry may affect the sensing properties. This chapter describes the various structures and properties of the electrode and how these different conditions affect the contribution to the overall electrical conductance, together with the presently available knowledge about the interaction of gases at the boundaries between the electrode and the sensing layer. In addition, considerations are made on how to connect the influence of the electrode to noble metal additives, which are distributed inside the sensing layer.

3.1 Scientific point-of-view

Contacting two materials such as an n-type semiconductor and a metal, with different work functions, causes a formation of an additional energy barrier. The work function of the semiconductor, which is defined as $\Phi_{SC} = (E_C - E_F)_{bulk} + qV_S + \chi$, differs from the work function of the metal (Φ_M). The values for several metals (measured in vacuum [Mic77]) can be found in Table 3.1, which are assumed to be higher than the work function of the n-type semiconducting metal oxides commonly used in gas sensing devices. As the two materials are brought in contact, the Fermi energy (E_F) of both components must be aligned at thermal equilibrium, which is why electrons from the semiconductor move into the metal forming the energy barrier, with a magnitude equivalent to the initial difference between the work functions.

Table 3.1: Workfunction of metals in [eV] [Mic77]

Al	Ti	W	Mo	Cu	Ni	Au	Pt
4.28	4.33	4.55	4.6	4.65	5.1	5.15	5.65

Given the characteristics of the system concerned here, the following conclusions can be drawn in the light of the experience acquired to date. Barsan et al. were stating that the electrical influence on the change of the overall electrical resistance in a thick film gas sensor - as described there - are negligible during the operation of a sensor [Bar01]. Different initial band bendings will result in the same barrier between metal and semiconductor which depends on the proper bulk values of the work function, as long as the electron affinity (χ) remains constant (case 1 & 2 - Figure 3.2). A change in the electron affinity (χ), before or after the initial equilibrium of the Fermi levels, is the only parameter that may influence the barrier height (case 3 - Figure 3.2). χ can be influenced by the formation of a dipole on the surface, but since the field of such a dipole is rather spatially limited in distance (see Figure 3.3) the influence is assumed to be negligible.

Through close observation and deductive reasoning the electrical influence of the electrode on a working thick film sensor can be considered negligible. Other studies have revealed the influence of different transducer designs & geometries. Several authors have noted the significance of positioning of the electrodes. In 1990 Jain et al. conducted research studies on electrode configurations which are inside and outside the exposed face of the sensing layer. Numerical calculations demonstrated that based on the rate constant of the reaction of a reducing gas or oxygen, the electrode which is placed on the facing side of the gas exposure (back contact) will show higher

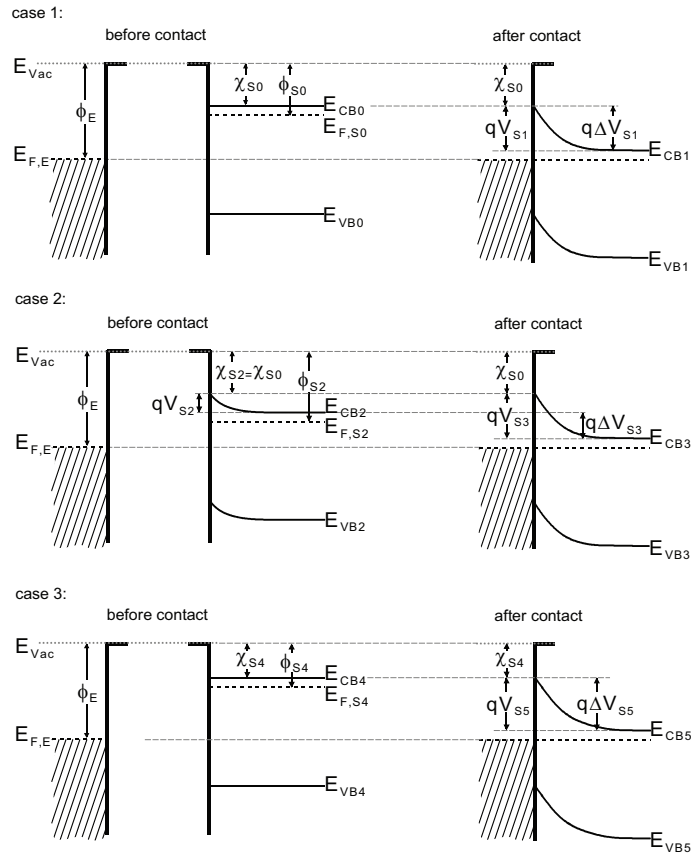


Figure 3.2: Three different cases describing the situation before (left) and after (right) contact between the electrode and the semiconductor. Case 1 & 2: In both cases the electronic affinity is assumed to be equal. After the contact between both materials the Fermi levels equilibrates, which results in a band bending independent of the initial band bending (before contact). Case 3: The electronic affinity is different compared to case 1 & 2, which results in a different barrier height after contact of the metal and the semiconductor. After [Bar01]

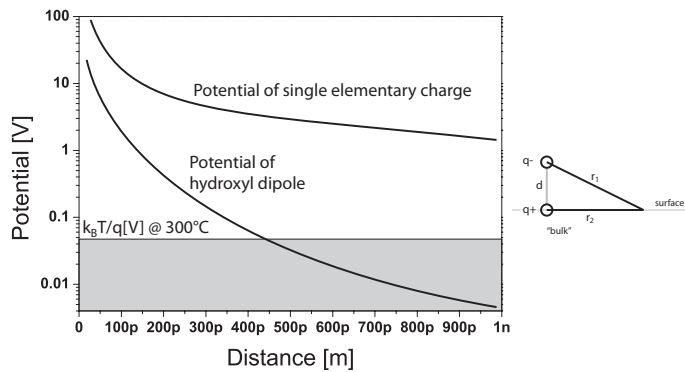


Figure 3.3: Potential of a single elementary charge (q^+) and a hydroxyl dipole (q^+ & q^-). The area shaded in grey is giving the potential of the thermal energy. q^+ is the origin of the x-axis, while the distance [m] is represented by r_2 . For more details & explanations of calculations see [Bar01]

selectivity for moderately reactive gases compared to less or more reactive ones - as could be seen also for commercial sensors (e.g. Figaro). Conversely, contacts on the exposed side show high sensitivities but a much lower selectivity. The purely geometric effect occurs because of the non-uniform change in layer conductance, when exposing it to a certain gas - if a gas molecule hits the surface, then it must first diffuse through the whole film to induce an effect at the bottom electrodes [Jai90]. Moreover, Vilanova et al. (1995) and Durrani et al. (2006) found in their surveys about electrode geometry broadly the same results as those obtained by Jain et al. However, lower sensitivity for sensors with electrodes placed on the bottom (back contacts) can slightly be increased by widening the electrode gap [Dur06; Vil98]. Starting from the empirically demonstrable differences between varying-sized electrode gaps, Hofer et al. have made an attempt to systematically examine the various influences on sensitivity and selectivity depending on the distance between the electrodes. After numerous investigations on TLM (transmission line model) sensor arrays [Hoe95], thin film sensors with a highly asymmetric electrode configuration, an exemplary simple and low-cost integrated sensor system with improved selectivity which differs only in the electrode gap could be developed. It was thus possible, for instance, to selectively measure NO₂, which requires a high Schottky barrier, and CO, which presupposes short contact separations and wide sensitive layers [Hoe98]. Apart from the geometry effects of Au and Pt electrodes, Capone et al. focused on the stability of the electrode material. In their work in 2001 and 2006 they found a reduced thermal stability of the gold electrode. The possibility of a partial decomposition of the gold electrode and a subsequent diffusion of Au atoms into the sensing layer explained - on the one hand - why the sensitivity towards e.g. CO was increased, comparable to an Au-doping effect [Cap01]. On the other hand, such time-dependent destabilization has been associated with an ageing-effect or rather drift-effect by the authors [Cap06].

As depicted by the previous examples, the general setup of a chemo-resistive sensor consists of a two-probe electrode configuration. One further consideration that an applied voltage is necessary in order to measure the change in conductance brings us to another obstacle that should not be underestimated. The typical characteristic I - V curve of a Schottky junction shows a non-linear behavior. Thus, the applied voltage in a dc resistance measurement has to be selected carefully and scrutinized in order to estimate how the measured current depends on the voltage, especially for thin film sensors, where an electrical contribution of the contacts cannot be

excluded. Weimar et al. published in their work about improving selectivity and sensitivity with ac measurement techniques a variety of different probe setups in order to discriminate the influences of different sections of the sensor [Wei95].

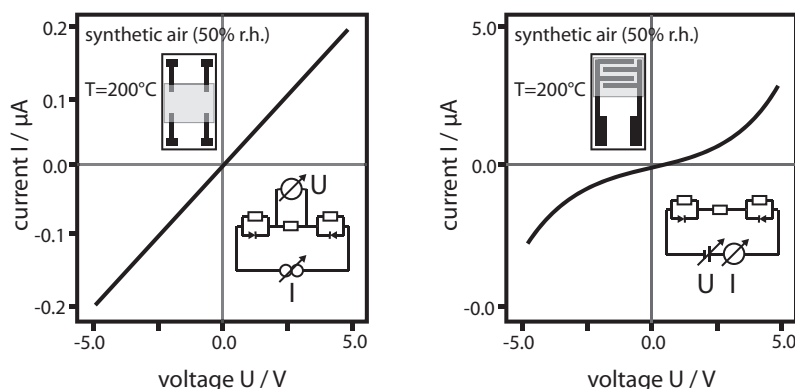


Figure 3.4: Ohmic behavior of the four-probe measurement readout of a SnO_2 sensor at 200 °C in 50 % r.H. (left) non-ohmic behavior of the two-probe measurement readout of a SnO_2 sensor at 200 °C at 50 % r.H. (right). For details see [Wei95]

While dc measurements on a SnO_2 thin-film sensor with a two-probe setup showed a non-ohmic behavior for all tested conditions, the four-probe setup (Van-der-Pauw method [Van58]) indicated an ohmic behavior, and therefore elimination of the contact contribution (see Figure 3.4)[Wei95]. One should mention, as a separate matter, that this work resulted in decisive key-findings on the detailed understanding of the conduction mechanisms, those times. Faglia et al. and Gerlich et al. presented concepts of measuring sensors on the basis of four-point structures, that allow for the detection and discrimination of different target gases [Fag98; Ger03]. All these examples indicate the potential for using the contact contribution in terms of a well-considered transducer design for enhanced sensitivity and selectivity. Moreover, many other contributions in scientific journals provided a crucial proof that the sensor performance is not only affected by the geometry or structure of the contacts, but also by the choice of the material. Table 3.2 summarizes some of the results of surveys made on this topic. A comparison of the results shows that there is considerable interest in understanding the influence of the nature of the electrode.

While starting from the early 1980s a general difference between gold and platinum electrodes in the sensing performance has been observed by Lalueze et al. [Lal84], especially in the mid 1990s a lot of work was carried out to systematically gather information about the significant differences. While some authors simply described the recorded diversities like the increased selectivity or sensitivity for miscellaneous gases using particular electrode materials [Gol94; Sau03; SB97] or the temperature

Table 3.2: Literature review on electrode effects

Electrode materials	Sensor material	Measurements	Results	Ref.
Au, Pt	SnO ₂ (pellets)	Conductivity measurements at different temperatures of SnO ₂ pellets connected via platinum or gold wires	Depending on the type of the SnO ₂ - metal junction the maximum in conductivity in air and in different benzene and SO ₂ concentrations appears at different temperatures	[Lal84]
Au, Pt, Pt/Au, Ag/Pd, Ni	Fe ₂ O ₃ , SnO ₂ (thick film)	Measurements in 50 % r.h. with methane at 400 °C and CO at 300 °C Depending on deposition techniques & firing temperatures of the electrode	Ag/Pd: Migration of silver in the oxide resulting in a short circuit Ni: very high resistance of the sensor, negligible sensitivity, oxidation of the sensor material Pt/Au: Response ten times smaller than with only Au or only Pt electrodes	[Dut92]
Au, Pt	SnO ₂ , SnO ₂ /Sb (thick film)	Temperature dependent (100 - 550 °C) conductance measurements in dry air and 1000 ppm H ₂ O	Lower conductance for Au electrodes at lower temperatures. Conductance for Pt electrodes remains nearly constant	[Yli93]
Pt, Au, RuO ₂ , NiP	SnO ₂ (thick film)	Methanol, Ethanol, Acetone, ethyl acetate 300 - 400 °C	Increased selectivity by using RuO ₂ or NiP electrodes, but not stable upon 350 °C	[Gol94]
Ag, Au	SnO ₂ , SnO ₂ /Pt (thick film)	H ₂ & CO 350 °C	Increased sensitivity for sensors with Ag electrodes. Migration of Ag into the sensing layer ("auto-doping")	[Mis94]
Au, Pt	SnO ₂ , SnO ₂ /Pt	CO 230 - 420 °C	Higher sensitivity for Pt electrodes at all temperatures	[SB97]
Stainless steel	SnO ₂ (thin film)	Ethanol 550-750 K	Increased sensitivity at a certain temperature, explained by an accumulation of adsorbed oxygen at the electrode-sample contact region	[Var98]
Pt, Pd, Au	SnO ₂ , SnO ₂ -Mn ₂ O ₃	H ₂ in N ₂ 300-550 °C	no difference in response along with the nature of the electrode, but the Pt electrode samples were the more resistant	[Gou99]
Au, Pt different gap	SnO ₂ (thin film)	CO 150-450°C	Higher response towards CO for Au electrodes, explained by Au migration. Less stability of Au electrodes, higher resistance of Pt electrodes.	[Cap01]
Au, Pt	SnO ₂ /Sb (thick film)	CO, H ₂ 230-470°C	With Pt electrodes more sensitive to H ₂ , with Au electrodes give better response to CO.	[Sau03]

dependence in conductivity under air [Yli93], others tried to find logic explanations for any deviations like migration processes or catalytically activated processes induced by the electrode [Cap01; Var98]. Concluding, the key elements are as follows:

- Temperature dependency - e.g. better responsiveness for sensors with gold electrodes at lower temperatures compared to sensors with platinum electrodes
- Instability of some electrode materials - one must be cautious here, because the production process of the electrode itself may differ significantly from case to case
- Activation of catalytic processes on the electrode or next to the electrode

Consequently, there are many facts available, but, still, clear findings and evidences are missing which are able to describe the material related differences in a proper manner. The acceptance of a non-significant influence on the electrical properties and the first indications of activated gas reactions on the surface bring us to a stage where it is reasonable to consider mainly chemical contributions of the electrode as main impact factor. Considering, furthermore, how much work was put into the understanding of noble metal / metal oxide interactions and the assumption that this case is broadly similar to those of electrode / metal oxide interactions, maybe it helps to look in recent publications to shed light on the processes taking place on the noble metal / sensing layer interface which are supposed to improve the efficiency.

According to the discussion in the first chapter, the interaction between the target gas molecules and the sensing layer can be tuned to obtain better sensor performance (in terms of sensitivity, selectivity or operating conditions) by preconditioning of the gas atmosphere reaching the metal oxide surface or changing the material properties themselves. While the former considers the implementation of an active filter on the surface or next to the surface, the latter can be realized by "doping"¹ of the material with noble metal additives. The influence of these dopants is primarily determined by their localization, aggregation and/or chemical state. These parameters are basically driven by the introduction step respectively by the sensor fabrication. The performance-enhancing effect that doping may elicit has been known for a long time - and it has been the subject of intensive research effort because of the extraordinary

1 in metal oxide gas sensors the term "doping" intend the addition of noble metals during or after the synthesis of the oxide material - not to be confused with the classical "doping" in semiconductors

opportunities it offers. With the assumption that noble metal additives establish a separate phase, certain possible interactions are sketched in Figure 3.5.

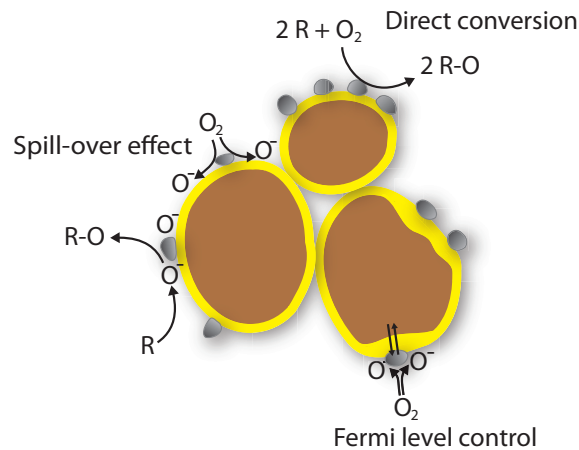


Figure 3.5: Effect of noble metal additives at the surface of n-type metal oxide grains

- Noble metals like platinum, palladium or gold are widely used in the field of catalysis and were investigated in this context in many publications. It is precisely this feature which is also important in sensor research. As stated by many authors, noble metal additives have an increased activity in **direct conversion** of a certain gas without having an effect on the electrical properties of the semiconducting sensitive layer [Kap01a].

On that account, one has to consider further synergies explaining the enhanced sensor performance, which include:

- **Fermi level control mechanism:** a direct reactions of the target gas at the surface of the additive removes electrons from the noble metal. The loss of electrons is compensated by withdrawing them from the closely contacting semiconductor. The further decrease of charge carriers changes the depletion layer and band bending of the metal oxide [McA88]
- **Spill-over effect:** There is an increased probability of gas adsorption/activation on the noble metal due to the lower required activation energy, that may subsequently leads to an diffusion or migration of the adsorbed species on the neighboring metal oxide grains [Yam91].

The influence of placing metallic films on the top or underneath the sensing layer was investigated, with the results of comparable effects as in the case of additives distributed in the layer [Mon03; Mon02]. These models remain valid as long as the

additive forms metallic clusters as described above. Besides that, it could be recently demonstrated by the means of operando EXAFS spectroscopy that palladium and platinum additives are present in an oxidized form, whose direct impact is more difficult to assess [Hue11b; Koz09]. All the results of these surveys provide an insight into the influencing factors of noble metals in general, however, a fundamental understanding from the chemical point of view or a detailed characterization of the chemical activation and reaction of gas molecules on the three-phase boundary is still missing.

The comparability of noble metals as additives in a metallic state, films, membranes as well as electrodes probably could combine all the efforts in order to gather more basic information. Consequently, the motivation of this work was to take on with this challenge and a host of measures has been taken to meet the aim of finding a spectroscopic proof for the models and theories mentioned above or possibly finding other explanations why different metallic noble metals in contact with the sensing layer cause such remarkable differences.

In accordance with Section 1.4 and Section 1.5, a fundamental understanding of sensing properties is not only a sustainable progress towards further research; it always leads to insights and possibilities with a focus on remarkable improvements in applications.

3.2 The sensors investigated in this work

Metal oxide gas sensors, in particular SnO₂ gas sensors, are available in many forms. The differences in material synthesis, morphology and transducer design, etc. influence the sensing characteristics to a large extent. The system investigated within this work is a screen printed thick film sensor on an alumina substrate with the sensitive layer and electrodes on the front side and the heater structure on the backside (Figure 3.6). This system was already the basis for numerous surveys [Gro12a; Hah02; Hue11a; Kap01b; Koz06; SB98; Wei01] and, therefore, provides a common ground for further research. However, various electrode materials, which were used for a variety of reasons, delivered fundamentally different results regarding the detection of various gases - again and again realizing the differences in terms of sensitivity and selectivity related to the nature of the electrode. As a consequence of the broad knowledge about this specific system, it is therefore not considered to repeat most of the standard measurements, which has to be done usually in order to generate a comprehensive know-how of the system characteristics. The focus

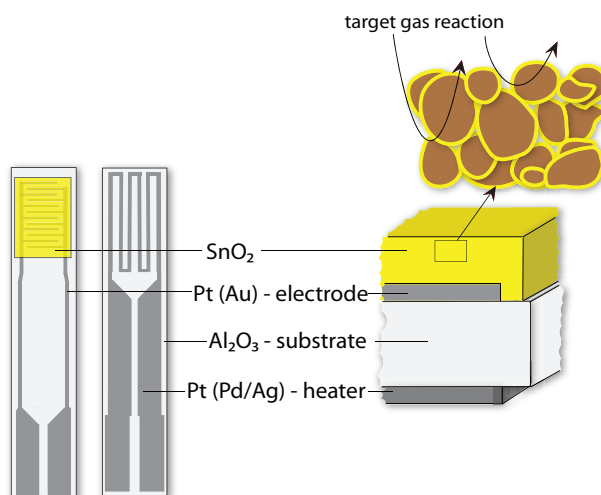


Figure 3.6: Schematic layout of the typical "IPC" SnO_2 sensor. The sensing layer is deposited via screen-printing on an alumina substrate. The interdigitated electrode structure beneath the sensing layer is out of platinum or gold. The heater structure on the backside is out of platinum or a palladium/silver-alloy.

here is exclusively on gaining a comprehensive understanding of the influence of the electrode material itself. That is why the first step was basically a fast screening of the already known material on the common alumina substrates with either gold or platinum electrodes. In this experiment the resistance of two SnO_2 sensors equipped with either gold or platinum electrodes have been recorded upon exposure to 25 ppm and 250 ppm carbon monoxide at a sensor working temperature of 250 °C and 350 °C. The normalized data is plotted in Figure 3.7. It is easy to grasp that the

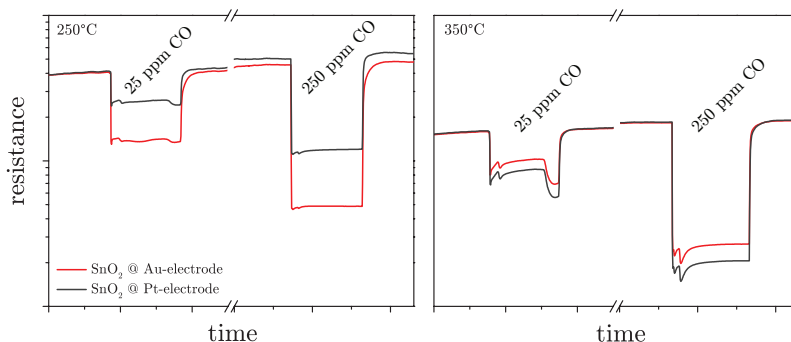


Figure 3.7: Normalized measurement of the resistance of two different SnO_2 sensors equipped with either platinum or gold electrodes at 250 °C and 350 °C under exposure to 25 ppm and 250 ppm carbon monoxide

difference in performance is temperature dependent. While at 250 °C the decrease in resistance upon exposure to a reducing gas is higher in the case of tin oxide sensors equipped with gold electrodes, the difference at 350 °C is not significant any more.

CHAPTER 4

Experimental

Well-controlled sample preparation, high reproducibility, good stability - are just a few of the keywords, which underline the requirements for a trustful study. As previously mentioned, in the present case of SnO₂ gas sensors, one can easily resort to existing knowledge [Kap01b; Wei01] when it comes to material synthesis and sample preparation. Still, the following section shortly summarizes the preparation route of the measured samples but also provides a complementary picture concerning different, novel type of samples, which have been prepared for well grounded reasons. Secondly, the various methods, which have been used in order to gain a full phenomenological and spectroscopic characterization of the material, are presented. For each of the used measurement technique, additional information is provided regarding the basic principles of the respective technology.

4.1 Material preparation and sensor fabrication

The manufacturing process for SnO₂ thick film gas sensors can be divided into powder preparation or material synthesis and the fabrication of sensors based on these powders. Both production steps are summarized in Figure 4.1 and will be described in detail in the following sections.

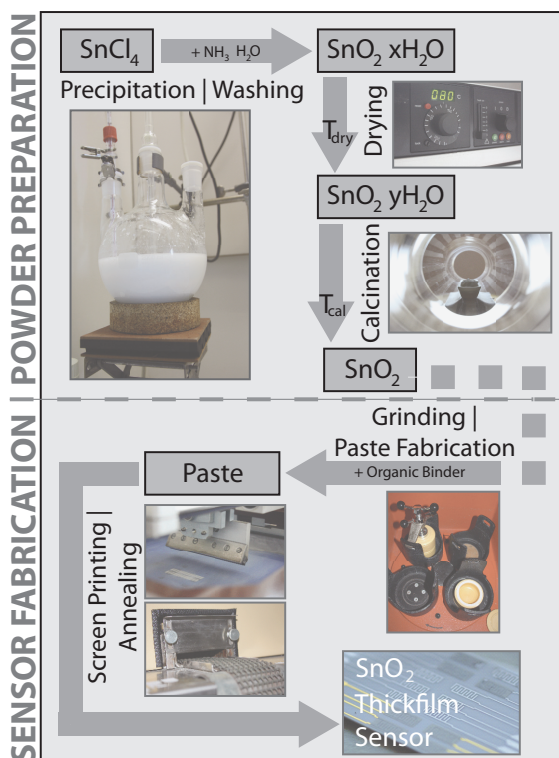


Figure 4.1: Flowchart describing the SnO₂ powder preparation and the sensor fabrication process

4.1.1 SnO₂ Synthesis

SnO₂ is usually commercially available with the limitation that certain parameters are already set. By the described preparation route one can tune different parameters, i.e. grain size, crystallite quality and defect concentration, as desired. The preparation process of the ready-to-use tin oxide can be divided into two parts - the synthesis of the hydrated tin oxide and the post processing to adjust specific parameters of the final SnO₂.

Synthesis - SnCl₄ is added drop-wise to ice-cooled water to get a 2 M water solution of SnCl₄. Since dissolution is highly exothermic and can lead to the premature

hydrolysis, the mixture should be continuously cooled and intensively stirred. The aqueous, ice-cooled SnCl_4 solution is then added drop wise at a controlled speed to an ice-cooled, aqueous solution of NH_3 . The temperature of the resulting mixture should remain fairly close to $0\text{ }^\circ\text{C}$ to reduce the reaction speed and to ensure a homogenous precipitate with a small mean grain size. Thereafter, the precipitate is washed several times with bi-distilled water in order to remove the remaining chloride and ammonia. After making sure that no remaining chloride or ammonia can be detected (conductivity measurement, pH measurement), the suspension is centrifuged and dried at $80\text{ }^\circ\text{C}$ in a drying oven.

Post processing - In the post processing step the resulting hydrated SnO_2 is calcinated in a tubular furnace at $1000\text{ }^\circ\text{C}$ for 8 h. This temperature treatment removes the remaining water and enables the grain growth to form SnO_2 with a well-defined grain size. Aside from a synthesis under precisely controlled conditions, the post processing part determines the material parameters which are essential in order to tune the sensor characteristics. The dependence of the preparation and synthesis parameters on the material characteristics has been thoroughly investigated [Kap01b; Wei01] and will be shortly summarized in the following.

Influence of synthesis temperature - Since SnCl_4 is highly reactive and its interaction even with water energetically very favorable (releasing 125 kJ/mol), there is a need to suppress its reactivity to avoid premature uncontrollable hydrolysis. To suppress chemical reactivity between the compounds the mixture has to be cooled. In addition, hydrolysis itself is an exothermic reaction and without heat removal the hydrolysis rate will increase by 2-4 times upon temperature increase by $10\text{ }^\circ\text{C}$ (van't Hof rule). The increased rate will result in non-uniform particles, agglomerates and microstructure of the precipitate, which should be avoided.

Influence of pH - The pH drastically changes the nature of the ligand type in the hydrolyzed tin complex. Therefore it can accelerate condensation or suppress it. In the described synthesis route a drop of SnCl_4 water solution is added into ammonia water solution, which means that hydrolysis occurs under very basic conditions, favoring formation of *oxo*-ligands rather than *hydroxo* ones, which results in high condensation rate and bigger primary particles.

Calcination - after the synthesis the obtained precursor - hydrated SnO_2 - is going

through a thermal treatment, providing thermal energy and initiating the growth of SnO₂ particles. Consequently, the size and the crystalline quality determined within this procedure are heavily influenced by the temperature and time of the calcination process. The particle size is increased with increasing the calcination temperature. The dependency of the average grain size of the herein used SnO₂ on the calcination temperature was investigated in [Kap01b] and is illustrated in Figure 4.2. Secondly, the defect concentration (oxygen vacancies) is determined as well by the calcination step. In general, the concentration increases with the calcination temperature. At higher calcination temperatures, the thermal energy enables a reorganization of atoms and a healing of dislocations inside the grain. In a further step, the prepared

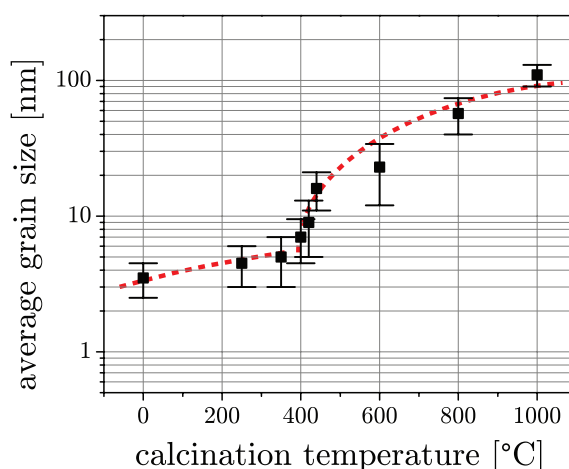


Figure 4.2: Average grain size of SnO₂ (wet-chemistry synthesis) as a function of calcination temperature. Data determined by TEM in [Wei01]

material has been examined in order to determine the specific parameters such as the specific surface area, the crystalline quality and the particle size. The specific surface area of the as-obtained tin oxide is about 10.3 m²/g and was evaluated by means of the Brunauer-Emmet-Teller method (BET). The crystalline quality and the particle size were determined by X-ray diffraction (XRD) in the laboratory of Lutz Mädler at the University of Bremen. The calculated crystallite size from Rietveld refinements that fit well to tetragonal SnO₂ (ICSD 39173 CIF file), is around 106 nm ± 34 nm.

4.1.2 Sensor fabrication

As previously mentioned, metal oxide thick film sensors are considered to be the most suitable for gas sensing, both in terms of research and in terms of application devices. Screen printing provides a simple and reproducible way to fabricate these types of sensors. All sensors which have been investigated were obtained by screen

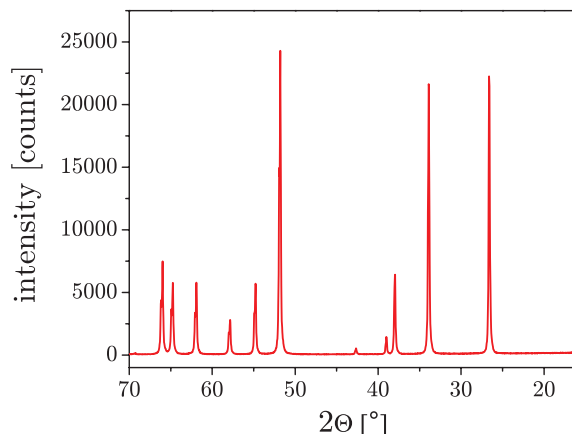


Figure 4.3: XRD pattern of SnO_2 calcinated for 8 hours at $1000\text{ }^\circ\text{C}$

printing SnO_2 based pastes onto alumina substrates provides with either Pt or Au electrodes - and respectively a platinum or silver/palladium heater on the backside. Therefore, the SnO_2 with defined parameters, obtained in the previous step - the powder preparation, has to be transformed into a homogenous paste. Due to the calcination step the tin oxide powder contains large agglomerates, which complicates the fabrication of a homogenous paste. Inhomogeneity in the paste would unduly complicate the printing process and would even cause cracks in the final sensing layer. Hence, after adding an appropriate amount of organic binder (propanediol), a milling process as depicted in Figure 4.4 is mandatory. The homogenous paste

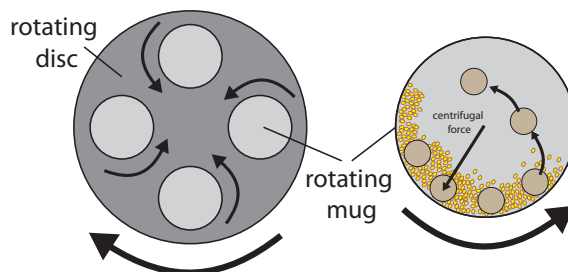


Figure 4.4: Preparation of the SnO_2 paste in a planetary ball mill. ZrO_2 balls in the ZrO_2 mug ensure an effective milling of the SnO_2 + propylene glycol slurry. [Kap01b]

obtained is then transferred onto the ceramic substrate (Cermatec©) with the screen printing method illustrated in Figure 4.5. Hereby a rubber squeegee presses the paste through the undeveloped part of the screen. By this method SnO_2 layers with a thickness of around $50\text{ }\mu\text{m}$ are obtained. After the screen printing process the sensor stays at room temperature for about one hour to let the paste settle. Next, it is kept for 24 h in a drying oven (Heraeus) set at $80\text{ }^\circ\text{C}$ followed by a final annealing (firing) in a moving belt oven (Centrotherm Centronic DO 1600-60-D5)

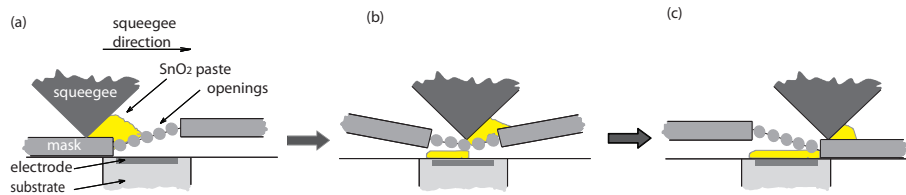


Figure 4.5: Fabrication of the sensors via screen printing. A rubber squeegee presses the viscous paste through the undeveloped part of the screen on the alumina substrate. By adjusting the speed, pressure and distance a defined and reproducible layer thickness is achievable. [Kap01b]

with 4 different temperature zones (300 - 400 - 600 - 400 °C). During this step, the organic binder is fully removed and the layer becomes mechanically stable and firmly attached to the substrate. A schematic layout is given in Figure 4.6 and a picture of the sensor, including zooming in the sensitive layer and the individual electrodes, is illustrated in Figure 4.7. It should be pointed out here that in the case of gold electrodes the heater structure is a palladium / silver alloy instead of platinum, which is used for the substrate provided with platinum electrodes. The SEM scanning on the electrode revealed a comparable structure of the gold and platinum electrodes. In general SnO₂ thick film gas sensors on ceramic substrates

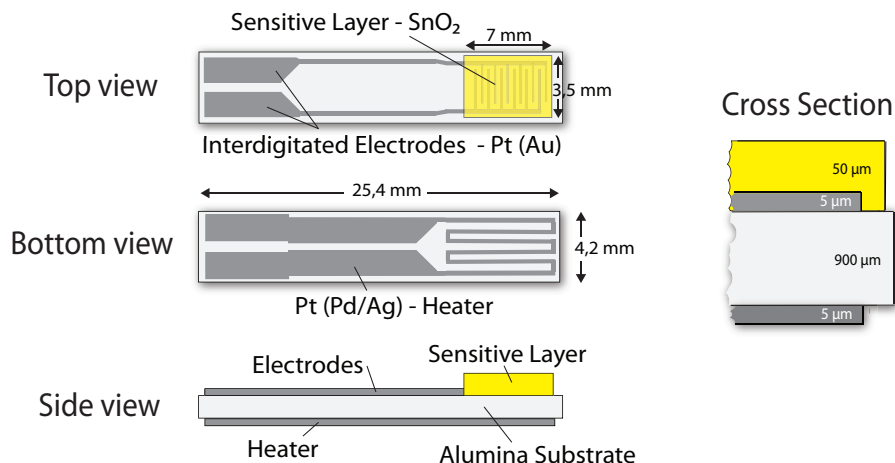


Figure 4.6: "IPC" sensor geometry from top view, bottom view, side view and cross section. [Bar03]

are operated at temperatures between 200 and 400 °C. Our sensors are equipped with a platinum heater structure. By applying a certain voltage the current will pass through the heater and increase the temperature. Due to the reasonable heat conductance of Al₂O₃, the sensing layer on the opposite site of the heat circuit will also be heated. Since the printed sensors are not necessarily similar - each sensor is individually printed, and by this a small difference in layer thickness may occur -

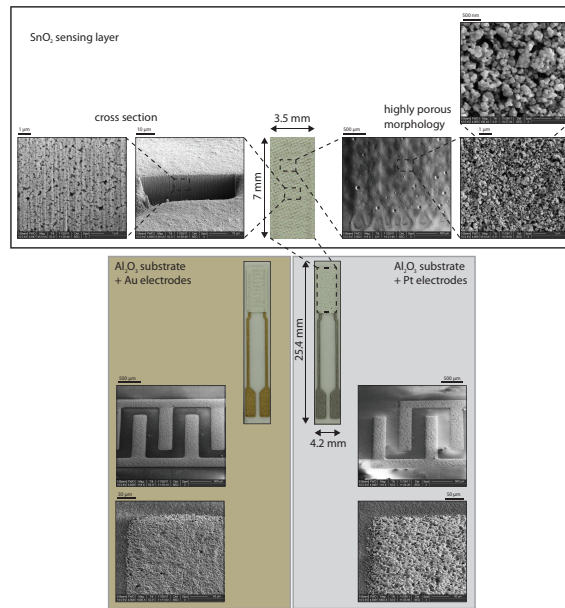


Figure 4.7: The "IPC" sensor device. SEM pictures (top - right) are showing a highly porous morphology of the SnO_2 sensing layer which extends through the entire layer (FIB cut; top - left). The platinum electrode as well as the gold electrode is showing a comparable porous morphology (bottom)

one have to apply a temperature calibration for each single sensor. While increasing the heating voltage, the temperature of the sensing layer is measured by an infrared thermometer Figure 4.8. Thus, a resistance vs. temperature calibration can be obtained by recording the current and the temperature at a given voltage.

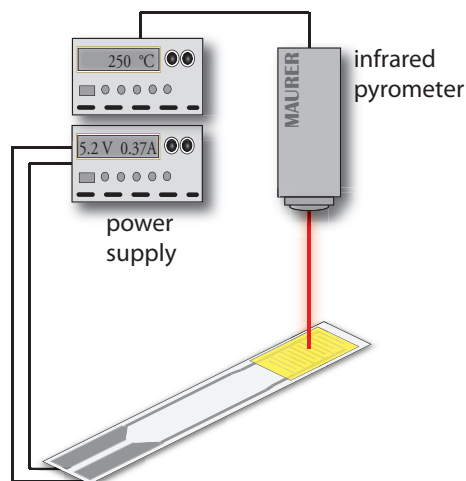


Figure 4.8: Temperature calibration of the sensor device using an infrared pyrometer.

4.1.3 SnO₂ + Au / SnO₂ + Pt powder mixtures

As will be explained in a later section, spectroscopic measurements on powders were considered in order to investigate the chemistry or rather the surface species on SnO₂, respectively next to the three phase boundary, upon gas exposure. The SnO₂ sensing layer, deposited via screen printing onto the alumina substrate consists of a number of interconnecting SnO₂ grains contacting the electrode structure. As described in the previous section, there is a spacing of about 300 μm in between two electrode fingers, providing a rather large space occupied by tin oxide grains which are not in contact with the electrode material. A considered influence of the noble metal / metal oxide interface wouldn't affect this part of the sensor, as discussed in Section 5.4 infra. In powder mixtures micro sized gold and platinum particles, which are obtained from FERRO© and ought to represent the metallic electrode, were mixed with the tin oxide powder and therefore constitute a model system which mimics the metal oxide / noble metal interface but with a more spatially distributed contact area. The physical data of the noble metal particles are given in Table 4.1: Based on this data and using the previous results about the basic properties of the

Table 4.1: Surface area and particle size distribution for noble metal powders obtained from Ferro©

	Gold powder	Platinum powder
Surface area	0.1 - 0.3 m ² /g	0.2 - 0.6 m ² /g
Particle size distribution	10 % 0.5 - 2.0 μm	10 % 1.0 - 2.0 μm
	50 % 1.0 - 3.0 μm	50 % 2.0 - 4.0 μm
	90 % 2.5 - 5.0 μm	90 % 3.0 - 6.0 μm

synthesized SnO₂ powder, an approximate proportion of weight was calculated in order to ensure a comparable contact area between the tin oxide and the noble metals as it can be found in the real sensor case. For the mixture preparation 5 wt. % of the respective noble metal powder was mixed with the appropriate amount of SnO₂. A final heat-treatment, equal to the annealing step in sensor fabrication, was carried out in order to have a high comparability.

4.2 Measurement techniques

Although considerable efforts have been made in order to understand the fundamental characteristics of metal oxides and their reaction with certain gases, most of these basic studies were carried out in conditions of that kind which could not

reasonably be foreseen in an application-like environment. A chemical MOX-type gas sensor is typically driven at elevated temperatures between 200 and 400 °C and is surrounded by normal atmosphere pressure - per definition. Usually, most of

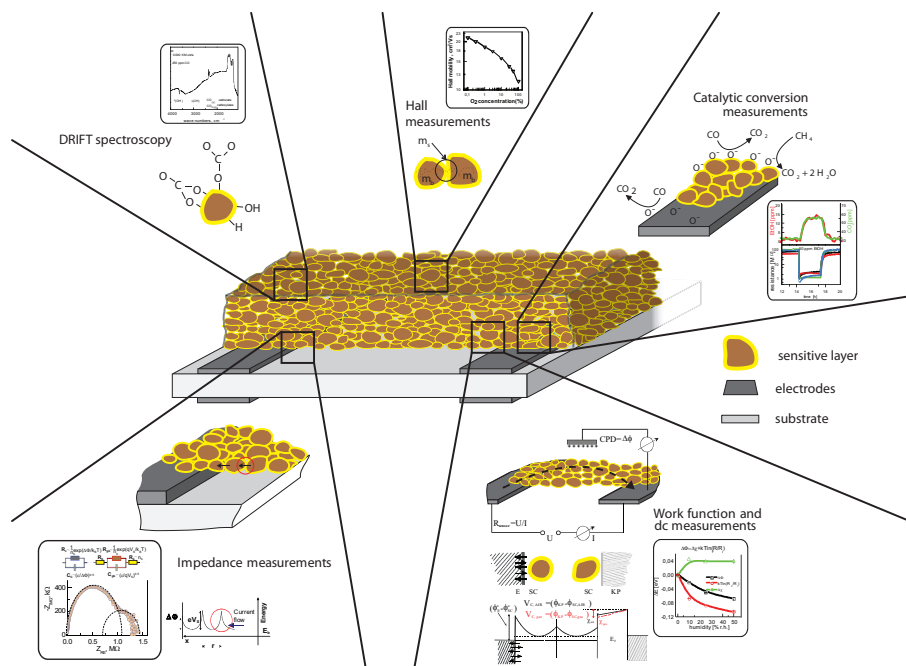


Figure 4.9: Overview of the different "operando" measurement approaches used at the Institute of Physical Chemistry at the University of Tuebingen. For more details see [Bar07]

the applied spectroscopic techniques are conducted in ultra-high vacuum at much lower temperatures. To gain access to detailed knowledge about the fundamental principles of the gas sensing process, and further, be able to improve the sensor performance, it is necessary to characterize the sensors when operated close to their working conditions. Since this aspiration is also a huge challenge in the field of catalysis, the concept of "in situ" measurements is relatively common, describing a characterization in working conditions. An "operando" measurement, which describes an in-situ characterization with the associated performance readout, is an ideal supplement to it. This concept can be easily transferred to sensor research and is therefore the basis for efficient and comprehensive studies since a long time. The combination of electrical measurements and spectroscopic methods has proven very beneficial and are reflected in Figure 4.9. The following sections briefly explain the main methods which have been used in this work. A comprehensive review of operando measurement for the characterization of metal oxide sensors can be found in [Bar07; Gur07].

4.2.1 Gas mixing system

The gas mixing system (GMS) provides the desired gas atmosphere in order to test the gas sensors. The typical setup of a gas mixing system, which consists of a couple of computer controlled mass flow controllers (MFCs) and computer controlled magnetic valves, is shown in Figure 4.10. By means of such a system, several test gases can be mixed with either dry synthetic air (Westfalen Gas) or nitrogen (Westfalen Gas), which are usually used as carrier gases. The relative humidity (r.H.) can be adjusted by flowing a certain share of the carrier gas through water-filled vaporizers. The gas mixing system is operated by customized software (Agilent VEE), which allows the adjustment of the gas flow through the individual channels. The tubing of the gas channels consists mainly of polished stainless steel pipes or vacuum tight teflon tubes.



Figure 4.10: Gas mixing system used in the laboratory at the University of Tuebingen

4.2.2 Electrical measurements

The typical measurement technique for semiconducting metal oxide material (MOX) sensors is the one of their conductance or resistance. A change in the surrounding atmosphere causes a change in the resistance / conductance of the sensors. There are different ways to operate or measure a metal oxide sensor, spanning from constant operation temperature and permanent polarization to modulated operation temperature and periodic dc tests. However, the resistance of the sensor is not only influenced by surface reactions and the related changes in the grain-grain potential barriers, as particularized previously. In this regard, it is important to understand how the sensors are measured and how the measurements respectively the results, are influenced by the measurement conditions and parameters.

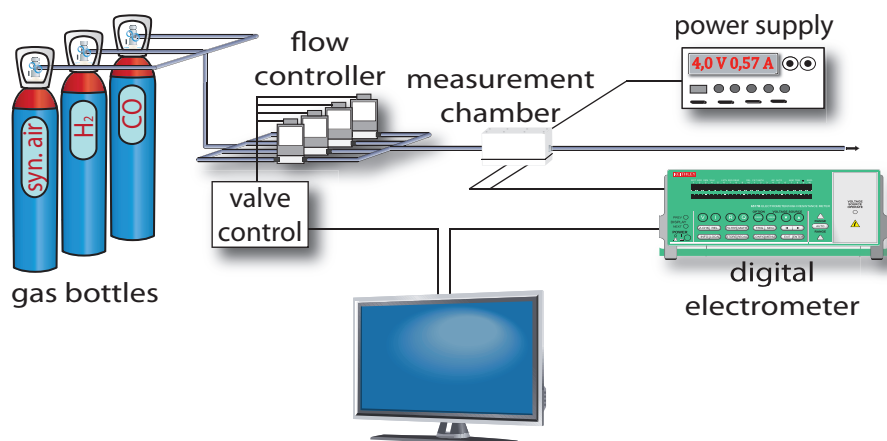


Figure 4.11: Experimental setup for electrical measurements. Gas mixtures are controlled via a computer controlled gas mixing system. Resistance readout of the heated sensors is performed via a digital multimeter.

For measuring the resistance, the sensors are placed in home-made Teflon chambers, typically four sensors in series as illustrated in Figure 4.11. While the heating is ensured by applying a certain voltage - according to the previous calibration data - the readout of the resistance is realized with a digital multimeter (Keithley DMM 199), operated in constant current mode. The resistance readout is performed in a fixed resistance range, for the simple reason that measuring in auto-range mode can be distorted by varistor or polarization effects.

4.2.3 DRIFTS

Infrared (IR) spectroscopy exploits the fact that molecules absorb specific frequencies that are characteristic of their structure [Atk06]. Infrared light will not cause electronic transitions, but rather interact with a molecule stimulating rotational and vibrational changes. Specific frequencies of the incident infrared light matches with the frequency of an atomic bond or a specific group and thus can be absorbed - therefore, these absorptions are called resonant frequencies. The energies are determined by the shape of the molecular potential energy surfaces, the masses of the atoms, and the associated vibronic coupling. Whether a vibrational mode is IR active depends on the selection rules. In a simplified manner it must be associated with a change in the dipole.

Diffuse Reflectance Infrared Fourier Transform spectroscopy (DRIFTS) is a special technique of the infrared spectroscopy. When the infrared light encounters the sample - powder or highly porous solids - it can be absorbed, directly reflected (externally), internally multi-reflected or diffuse reflected. However, the share of

specular reflection, consisting of the directly and multi-reflected light, is undesirable. The diffuse reflection, on the other hand, achieves much higher information content due to its penetration through the whole sample. It contains information about the absorption properties of almost the whole sample surface and is therefore the component of interest in DRIFTS. It is impossible to measure the ideal case of sole diffuse reflectance, as it was described by Lambert. Thus the intensity of radiation reflected (re-emitted) from a completely mat surface is of the same intensity all over, independent on angle of observation ϑ and incident α (Figure 4.12). The flux of the remitted radiation I_r in area df and solid angle $d\omega$ is a function of the cosine of the angle of incident and the angle of observation (Lambert's cosine law for diffuse reflection):

$$\frac{dI_r/df}{d\omega} = \frac{CS_0}{\pi} \cos\alpha \cos\vartheta = B \cos\vartheta \quad (4.1)$$

Since this seems only to be valid for a black body radiator and an ideal diffuse reflector

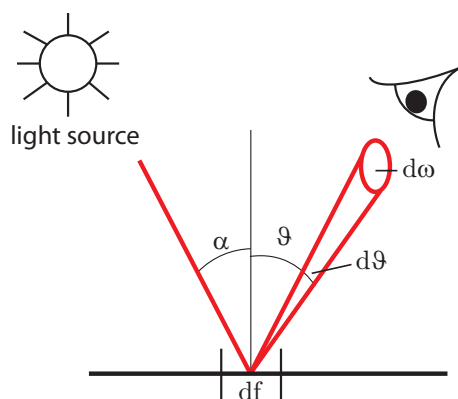


Figure 4.12: Visualization of the variables used in Lambert's cosine law

has never been found, there is a need to find a different way to separate the coherent diffuse and specular reflectance. By using an operando-chamber (phenomenological and spectroscopic readout in parallel) in a commercial available DRIFTS optics unit (Praying Mantis - Harrick Scientific Products, Inc.), the percentage of normal specular reflectance is reduced to a minimum due to a specific mirror alignment Figure 4.13. Secondly, a SnO_2 particle size of around 100 nm, which is several orders of magnitude smaller than the used wavelength in the MIR range (used in the recent experiments ($1.6667 \cdot 10^{-2}$ mm - $2.5 \cdot 10^{-3}$ mm)), ensures that specular reflectance is non-dominant.

In order to make quantitative statements about the diffuse reflectance the approach

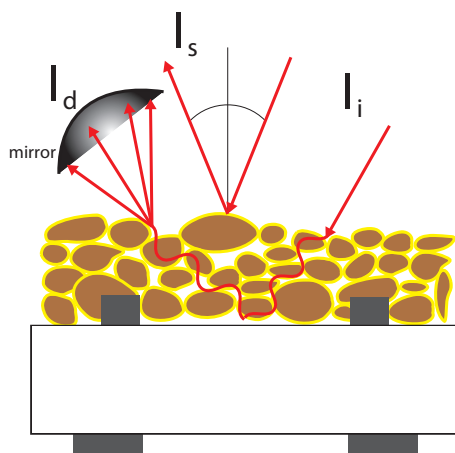


Figure 4.13: Different shares of the incident beam (I_i). Specular reflectance (I_s) occurs on grains with a larger diameter than the wavelength. A special mirror alignment reduces the normal specular reflectance to a minimum and is mainly capturing the diffuse reflection (I_d).

of Kubelka and Munk can be applied [Kub31]. The Kubelka-Munk theory is a phenomenological approach to describe the radiation transport in a medium with scattering or absorbing properties. Put in highly simplified terms, the light transmission is only to be considered perpendicular into the medium or reverse again, thus only in two directions. In another crucial assumption it is assumed that the scattering is isotropic and the light distribution has a purely diffuse character within the layer due to multiple scattering processes. Further details can be taken from different scientific reviews [Voe01]. An obstacle in measuring semiconducting samples, such as metal oxide gas sensors, is the effect of free charge carrier absorption. The solution of the acceleration of free charge carriers in a semiconductor by the oscillating electrical field, within the framework of classical electrodynamics, derives [Hah03] the following dependence between the absorbance coefficient (α) and the free charge carrier concentration (n_e):

$$\alpha = \frac{\sigma_0}{n' C \varepsilon_0 (1 + \omega^2 \tau^2)} \quad (4.2)$$

with ε_0 is permittivity of free space, ω - frequency, τ - relaxation time (factor sensitive to the temperature and purity in any substance), c - light velocity in free space, n' - real part of the complex index of refraction. Limiting the consideration to IR

wavelength range, where $\omega\tau \gg 1$, the latter equation can be reduced to

$$\alpha = \frac{\sigma_0}{n' C \epsilon_0 \omega^2 \tau^2} = \frac{n' \lambda_0^2 e^3}{4\pi \epsilon_0 m^{*2} c^3 n_e \mu} \quad (4.3)$$

where: μ is the mobility, m^* is the effective mass of the free carriers, λ_0 is the wavelength in free space, n_e - concentration of the electrons per unit volume. According to Equation (4.3) the absorbance of a material at a given wavelength is directly related to its electrical conductivity. Within this work, the determined absorbance spectra are basically calculated out of two spectrums recorded in different gaseous atmosphere. Most likely, the free charge carrier concentration is changed when changing the atmosphere, e.g. upon exposure to an oxidizing or reducing gas. Fundamental assertions on the absorbance in specific regions of the spectra should therefore always be examined critically, since an increase or decrease in absorption due to a change in the free charge carrier concentration may mask the absorption bands of the specific surface species. The DRIFTS measurements in this work

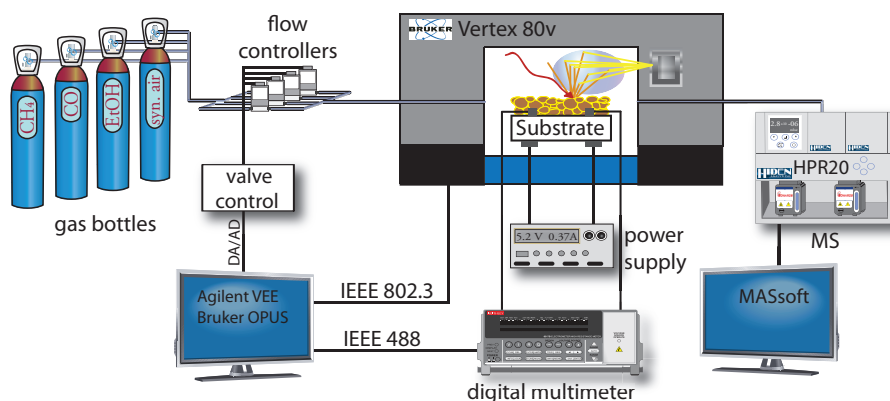


Figure 4.14: Experimental setup for simultaneous DRIFTS and resistance measurements. Gas mixtures are controlled via a computer controlled gas mixing system. Resistance readout of the heated sensors is performed via a digital multimeter. Spectroscopic information is gathered via a FT-IR spectrometer equipped with a DRIFTS unit.

have been performed on a FT-IR spectrometer (Bruker Vertex 80V). The sample is mounted in a homemade chamber where different mixtures of gases can be adjusted by means of a gas mixing system as described in a previous section. While the sample compartment is kept at normal pressure and therefore in operando, the spectrometer itself is evacuated in order to diminish disturbing compounds like gaseous water or carbon dioxide. A special DRIFTS chamber (Harrick Praying Mantis) ensures that primarily diffuse reflected light reaches the MCT detector (mercury cadmium

telluride detector - which has to be cooled with liquid nitrogen). In case of real sensor samples, the resistance is measured according to the previously mentioned principle. The exhaust gas is analyzed on the basis of a mass spectrometer (HIDEN, HPR 20, quadrupole mass analyzer)

4.2.4 Catalytic conversion

The fundamental mechanism for the detection of certain gases, e.g. carbon monoxide and hydrogen, is the reaction with pre-adsorbed oxygen and further the conversion to its oxidized form - carbon dioxide and water respectively. As already indicated, such processes not only occur on the surface of the sensing layer. It is beyond of doubt that especially the noble metal parts (electrode & heater) as well as the alumina substrate have a great share in the consumption of the specific gases. Even more interesting than measuring sensors only, where a statement is obtained on the all-over consumption of the whole sensor - including electrodes, heaters and substrate, are measurement on powders and powder mixtures, where the individual sensor parts can be divided - even if only on a model basis. In order to measure the conversion,

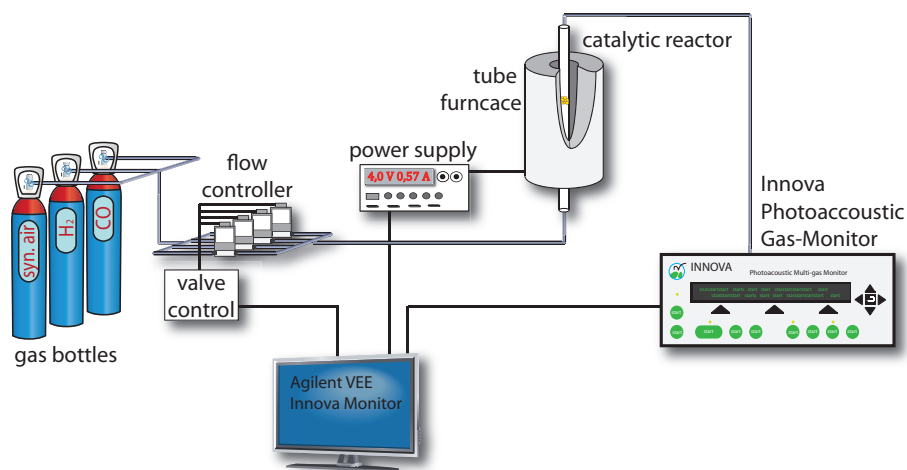


Figure 4.15: Experimental setup for catalytic conversion measurements. Gas mixtures are controlled via a computer controlled gas mixing system. The gas mixtures pass through a catalytic reactor which is heated via a tube furnace. The exhaust components are analyzed with a photo acoustic gas monitor.

the powder samples were placed inside a catalytic pipe with fittings ensuring a sealed connection to set the desired atmosphere. The samples were heated passively using a tube furnace enclosing the whole sample compartment (catalytic reactor). The atmosphere was adjusted by means of a gas mixing system as illustrated in Section 4.2.1. The exhaust gas, more precisely the concentration of CO and CO₂ was

measured by a photo acoustic gas analyzer (INNOVA 1312 LumaSense Technologies). The whole setup is depicted schematically in Figure 4.15. In experiments where the level of oxygen has to be monitored, the oxygen concentration was measured based on an electrochemical oxygen analyzer (ZIROX SGM400), which was connected downstream.

CHAPTER 5

Results & Discussion

In the context of this work a representative selection of samples was investigated using a variety of methods described in the previous chapter. As stated before, SnO₂ is one of the most investigated material when it comes to chemical metal oxide gas sensors and a large offer of products and applications in the field of gas sensing based on this material is available on the market. The current approach for developing sensor technologies is still mostly empirical. It primarily consists of optimizing material & device parameters to fulfill the application requirements, which does in fact result in a well-engineered instrument, but the general understanding of the sensing structure is far from complete. The attempts of basic research to represent the sensing mechanism on ideal structures by models are so far not target-oriented and functional when it comes to applications.

Consequently, the right approach towards the understanding of the sensing characteristics and material parameters is the combination of phenomenological and spectroscopic investigation methods - simultaneously, if possible, as seen in a number of surveys [Bar07; Koz06; SB98]. With test platforms whose materials and designs are comparable to commercial sensors and experimental conditions as close as possible to the real operational ones, it becomes feasible to develop universally applicable models by linking up different parameters gathered by various characterization techniques. Thus, a number of different SnO₂ samples, sensors and powders, which differ mainly by being in contact with either metallic gold or metallic platinum - here as electrode material or micro-particle additives, have been investigated by the means of DC conductance, consumption and DRIFTS measurements.

5.1 Sample overview

For the measurements described below, a variety of samples have been used. The following section provides an overview about the different samples and the basic properties. In all cases, SnO_2 , which has been synthesized in house, is the sensitive raw material. The wet chemistry based synthesis of the tin oxide was described in detail in Section 4.1.1. The subsequent calcination process defines the final crystal structure, defect concentration and grain size. Based upon the raw powder, further preparation processes were necessary depending on the individual experiments which have been scheduled. Figure 5.1 provides an overview of the different types of samples.

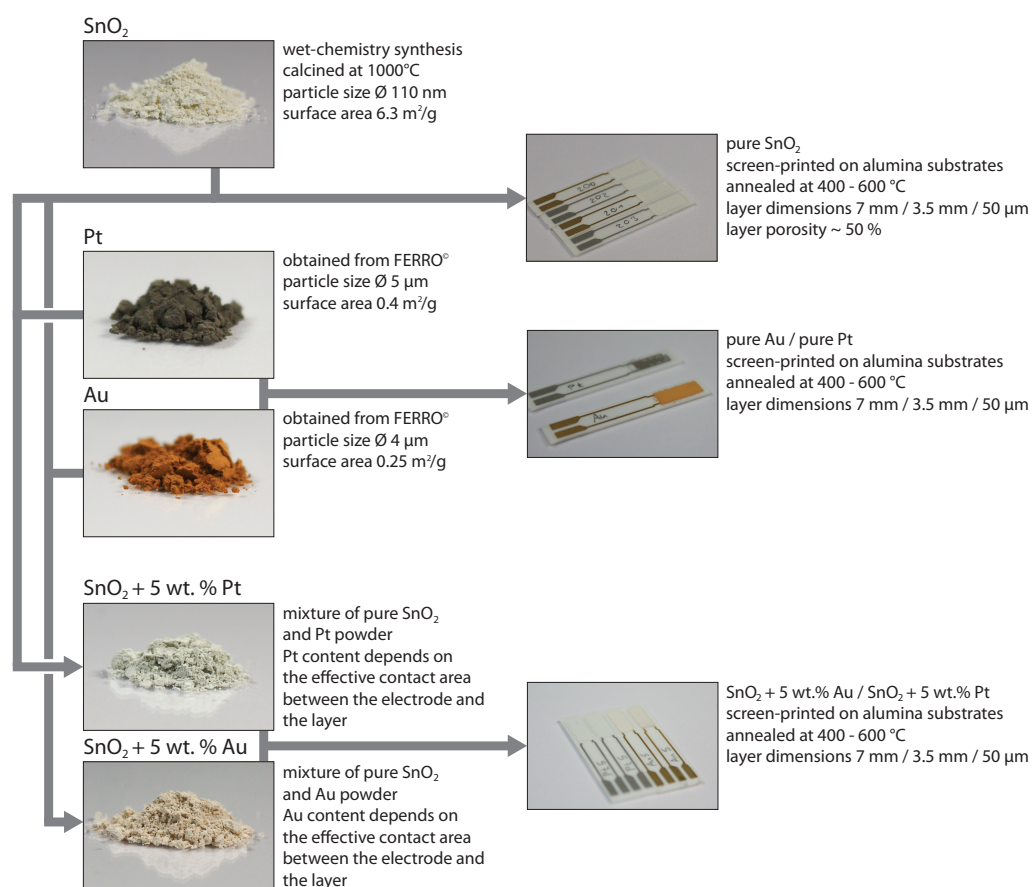


Figure 5.1: Overview of investigated samples

5.2 Electrical measurements I

As it was explained in the previous chapters, a sensor is a device which responds to a stimulus, whereas the stimulus is a chemical input - a gaseous species - and the resulting output is an electrical signal - a change in conductance. In order to understand a sensor, it is essential to get a comprehensive characterization of its performance. Accordingly, an electrical characterization is the starting point for further experiments. Commonly, such phenomenological investigations on real working sensors are performed in operando conditions, which implies that the sensors are heated up to a certain temperature, which is necessary to make them work, and exposed to different concentrations of target gases in a background of synthetic air at standard atmospheric pressure (1013 mbar). Carbon monoxide and hydrogen are commonly selected for a first characterization. Moreover, a variation in humidity should not miss since it is well known that metal oxide based gas sensor performance is strongly influenced by water vapour.

5.2.1 Results

A set of undoped SnO₂ sensors with different electrode materials were exposed to various concentrations of carbon monoxide and hydrogen in synthetic air at 0 % and 50 % relative humidity. The through-flow (250 ml/min) and the concentration of the gas were adjusted by a gas mixing system, as explained in the previous chapter. The sensors were mounted in a Teflon chamber and heated by a power supply; resistance was monitored with a scanner multimeter (Keithley DMM 199). After a variation of the background atmosphere or after a change in the working temperature, respectively in the very beginning of each experiment, a minimum of 2-3 hours were allowed in order to ensure a thermodynamic equilibrium of the surface conditions, before inducing a certain concentration of test gas.

In the first experiments the sensors were exposed to pulses of 30, 50, 100 and 200 ppm hydrogen followed by 25, 75, 125 and 250 ppm of carbon monoxide in dry synthetic air with a pulse duration of one hour and one hour of recovery time in between. Subsequently, this exposure sequence was repeated in an atmosphere with 50 % relative humidity. The sensors were operated at a working temperature of 200, 250, 300 and 350 °C. The change in resistance over time, dependent on the actual composition of the gas atmosphere, is shown in Figure 5.2.

Assessing the response and recovery time there are no remarkable differences between gold electrodes and platinum electrodes. The response and recovery times

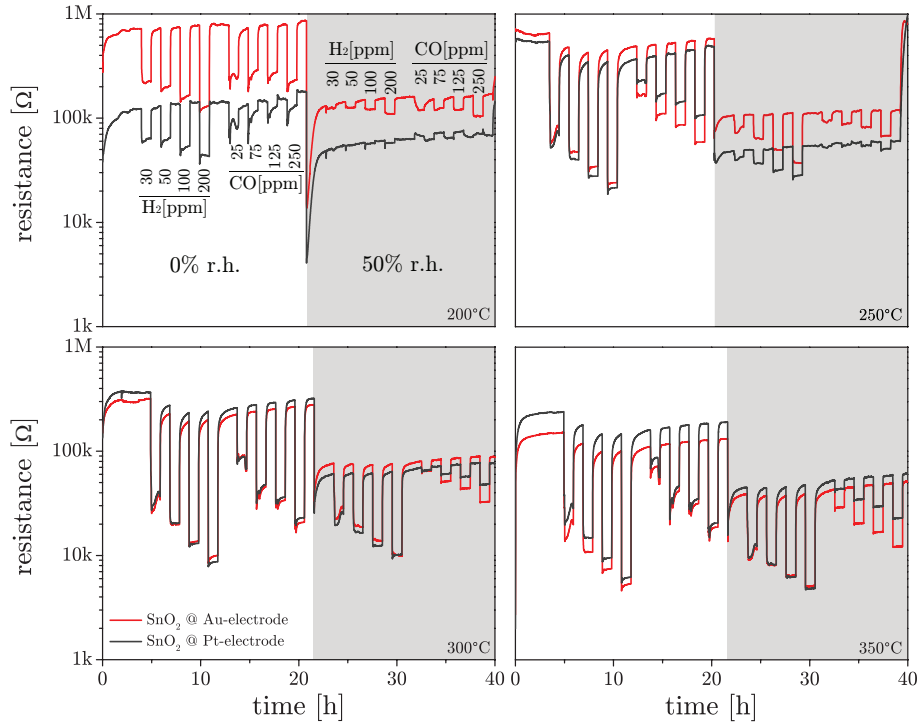


Figure 5.2: Time-dependent measurement of the resistance for two different sensor types (SnO_2 on substrates with Au-Electrodes & SnO_2 on substrates with Pt-electrodes). Measurements performed in dry air and 50 % r.H. for pulsed, subsequent increasing concentrations of hydrogen (30, 50, 100, 200 ppm) and carbon monoxide (25, 75, 150, 250 ppm). The sensors were heated up to 200 °C (top left), 250 °C (top right), 300 °C (bottom left) and 350 °C (bottom right)

are quite fast for all measured conditions. An exception is the sensor with platinum electrodes at 200 °C working temperature in 50 % relative humidity, where the responses are too low to make a clear assessment. In the specific case of carbon monoxide exposure it is even worse so that the resistance is increasing under carbon monoxide exposure which is not the expected behavior for a n-type semiconducting material. This might be explained by very small levels of impurities (H_2O) in different gas bottles or a slightly different temperature of the carrier gas and the test gas, which causes a higher effect on the sensor than the test gas itself.

The sensor signal, id est the ratio between the baseline resistance and the resistance during target gas exposure, provides information about the behavior of the sensor. In Figure 5.3 and Figure 5.4 the logarithm of the sensor signal is plotted against the logarithm of the concentrations for each electrode material and each measured atmospheric condition. It is important to note that the figures given are average values complete with error bars reflecting multiple measurements taken on 8 - 12

samples.

The results for hydrogen concentrations between 30 and 200 ppm are as follows: In 0 % relative humidity the sensor signals are higher for all conditions measured in these experiments when compared to recorded at 50 % relative humidity. Furthermore,

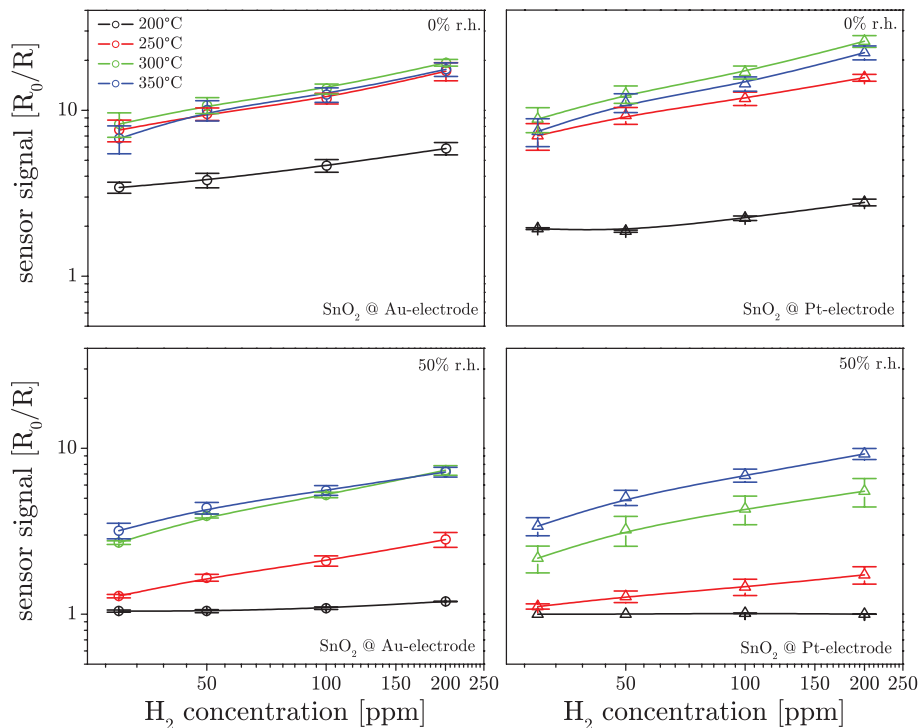


Figure 5.3: Sensor signal as a function of the hydrogen concentration for the different sensor types in dry air and 50 % r.H. at the four different temperatures

no saturation effect is observable within the measured range of concentrations, except for the sensors with platinum electrodes at the lowest measured temperature at 50 % relative humidity where almost no signal is observable. A closer look into the temperature dependence in the case of 0 % relative humidity suggests that the main difference appears between 200°C and 250°C; at temperatures above 250°C only the sensors with platinum electrodes show temperature dependent effects. At 50 % relative humidity this trend appears to be shifted to higher temperatures. For the gold electrode sensors, a difference is still visible between 250°C and 300°C and differences between the specific temperatures are more pronounced for the platinum electrode types.

For the sensor signals upon exposure to different levels of carbon monoxide, as can be seen in Figure 5.4, the situation can be described as follows. Over the entire range of CO concentrations no saturation effect can be observed, except for the weak signals

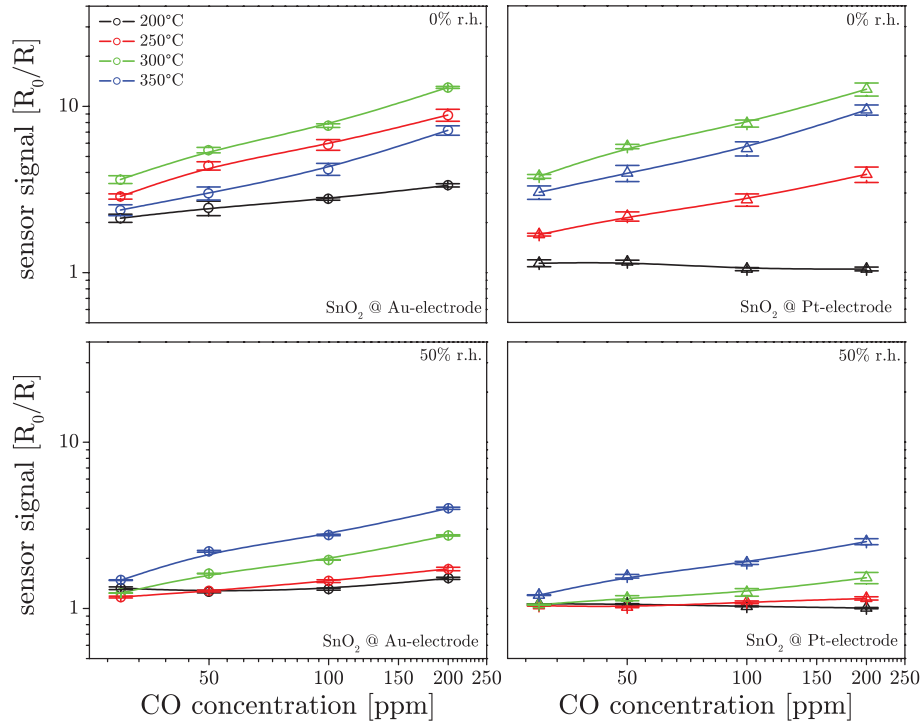


Figure 5.4: Sensor signal as a function of the carbon monoxide concentration for the different sensor types in dry air and 50 % r.H. at the four different temperatures

of the platinum electrode sensor at 50 % relative humidity, as previously described. For carbon monoxide, a decrease in the sensor signals is detectable when increasing the humidity, which holds true for both types of electrodes. Differences within a certain condition and electrode type are visible from the minimum operating temperature up to the maximum operating temperature. The temperature dependency is more significant already in dry air compared to the results obtained for hydrogen.

In the following, the results are plotted in a different way and made more detailed in order to include the temperature effect in a clearer manner: The sensor signal for the highest measured concentration of each test gas (200 ppm H₂ & 250 ppm CO) is plotted versus the working temperature of the sensor (Figure 5.5). Regarding the main focus of this work, alongside the effect of the above mentioned temperature dependencies within a sample and condition, a clear trend is observable regarding the different electrode materials. In all cases the sensors equipped with gold electrodes show higher signals than the sensors with platinum electrodes at 200 °C. This tendency continues until inversion is reached or the difference in sensor signal is no longer significant. Also here observations can be made, whereby humidity is enhancing the effect to a higher temperature, e.g. for carbon monoxide in a wet atmosphere the

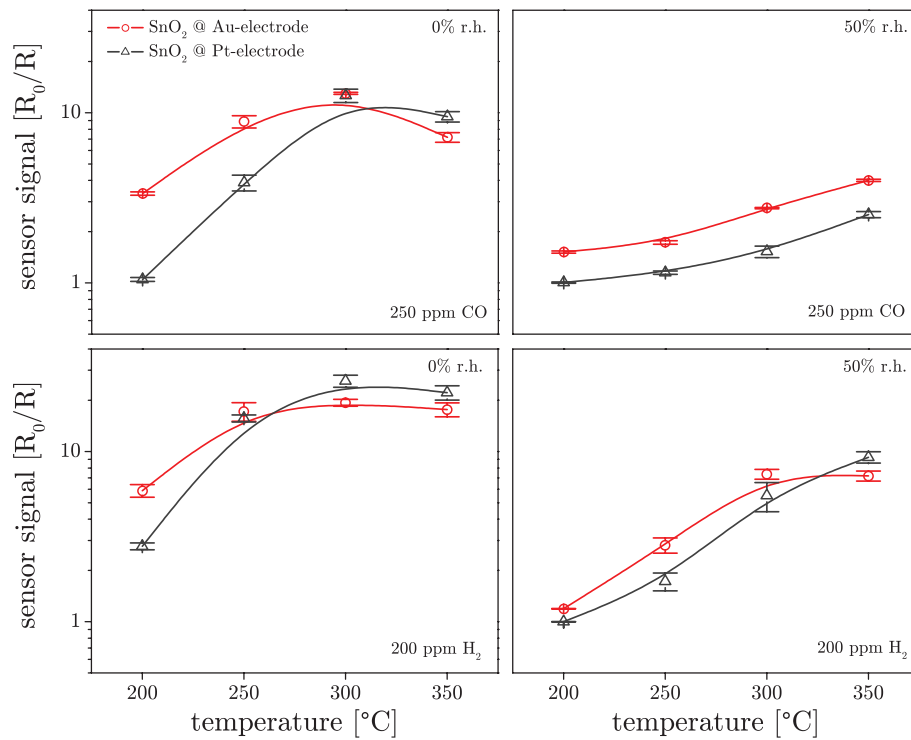


Figure 5.5: Sensor signal as a function of the working temperature of the different sensor types at 250 ppm carbon monoxide in dry air (top left), 250 ppm carbon monoxide in 50 % r.H. (top right), 200 ppm hydrogen in dry air (bottom left) and 200 ppm hydrogen in 50 % r.H. (bottom right).

sensors with gold electrodes are dominant over the entire temperature range, while in dry air the inversion is clearly around 300 °C. The data for low concentration measurements, which are not shown here, show the same trend.

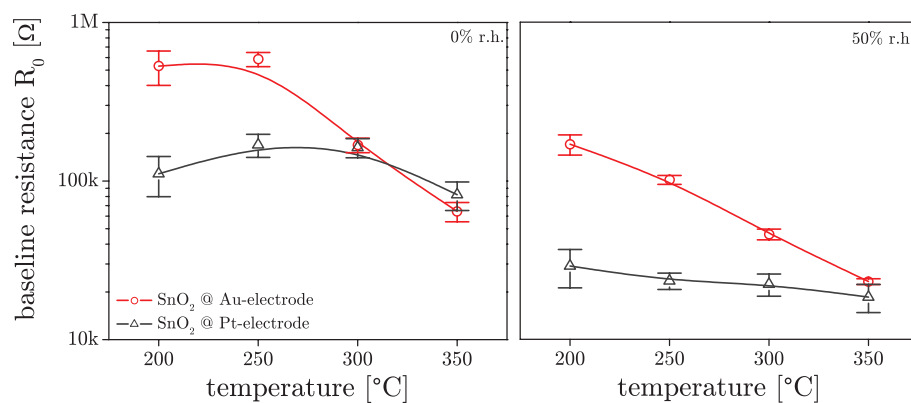


Figure 5.6: Baseline resistance (R_0) - measured right before gas exposure - as a function of the working temperature of the different sensor types in dry air and at 50 % r.H.

In a further evaluation step, the baseline resistance in dry and humid air is plotted

versus the temperature for both types of electrode materials (Figure 5.6). The data reveals a slightly surprising picture, in which a temperature dependency between both materials is also observable in the raw resistance values in synthetic air without any influence of the used test gases. At the lowest working temperature, the resistance of the sensor with gold electrodes is increased by around one order of magnitude, while at elevated temperatures the values of the resistance are converging until they are indistinguishable around 300 °C in the case of dry air and at 350 °C in the case of 50 % relative humidity. It is apparent, therefore, that differences caused by the electrode material not only influences the reaction with the specific target gases CO and H₂. In this context it is worth to note, that the synthesis and preparation processes for both types of sensors are perfectly equivalent.

5.2.2 Discussion & Summary

The main findings of the electrical measurements can be summarized as follows:

- The highest sensor signals in general are obtained at temperatures between 300 and 350 °C
- Undoped SnO₂ Sensors with gold electrodes show higher sensor signals at lower working temperatures
- Response and recovery times are very comparable for both types of electrode materials
- The baseline resistance in dry and humid conditions depends on the electrode material, with respect to the temperature
- The prevalent effect of the sensors with gold electrodes at lower temperatures is still visible at higher temperatures at 50 % relative humidity.

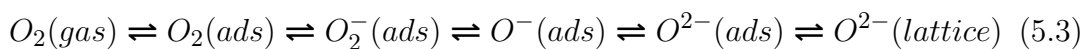
With the background knowledge on the electrical influence of the electrode contact outlined in Section 3.1 and the resulting conclusion of mainly chemical influence, it is necessary to understand the processes which might appear at the surface of the metal, the metal oxide and the boundary between them both. First and foremost the reaction of a specific gas with the metal oxide surface affects the potential barrier at the grain-grain boundary, respectively the resistance. The reaction of carbon monoxide and hydrogen in synthetic air has been thoroughly investigated and can be found in many publications [Bar99; Wei01]. It is proposed that the reaction of reducing agents like carbon monoxide and hydrogen proceeds by an interaction with the pre-adsorbed oxygen on the tin oxide surface, which results in the release of

electrons and can be described by a quasi-chemical equation using the Kroger-Vink notation [Kro56] (Equation (5.1) & Equation (5.2)).



In both cases the availability of pre-adsorbed oxygen is required for these reactions - even if other surveys have shown the possibility of CO and H₂ detection in the absence of oxygen via different reaction paths [Bar11; H11; Ran09].

Many authors have extensively studied the adsorption and reaction of oxygen on SnO₂ (see [Bat05; Gur06] and references therein). The adsorption of oxygen itself is described as a temperature dependent process. By using EPR measurements Chang et al. were able to identify a transition temperature at around 150°C, below which oxygen adsorbs mainly in its molecular form as O₂⁻. At higher temperatures, atomic oxygen in the form of O⁻ or O²⁻ can be found. These differences were confirmed on the basis of TPD measurements: Yamazoe et al. found a low temperature peak at around 100 °C which could be only observed for oxygen adsorption below 150 °C and can be attributed to the molecular oxygen species [Yam79]. At higher adsorption temperatures (~400 °C) a second peak at around 500°C was found, which implies ionisorbed atomic oxygen species. A roundup of the surveys describing the possible adsorbed oxygen species is illustrated in Figure 5.7. The adsorption procedure is a quite complicated process. In general there are several ways or reaction paths a molecule can follow to reach its target - the chemisorbed state. For each reaction path there is a limiting factor in which the system must procure the activation energy, e.g. the dissociation of oxygen as a conceivable option. Unfortunately in most of the cases the surface of solids is far too complex to identify this activated state. There are some attempts to specify the activation or dissociation of oxygen on TiO₂ and SnO₂ [110] surfaces (see [Gur06] and references therein). However, there are still a number of ambiguities, especially when it comes to reaction paths with lowered activation energies of the activated state, where the sophisticated approaches to describe different pathways are considering interaction of additives or surface heterogeneity [Mor77a], just to name a few. At the risk of oversimplification, the oxygen interaction with SnO₂ can be summarized as follows:



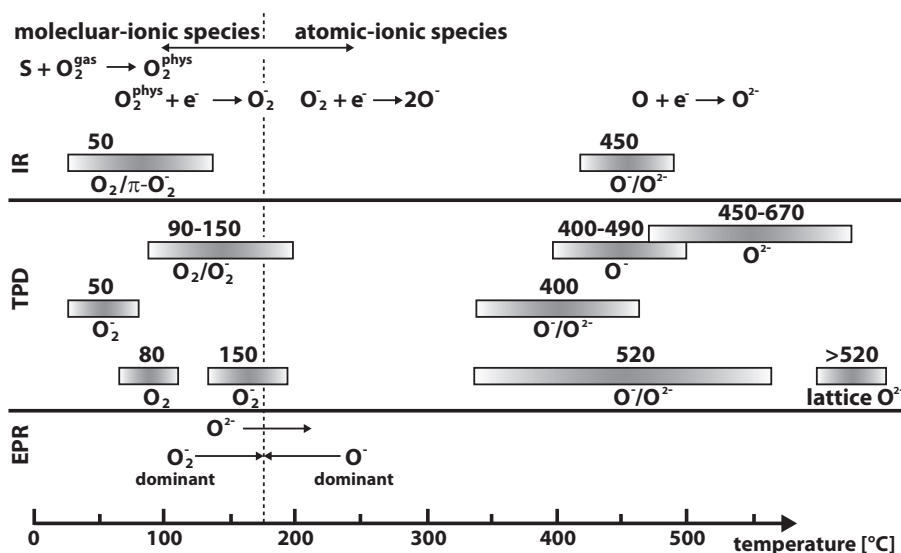


Figure 5.7: Literature review of oxygen species at the SnO_2 surface dependent on the temperature detected by the means of IR (Infrared) - spectroscopy, TPD (Temperature Programmed Desorption) and EPR (Electron Paramagnetic Resonance) [Bar99]. For details see [Cha80; Gil76; Jol86; Len95; Vol81; Yam79]

The complexity arises when it finally comes to ionosorption where the electron transfer plays a decisive role. It is important to note that the ionosorption and the resulting transfer of free charge carriers is the essential step for having a change in resistance upon exposure to oxygen. A comprehensive review about the different aspects of oxygen ionosorption and the influence on space charge effects is given in [Mad89; Mor77b]. It can be argued that the limiting factor for ionosorbed oxygen on a metal oxide surface is not the potential adsorption sites on the surface, but rather the availability of electrons.

A larger amount of ionosorbed oxygen on the surface would explain, on the one hand a higher baseline resistance under synthetic air; on the other hand more potential reaction partners for gases like carbon monoxide or hydrogen would mean higher sensor signals. Both these effects can be seen in the first experiments for SnO_2 sensors with gold electrodes at the lowest working temperature (200 °C). The question, therefore, is whether the gold electrode respectively gold in general is activating the adsorption of oxygen.

When and how metallic particles or additives interact in a metal-oxide setting has been discussed in great detail, but the investigated systems were far too unique for a general understanding. Especially in the field of catalysis, the interaction of small gold particles in the surrounding of metal oxide supports attracted considerable

attention by many surveys [Gru99; Lop04]. Unsupported gold particles or supported on metal oxides seem to be very active in various oxidation reactions like the oxidation of CO to CO₂, water-gas shift reaction ($CO + H_2O \rightleftharpoons 2CO_2 + H_2$) and oxidation of hydrocarbons. The nature of the high catalytic activity of gold catalysts has been strongly discussed and even if models have been presented there is still a question which remains unanswered: how is the oxygen activated? Miller et al. were able to demonstrate the oxidation of gold by air with Au/Au₂O₃ catalysts by the means of EXAFS analysis [Mil06]. Bronkhoven et al. observed a strong interaction of oxygen with small gold particles on an Au/Au₂O₃ catalyst as well [Bok06].

Despite the rigorous research directed towards catalysts, the corresponding equivalent to metal oxide gas sensors is rather limited. Nevertheless, some approaches to elucidate the interaction between noble metals and metal oxides in gas sensitive materials are particularly promising. Therefore, in addition to the general approach describing the three adequate familiar potentialities of additives (Spill-over, Fermi-level control & catalytic conversion) mentioned in Section 3.1, there are investigations dealing with the activation of oxygen on Au/SnO₂ interfaces in particular. Montmeat et al. studied the influence of metallic films, membranes and particles in several works [27,28]. In a study about the physico-chemical contribution of gold metallic particles they were able to demonstrate a synergistic effect between tin oxide, gold and oxygen on the three-phase boundary. These results were supported by conduction measurements on a particular test bench, separating the atmosphere seen by the three-phase boundary from the atmosphere seen by the remaining sensor parts as well as gravimetric measurement on this setting [Mon03]. Huebner et al. found valid reasons for drawing basically the same conclusion. By means of work-function measurements corroborated by spectroscopic observations (operando EXAFS) a higher oxygen coverage could be demonstrated on Au-doped SnO₂ sensors [Hue12].

5.3 Electrical measurements II

In order to verify the idea of an enhanced activation of oxygen adsorption on metallic gold even for the gold electrode / sensing layer interface, the given system of an undoped SnO₂ sensor with gold electrodes or platinum electrodes had to be analyzed carefully. According to the previous considerations the DC sensor resistance is mainly determined by the surface reactions. In an atmosphere of nitrogen and oxygen, at a given working temperature of the sensor, the change in resistance should be only affected by the amount of oxygen which ionosorbes on the surface. Since the Weisz-limitation can be excluded, a change of the oxygen concentration in the atmosphere with an increased ionosorption on the SnO₂ surface due to a potential activation of the oxygen on the gold electrode should be verifiable by a bigger change in resistance compared to sensors equipped with platinum electrodes.

5.3.1 Results

For the first experiments, sensors based on fresh/newly prepared undoped SnO₂ from the same batch like the ones in the previous experiments were used. The sensors were exposed to 0 %, 1 % and 2 % oxygen in dry synthetic air. The gas flow (250 ml/min) and the oxygen concentration were controlled by a gas mixing system. DC measurements were performed using a Keithley DMM 199 multimeter. The operating temperatures of the sensors were similar to the previous experiments, namely 200, 250, 300 and 350 °C. The sensors were allowed a reasonable period of time (~40 hours) to equilibrate at a given temperature and oxygen concentration. The time-dependent change in resistance as a function of the actual composition of the gas atmosphere is presented in detail in Figure 5.8.

Since it is well known that freshly produced sensors need sufficient time to equilibrate it was essential to wait a certain amount of time before changing the atmosphere. Considering the time period, which was allowed between the modulations of the oxygen concentrations, one can admit that the equilibrium is reached in each single case. Even if in the starting atmosphere no oxidizing or reducing gaseous species is present, the resistance at intended 0 % oxygen is slightly different for the both types of sensors with various electrode materials. The sensor with gold electrodes shows a higher resistance in intended 0 % oxygen at 200, 250 and 300 °C while at 350°C the resistance of the sensor with the platinum electrode is higher. The observed differences are due to oxygen impurities even at a setting of 0 % oxygen due to some leaks in the gas mixing system (fittings) and a too small flow rate.

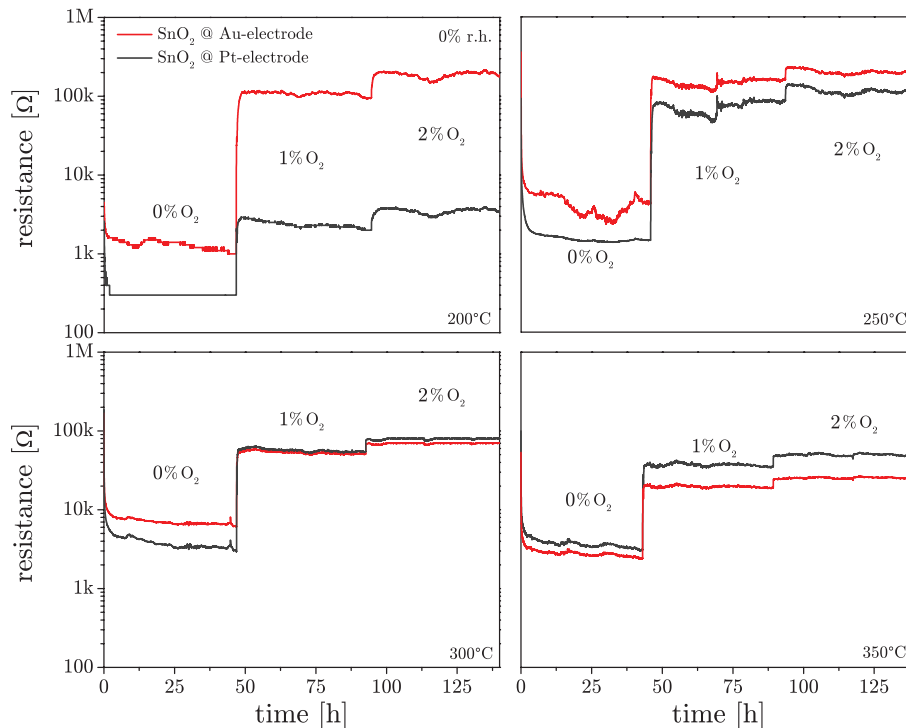


Figure 5.8: Time-dependent measurement of the resistance for two different sensor types (SnO_2 on substrates with Au-Electrodes & SnO_2 on substrates with Pt-electrodes). Measurements performed in nitrogen for subsequent increasing concentrations of oxygen (1, 2 %). The sensors were heated up to 200 °C (top left), 250 °C (top right), 300 °C (bottom left) and 350 °C (bottom right)

The real oxygen concentration under intended pure nitrogen (N_2 (6.0) - Westfalen Gas - 0.0 - 0.5 ppm oxygen as minor component) in the system used for these measurements is around 25 ppm - a small value which has a dramatic influence as can be seen in the results. Nevertheless, concerning the assumed hypothesis of an enhanced oxygen adsorption in the case of gold electrodes these differences can be seen as a first hint in this direction. Especially the temperature dependency is quite noticeable and suggests that the above-mentioned effect is significantly stronger at lower operating temperatures. The difference between gold and platinum is highest at 250 °C, is smaller at 300 °C and at 350 °C it is inverted. By increasing the oxygen concentration the resistance is increased, as expected, for both types of sensors. The differences at an increased oxygen concentration between the sensors are decreasing with temperature, as it can be seen already in the raw measurement data. It ought to be restated that the sensor material for both types of sensors is out of one synthesis, furthermore, the sensor preparation and fabrication steps were done in parallel. In consequence, the sensors are absolutely identical except for the electrode material.

Differences in electrical measurements, as they are apparent here, are assumed to be present just because of various electrodes. Differences originated from the sensor position in the measuring chamber, as described in former surveys [Roe09], were eliminated by repeated measurements with sensors on swapped positions.

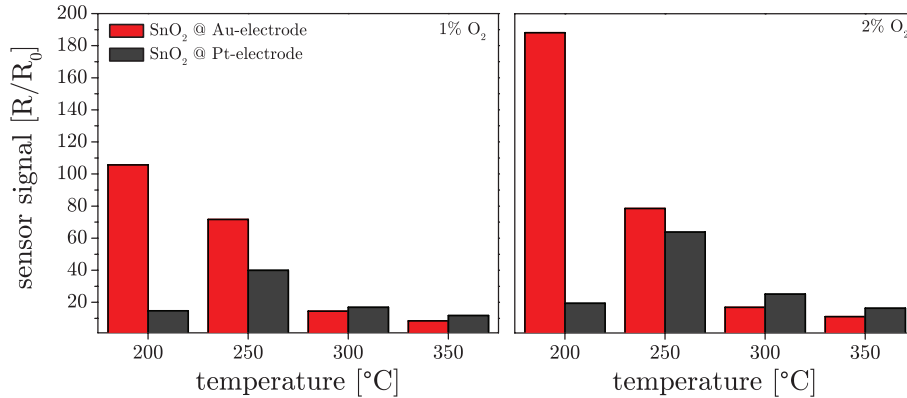


Figure 5.9: Sensor signal as a function of the working temperature of the different sensor types at 1 % oxygen in nitrogen (left) and 2 % oxygen in nitrogen (right)

The calculated sensor signals in Figure 5.9 perfectly mirrors the implied picture of an enhanced effect at an increase of the oxygen level for sensors with gold electrodes at lower operating temperatures. The changing point at a temperature of 300 °C, which was already mentioned in the discussion of the sensor signals upon exposure to different levels of CO and H₂, is visible here as well. Starting with 300 °C, the signal of the sensors equipped with platinum electrodes is higher but only with a little.

In view of the O₂ contamination problems in an adjustment value of 0 % oxygen in the latter experiment a different test bench was used ([Hö8]) in order to fulfill the requirements of an oxygen free atmosphere. The actual oxygen concentration - measured in the exhaust after the gas passes the sensor chamber - during a measurement was recorded by with an electrochemical oxygen analyzer (Zirox SGM 400). At a given concentration of 0 % oxygen (N₂ (6.0) - Westfalen Gas) and an increased flow rate (500 ml/min) plus improved fittings on the test bench, the measured amount of oxygen was in fact below the detection limit (< 3 ppm) of the oxygen analyzer. Again a new set of undoped SnO₂ sensors with different electrode materials was measured. The experiments were very similar to the latter ones, except for lower concentrations of oxygen levels. Starting over with pure nitrogen (N₂ (6.0) - Westfalen Gas), the oxygen concentration was increased in two consecutive steps by 200 ppm and 500 ppm; the measured O₂ concentrations in the exhaust were around 300 ppm and 700 ppm. The resistance data measured over time is shown

in Figure 5.10. These experiments also display the initial resistance under a very

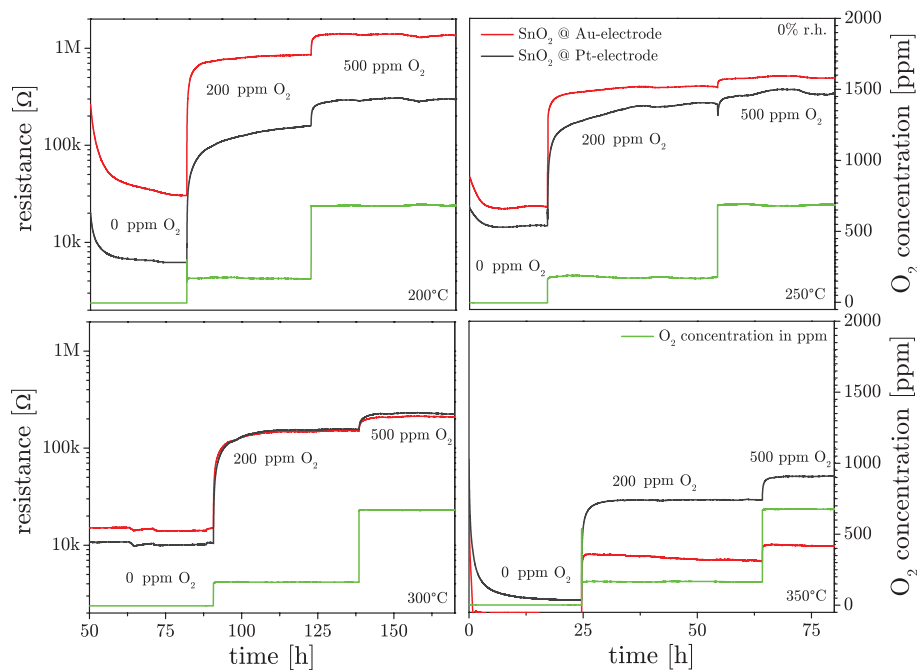


Figure 5.10: Time-dependent measurement of the resistance for two different sensor types (SnO_2 on substrates with Au-electrodes & SnO_2 on substrates with Pt-electrodes). Measurements performed in nitrogen for subsequent increasing concentrations of oxygen (200, 500 ppm). The sensors were heated up to 200 °C (top left), 250 °C (top right), 300 °C (bottom left) and 350 °C (bottom right). The actual oxygen concentration in the exhaust is monitored by an oxygen analyzer.

low concentration of oxygen to be diverging for both types of sensors which leads to the indication that there is an impact on the sensor resistance already at oxygen concentrations of below 3 ppm. With increasing the oxygen concentration at 200 ppm (actual: 300 ppm) and further to 500 ppm (actual: 700 ppm) the resistance increases in a comparable ratio to the previous experiments. Once more, a changing point at around 300 °C is detectable, where the resistance of the sensors with platinum electrodes, under various oxygen concentrations is higher than for the ones with gold electrodes.

The trend of an increased response towards oxygen for sensors with gold electrodes in a temperature dependent manner is further evidenced by the sensor signals plotted in Figure 5.11. With an increase of 200 ppm O_2 , a level which is quite low in relative terms compared to the concentration levels in regular air, the difference between the two types of sensors at 200 and 250 °C is significant. At an increase up to 500 ppm O_2 , the absolute values are somewhat higher, but relatively seen the trend is analogous.

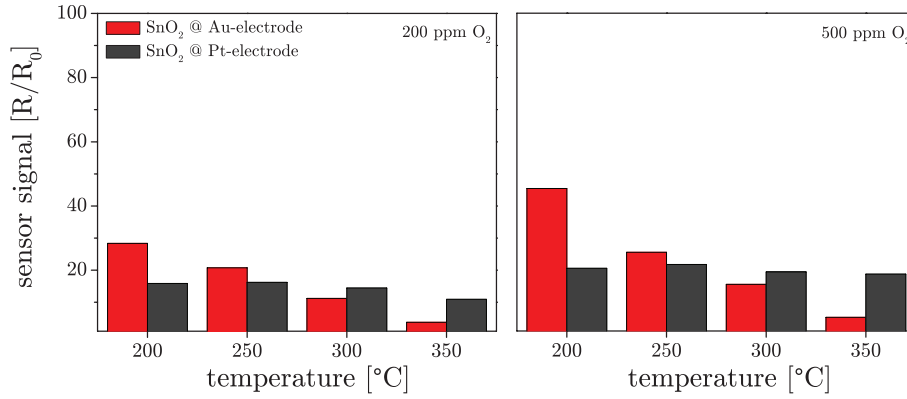


Figure 5.11: Sensor signal as a function of the working temperature of the different sensor types at 200 ppm oxygen in nitrogen (left) and 500 ppm oxygen in nitrogen (right).

5.3.2 Discussion & Summary

A summary of the findings made on the experiments above is that sensors with gold electrodes feature higher responses under oxygen exposure at 200 and 250 °C as the comparable sensors with platinum electrodes, as illustrated all in all in Figure 5.12. At higher temperatures, the differences between the two sensor types tend to become blurred in the range of the errors. While the general difference in response under

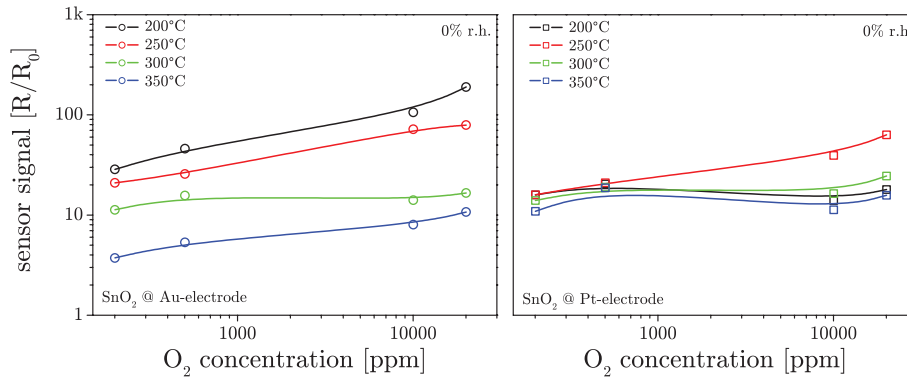


Figure 5.12: Sensor signal as a function of the oxygen concentration for the different sensor types - SnO₂ on substrates with Au electrodes (left) & SnO₂ on substrates with Pt electrodes (right).

oxygen exposure at lower temperatures is obvious, the difference in baseline resistance under 0 % oxygen - or at least an oxygen concentration as low as possible - between a sensor with gold electrodes and one with platinum electrodes at a given working temperature is mandatory to discuss. Of course, the leakages of the system leading to small oxygen impurities have an effect. On the other side it has to be considered if there are differences and/or errors of the set temperature. Due to a dual temperature

calibration (T vs. resistance (passively heated), T vs. resistance (actively heated)) and due to reproducible and constant calibration values for miscellaneous sensors over a long period, this concern can be safely ruled out. The temperature calibration of the sensors was explained in detail in Section 4.1.2.

Since the influence of deviating measuring parameters can be excluded, the enhanced activation of oxygen, the so called spill-over effect which has been discussed in previous chapters, appears the only reasonable explanation for the enhanced response behavior upon oxygen exposure in the case of tin oxide gas sensors with gold electrodes. This line of reasoning seems to be sound, however since there have been just phenomenological studies so far, there is a serious lack of evidence backing up this assertion. To verify the direct reaction of oxygen on gold would be the absolute proof, which in this case would mean a spectroscopic detection of activated oxygen on the gold surface. In the previous discussion about the detection of oxygen on the metal oxide surface it was clear to see how difficult it is to detect - and especially to differentiate - certain oxygen species and it can be anticipated that it was not possible to identify the activated state of the oxygen within this work. Therefore, by reason of the difficulty of this task, the phenomenological research has to be broadened and spectroscopic techniques needs to be adapted to find a way to delimit the theory of the spill-over effect and exclude different other possibilities.

A suitable approach would be to assume that an increase in the contact area between tin oxide and gold would modify the spill-over effect quantifiable. This could be achieved either by decreasing the grain size of the tin oxide or by enlarging the porosity of the electrode. Smaller grain sizes in the case of the metal oxide would change the basic properties which would result in incomparability with previous measurements. Also the structure of the electrode is more or less fixed due to the fabrication technique. Mixing gold particles with a fairly large grain size into the sensing layer would possibly have the desired effect of an enlarged contact area.

5.4 Electrical measurements III

If one looks at the sensor system as a whole, not that many metal oxide grains are in contact with the electrode, accordingly, a limited part of the sensing layer will be affected by the spillover effect. Even considering that the conduction pathway is mainly to be found at the bottom of the sensing layer directly between the electrodes [Bar03], there are still 300 μm of space in between them, which are unaffected by a potential spillover. Additional Au/SnO₂ contact points should therefore increase the spillover rate and the amount of ionosorbed oxygen on SnO₂.

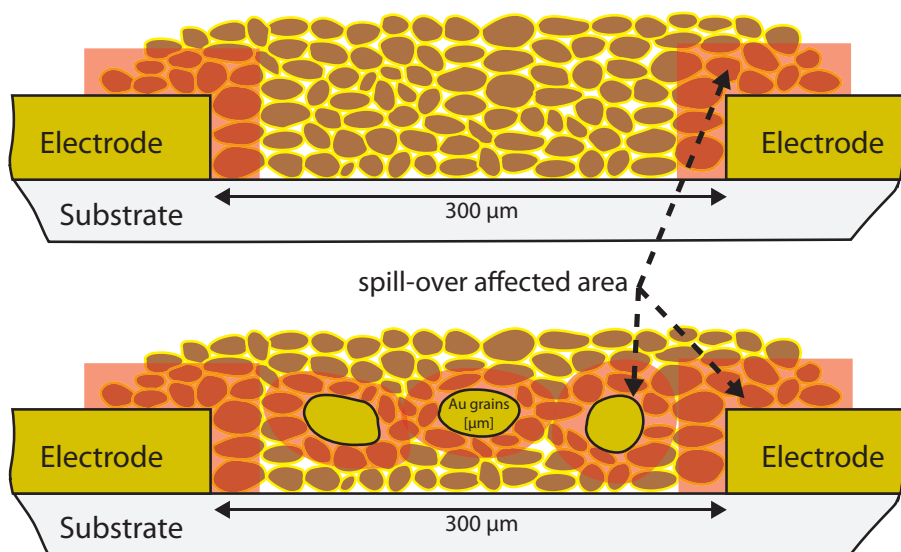


Figure 5.13: Schematic drawing of the sensor cross-section illustrating the area which might be affected by the spill-over effect on the electrode (top). An increased amount of metallic gold - distributed through the whole layer - would increase the affected area.

5.4.1 Results

To check that, the SnO₂ material was mixed up with 5 wt. % gold or platinum powder and printed on the substrates according to the description in Section 4.1.3. Thus, the previously indicated increased number of contact points could be realized. The same experiments like the ones described in ?? were carried out. Starting over with "pure" nitrogen, the oxygen concentration was increased in two consecutive steps by 200 ppm and 500 ppm. The sensors were heated up to 200, 250, 300 and 350 °C. Again, the actual oxygen concentration - measured in the exhaust after the gas passes the sensor chamber - was recorded with an electrochemical oxygen analyzer (Zirox SGM 400). The measured O₂ concentrations in the exhaust were around 300

ppm and 700 ppm.

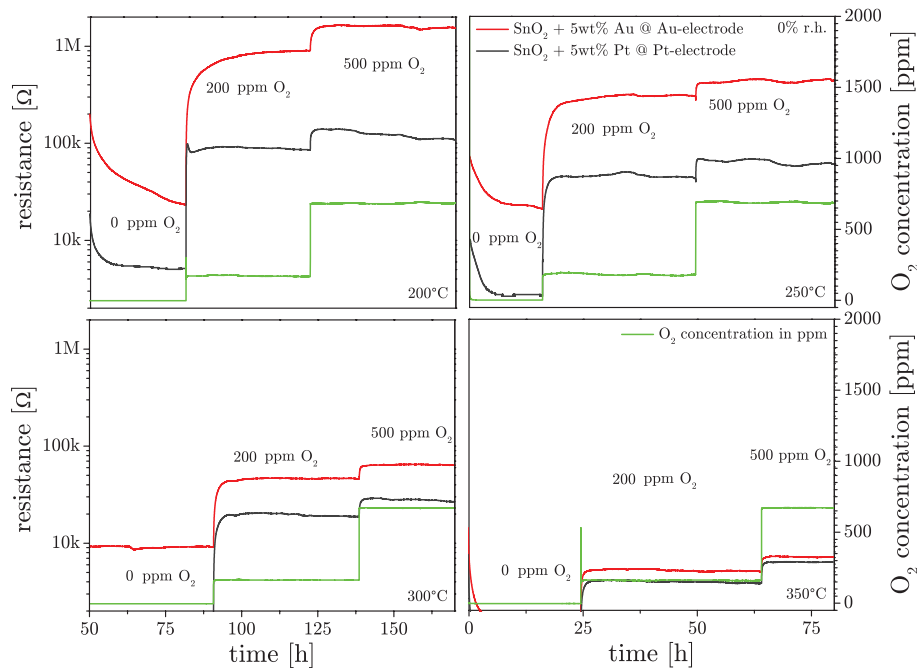


Figure 5.14: Time-dependent measurement of the resistance for two different mixtures printed on the regular substrates (SnO₂ + 5 wt. % Au on substrates with Au-Electrodes & SnO₂ + 5 wt. % Pt on substrates with Pt-electrodes). Measurements performed in nitrogen for subsequent increasing concentrations of oxygen (200, 500 ppm). The sensors were heated up to 200 °C (top left), 250 °C (top right), 300 °C (bottom left) and 350 °C (bottom right). The actual oxygen concentration in the exhaust is monitored by an oxygen analyzer.

The time dependence of the resistance is presented in Figure 5.14. The allotted time period before changing the atmosphere is sufficient to reach a stable baseline. Once more, the difference in resistance between the two sensor types in absence of oxygen is apparent - only with the difference that the sensor with gold electrodes shows higher resistances even at the highest temperature (350 °C). With increasing oxygen concentration the resistance increases just like in the previous measurements. The absolute resistance values can be found in the same regions like for the pure SnO₂ sensors. Nevertheless, with the high amount of allocated micro-sized noble metal particles, it is difficult to compare absolute resistance values since the conductance could be distorted or probably short-circuited in some regions. In general, the plotted sensor signals in Figure 5.15 present fairly the same picture like expected from the previous experiments. With a much stronger response under exposure to oxygen of the sensor with gold at 200 °C the assumption of oxygen activation through gold is becoming increasingly clear. The trend, according to which a changing point is

detectable between 250 and 300 °C, is also valid in this experiment.

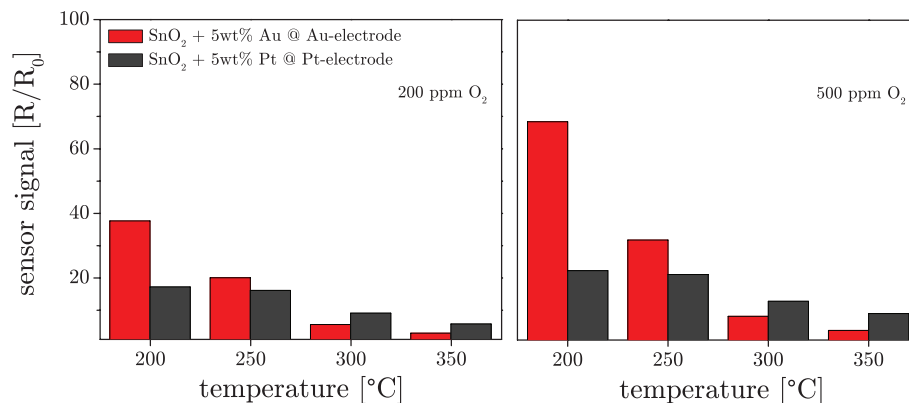


Figure 5.15: Sensor signal as a function of the working temperature of the different samples at 200 ppm oxygen in nitrogen (left) and 500 ppm oxygen in nitrogen (right).

Comparing these values with the ones gained in the previous experiments, it can be recognized that at 200 °C the sensors signals for the gold mixtures are indeed higher as the signals for the pure SnO₂ material. On platinum mixtures and at higher temperatures one obtains lower signals in the case of the mixtures. However, 5 wt. % noble metal particles allocated in the sensing layer do have a certain influence on the conductance apart from possible influenced interactions on the surface and therefore, it is necessary to be particularly careful with strong statements when analyzing the results.

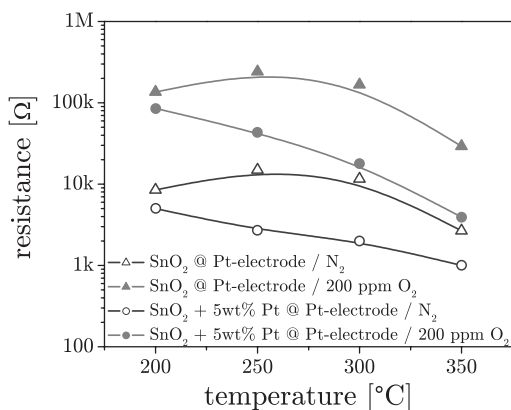


Figure 5.16: Actual measured resistance of SnO₂ sensors on substrates with platinum electrodes and a mixture of SnO₂ + 5 wt. % Pt on substrates with Pt electrodes upon exposure to nitrogen and 200 ppm oxygen as a function of temperature.

In Figure 5.16 the resistance for the sensor with platinum electrodes as well as the mixture of SnO₂ + 5 wt. % Pt printed on substrates with platinum electrodes in the absence of oxygen and at 200 ppm oxygen are plotted versus the working temperature. The sensor with pure SnO₂ on platinum electrodes shows a higher

resistance in the absence of oxygen (<3 ppm) as well as in presence of 200 ppm oxygen compared to the sensor with the imprinted mixture of SnO₂ + 5 wt. % platinum. Reports about adsorption of oxygen on platinum can be found in many scientific articles [Eic00; Lew68; Zam97]. With a reported formation enthalpy of -246 kJ/mol it is understandable that oxygen is strongly bound on platinum [Nag02]. Hence, chemisorbed oxygen on platinum will not affect the conductivity of the neighboring metal oxide and must therefore be treated as ineffective. A higher amount of platinum - as it is the case in the mixtures - is able to capture the oxygen, which is then not available anymore for the ionosorption on SnO₂. But also here, it is mandatory to remind the different properties of both samples. Micro-sized platinum particles inside the layer may influence the whole conduction path.

5.4.2 Discussion & Summary

By increasing the contact area between the noble metal and the metal oxide, the presumed effects increased considerably. Because one has to take into consideration that additional micro-sized metallic particles may influence the conduction of the sensitive layer, the comparability of absolute values is questionable. Nevertheless, it is possible to make a statement about the actual trend. At 200 °C the increased contact area between gold and tin oxide clearly increases the sensor signal upon exposure to different levels of oxygen, which can be explained by an enhanced spill-over activity. This effect is stronger at the lowest measured temperature, while the similarities between SnO₂ + 5 wt. % Au and SnO₂ + 5 wt. % Pt at higher temperatures can be explained by the available thermal energy and due to this a negligible impact of the spill-over effect.

All concepts which could be reconsidered in the light of the investigation that have been carried out are based on a direct reaction of oxygen with the tin oxide surface or reactions on the electrode which influence the tin oxide surface in an indirect manner. What must not be forgotten alongside are the target gases (CO & H₂) which have been measured in the former experiment. Assuming that the oxygen is interacting with the electrode or with noble metals in general must also allow interplay between carbon monoxide or hydrogen and the noble metal. Furthermore, not only the gold electrode can be seen as catalytic active. Platinum, well known for its high catalytic activity, has also shown interesting properties regarding the oxygen adsorption. It is, therefore, necessary to compare the catalytic properties of all materials with respect to the conversion rate of one of our target gases.

5.5 Catalytic conversion measurements

In order to study the CO - O₂ interaction on either the SnO₂ surface or on metallic platinum or gold, the CO consumption of different powder mixtures have been investigated. The objective is to examine how the conversion rate differs for five samples at different temperatures between 200 and 250 °C: pure SnO₂, pure gold, pure platinum and the mixtures SnO₂ + Au and SnO₂ + Pt. Hereby, the overall CO consumption can be divided into the contribution from the individual fractions; the electrode, mimicked by micro-sized grain powder, and the sensitive material SnO₂. It is known that carbon monoxide reacts with adsorbed oxygen to form carbon dioxide [Kap01a].

5.5.1 Test conditions & Results

The powder mixtures were placed inside a pipe with fittings ensuring a sealed connection to set the desired atmosphere. The samples were heated passively using a tube furnace enclosing the whole sample compartment. The temperature was increased in 50 °C steps starting at 200 °C up to 350 °C. The gas concentrations and the flow-rate (250 ml/min) of the test gas composition were adjusted with a gas mixing system. The exhaust gas, more precisely the concentration of CO and CO₂ converted by each 1 mg of the material, was measured by a photo acoustic gas analyzer (INNOVA 1312 LumaSense Technologies). After a short period of synthetic air, CO pulses were applied onto the powder and both, the concentration of CO₂ - resulting from CO reacting with oxygen - were measured in the exhaust gas. Figure 5.17 shows an example for measurements at 250°C. The results are showing a clear coincidence in time between the supplied carbon monoxide and the measured carbon dioxide. The signals corresponding to the CO₂ concentrations are quite noisy due to the instrument parameters of the gas analyzer. Hence, the lowest concentration of CO and respectively the formed CO₂ is too close to the lower detection limit to include it in further evaluation steps. Furthermore, the highest measured concentration is not giving appropriate results due to a limitation given by the calibration of the INNOVA gas analyzer. As a consequence only the measured CO₂ values corresponding to CO concentrations ranging from 50 to 200 ppm are further used.

Comparing the conversion rates of all samples at four different temperatures, averages of the measured concentrations (50 - 200 ppm) are calculated for each temperature, expressed as a percentage of turnovers by forming the quotient of the

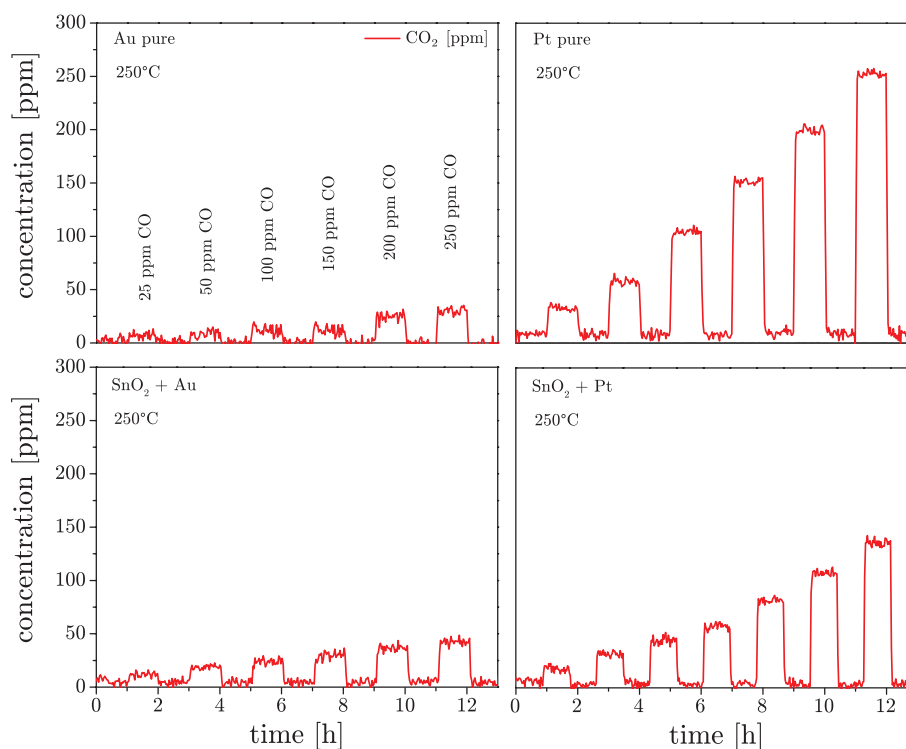


Figure 5.17: Time dependent measurement of the carbon dioxide concentration. A certain amount of the given carbon monoxide is converted by the powder samples. The amount of converted carbon dioxide is measured in the exhaust with a photo acoustic gas monitor. The depicted plots are showing the measured concentrations exemplary for measurements on four different powder samples (Au, Pt, $\text{SnO}_2 + \text{Au}$, $\text{SnO}_2 + \text{Pt}$) at 250 °C.

CO_2 concentration measured in the exhaust gas and the applied CO concentration. As shown in Figure 5.18 the conversion rate of pure SnO_2 increases slowly by increasing the temperature. By reaching 350 °C only about one third of the carbon monoxide is turned into the product (see Table 5.1 for all numbers). The CO_2 turnover of pure gold is even lower, especially with increasing the temperature the conversion rate is not really picking up. However, the measurements on platinum powder showed already at low temperatures a complete conversion of 100 %. The mixture of $\text{SnO}_2 + 5 \text{ wt. } \% \text{ Au}$ shows a higher conversion rate than the pure SnO_2 and the gold powder, while the mixture of $\text{SnO}_2 + 5 \text{ wt. } \% \text{ Pt}$ is somewhere in between its basic components.

As a next step, the theoretical conversion rate of the mixtures was calculated out of the data of the basic components by simply adding up the values in respect to their proportions in the mixtures. The calculated expected values for the platinum mixture are higher than the real measured ones, indicating an inhibiting factor for the

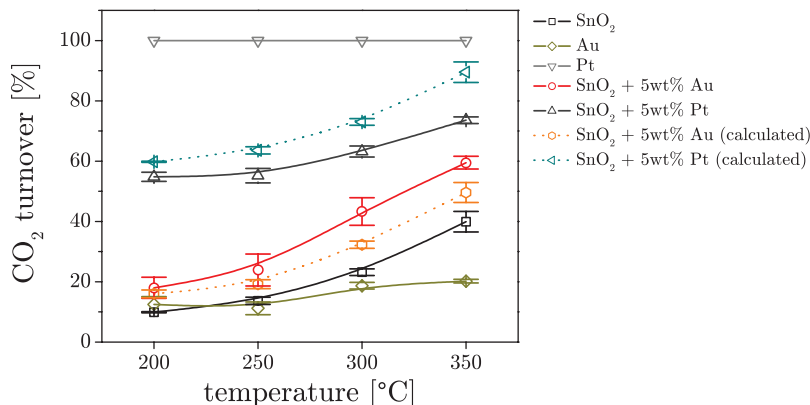


Figure 5.18: CO₂ turnover plotted as a function of temperature for the five different powder samples. The dashed lines are theoretical expected values for SnO₂ + Au and SnO₂ + Pt mixtures, calculated out of the values obtained for the "pure" samples.

CO to CO₂ conversion. Gold mixtures, on the other side, show a higher conversion in the experiment than the theoretical calculated ones, which confers additional credibility to a synergistic effect in the CO to CO₂ conversion.

5.5.2 Discussion & Summary

A clear conclusion can be drawn out of the conversion measurements. Regarding the very different conversion properties of SnO₂, gold, platinum and their mixtures, platinum seems to be an efficient catalyst already at low temperatures. Since the conversion rate reach a complete conversion of 100 % from 200 °C on, the catalytic activity of platinum is likely to be independent of the platinum concentration and the applied working temperature. These results are in line with statements which can be found in literature, whereupon platinum is an excellent catalyst for CO oxidation [Ber81; Cam80; Cou91]. Just as importantly, these results are entirely consistent with the studies of Kappler et al., in which they showed that a significant portion of the carbon monoxide is consumed by the platinum electrode [Kap01a][40].

In contrast, the measurements with gold show much lower conversion rates but in a temperature dependent manner. In the case of gold a weaker binding of oxygen is more likely, or even a prompt desorption is favored, which complicates the direct reaction. Consequently, this results in a lower conversion rate. Including theoretical conversion rates calculated by the summation of plain SnO₂ and the respective additive the trend becomes even clearer. Comparing the experimental gained rates for SnO₂ + 5 wt. % Au with the calculated rates, a non-additive behavior stands out. The experimental rate is much higher than expected indicating a synergistic effect.

The weak binding of oxygen in combination with this synergistic effect could be interpreted into a possible transfer of oxygen from the gold electrode to the sensing layer in real sensors.

Table 5.1: Turnover rate in percent for all measured samples at different temperatures

	SnO ₂	Au	SnO ₂ + Au	Pt	SnO ₂ + Pt
T = 200 °C					
25 ppm	39.2	21.7	40.6	100.0	76.0
50 ppm	16.4	24.5	28.2	100.0	60.0
100 ppm	9.8	16.4	22.2	100.0	57.0
150 ppm	10.2	11.4	19.1	100.0	54.0
200 ppm	9.6	11.0	16.7	100.0	54.0
250 ppm	9.9	11.3	14.0	100.0	54.0
\bar{x}	9.9	12.5	18.0	100.0	54.8
sdv(\bar{x})	0.2	2.6	3.5	0.0	1.5
T = 250 °C					
25 ppm	26.6	29.4	46.9	100.0	77.2
50 ppm	21.1	17.3	37.8	100.0	64.5
100 ppm	15.3	12.1	31.0	100.0	58.8
150 ppm	13.9	8.1	24.5	100.0	54.1
200 ppm	12.4	12.4	21.2	100.0	53.8
250 ppm	13.4	12.0	18.8	100.0	54.2
\bar{x}	13.7	11.2	23.9	100.0	55.2
sdv(\bar{x})	1.2	2.1	5.3	0.0	2.4
T = 300 °C					
25 ppm	32.9	13.9	56.5	100.0	80.4
50 ppm	25.9	13.4	52.5	100.0	64.5
100 ppm	24.8	19.2	48.8	100.0	62.2
150 ppm	22.3	20.0	44.8	100.0	61.8
200 ppm	22.6	18.3	41.7	100.0	63.0
250 ppm	23.1	17.3	37.9	100.0	65.9
\bar{x}	23.2	18.7	43.3	100.0	63.2
sdv(\bar{x})	1.1	1.1	4.6	0.0	1.8
T = 350 °C					
25 ppm	54.8	15.8	69.4	100.0	83.0
50 ppm	46.4	14.1	65.2	100.0	71.4
100 ppm	42.9	19.7	62.4	100.0	72.4
150 ppm	42.8	20.4	58.8	100.0	73.2
200 ppm	37.2	21.0	59.4	100.0	73.9
250 ppm	36.7	19.7	57.5	100.0	74.9
\bar{x}	39.9	20.2	59.5	100.0	73.6
sdv(\bar{x})	3.4	0.6	2.1	0.0	1.1

5.6 DRFITS measurements I

Ionosorbed oxygen species as well as intermediates formed in reactions between pre-adsorbed oxygen and target gases like carbon monoxide and hydrogen are considered to be responsible for charge transfers and ultimately for the change in resistance. In the preceding chapter, it was possible to gain an explicit sight into the electrical and catalytic properties of the material concerning the reaction with different gaseous components. Based on these phenomenological results a comprehensive knowledge base can be derived. Oxygen, as an adsorbed species, seems to hold a dominant position regarding the influencing factor of the three phase boundary. It was possible to identify clearly quantifiable synergy potential of metallic gold being in contact with SnO₂, which could be associated to a spillover effect of oxygen. Nevertheless, it is almost superfluous to mention that only phenomenological studies in different conditions are not sufficient to gain a complete insight into the certain effects occurring at the surface of either the sensing material or the electrodes. Even if electrical measurements are highly sensitive already at minor changes of the material, spectroscopic evidence is crucial for a better understanding of surface reactions. Here, a vital problem is in fact the operating conditions of metal oxide gas sensors. Temperatures above 200 °C and a surrounding atmosphere at normal pressure are not compatible with most of the spectroscopic techniques. Measuring the electrical parameters in parallel on a real working sensor system in atmospheric conditions additionally complicates the task. Moreover, the investigated sensitive layer is rather a polycrystalline sample than a defined crystal. To investigate the surface science of a polycrystalline layer at elevated temperatures reacting with gaseous molecules in very low concentrations the remaining window of appropriable spectroscopic techniques is fairly small. If finding a useable technique seems hard enough, the circumstances of detecting the adsorbed oxygen is also complicating matters. As mentioned in the previous chapter, numerous attempts were undertaken in order to understand the chemisorption or ionosorption of oxygen. EPR and TPD measurements resulted in important findings, anyhow, measurements on a working sensor with a coincident electrical readout are not feasible yet.

Diffuse Reflectance Infrared Fourier Transformed Spectroscopy (DRIFTS), a special infrared based technique which can be used to investigate polycrystalline samples, is well known for its applicability in the research field of catalysis, especially when it comes to "in situ" or "operando" conditions. A number of surveys have shown the strong potential of DRIFT spectroscopy in the frame of metal oxide gas sensors as

well [Bar07; Har05]. Admittedly, it is not possible to shed light upon the reaction of oxygen in a direct manner. Nonetheless, by combining pieces of knowledge of reactions between specific gaseous species and pre-adsorbed oxygen and a detailed investigation of the formed intermediates brought a wealth of additional insights. Experiments with carbon monoxide on SnO₂ gas sensors and the associated spectroscopic investigations have shown that for this specific reaction the intermediates are detectable by the means of DRIFT spectroscopy [Emi01; Koz06]. It reacts with adsorbed oxygen according to Equation (5.4).



It is not necessary to mention that this reaction depends on the availability of oxygen on the surface and a formation of carboxylates and carbonates is described as the most probable reaction pathway [Dav03; Emi01; Koz06]. Based on this model, the next step is the investigation of the intermediates, namely carboxylates and carbonates in the case of carbon monoxide reaction.

Even if DRIFT spectroscopy provides an outstanding capability to investigate surface phenomena in operando, it has disadvantages as described in detail in Section 4.2.3. Besides effects like free charge carrier adsorption, which is not quite easy to deal with, the signal-to-noise ratio is often very weak, especially when the investigated layer becomes very thin. This is attributed to the fact that the incident beam "collects" information of the whole layer by its diffuse reflectance. Simply put, the thicker the layer the higher the amount of information. In the particular case of investigations at the three phase boundary it is even more complex due to the underlying electrode. Measurements on powder mixtures, similar to the ones used for catalytic conversion experiments, could relativize some of the misfeatures, but paid for with the disadvantage of the impossibility of simultaneous resistance measurements. As described in Section 4.2.3 the powder chamber with its height of 5 mm is able to carry more material than it would be able to print on a substrate. Further, by mixing tin oxide with a specific amount of platinum or gold powder, which simulate the electrode, the contact area between the noble metal and the metal oxide is reasonable increased and more distributed in the whole sample as opposed to be found underneath a relative thick layer of pure SnO₂.

5.6.1 Results

To characterize the impact of the contact between gold respectively platinum and the tin oxide, powder mixtures equivalent to the ones used in the catalytic conversion measurements were measured. Accordingly, the common SnO₂ powder - synthesized and calcinated as described in Section 4.1.3 - was mixed with 5 wt. % micro-scaled platinum or gold powder (FERRO©) in order to simulate the contact surface between the electrode and the sensitive layer as in a real sensor system. The powder mixtures were placed in a special powder chamber suitable to the Harrick DRIFTS chamber (Harrick Praying Mantis). The chamber is equipped with a supply line for gases as well as an electrical connector for heating-up the sample compartment. A water cooling circuit diminishes the heating-up of the body parts of the chamber in order to minimize the thermal radiation. The sample compartment itself is isolated from the other inner parts of the spectrometer, which enables a controlled gas atmosphere in the sample compartment and an evacuated area around it. The gas atmosphere was controlled via a multi-channel gas mixing system as described in Section 4.2.1. In order to observe the formation and cancelation of surface species related to the reaction of carbon monoxide, the two different powder mixtures were measured at temperatures from 200 °C to 350 °C in a background of dry synthetic air. The measurement sequence consisted of 3 hours equilibration time in dry synthetic air, followed by a one hour pulse of 250 ppm carbon monoxide. It was of interest if the amount and type of intermediates, which are formed during the reaction of carbon monoxide and oxygen on the tin oxide surface differ, depending on the noble metal which is in contact with the metal oxide.

During the measurement, single channel spectra were recorded each 15 minutes out of 1024 scans with a resolution of 4 cm⁻¹. The second last single channel spectra before a change in the gas atmosphere was taken into consideration for the further evaluation steps. Figure 5.19 shows the proposed single channels at different temperatures in dry synthetic air and in dry synthetic air with 250 ppm carbon monoxide.

Based on the single channel spectra it is already possible to obtain extensive information about the surface compounds at each measured condition as well as information about the free charge carrier absorption which is indicated by a shift in the baseline. In all spectra a clutch of peaks is distinguishable in the range of 3700 and 3400 cm⁻¹. These peaks correspond to hydroxyl groups in different forms [Dav03]. The multiple peaks at around 2900 cm⁻¹ are linked or caused, in particular,

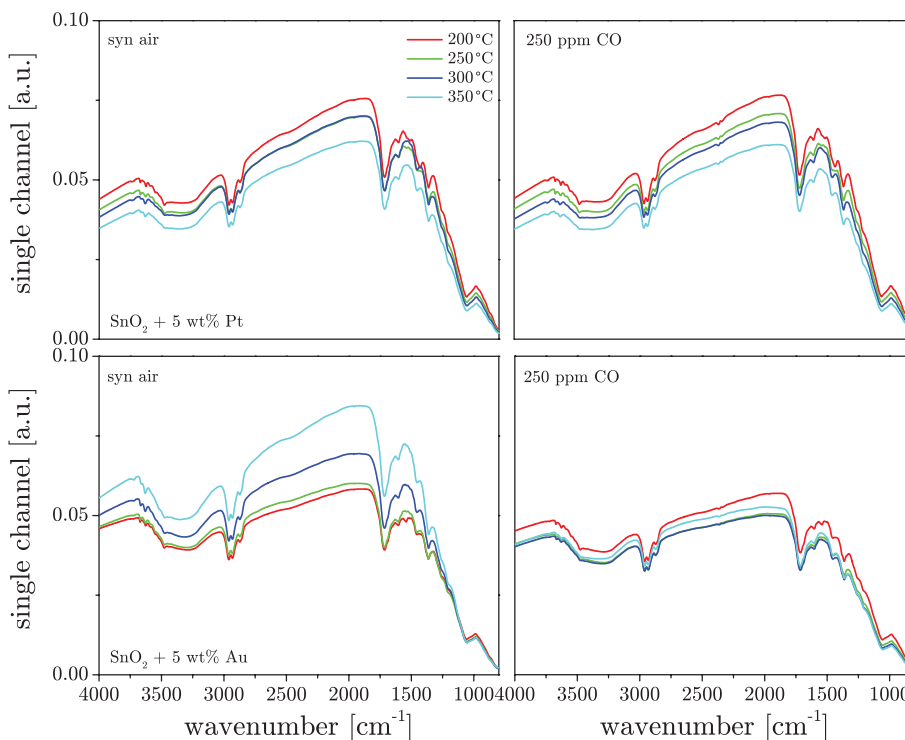


Figure 5.19: Single channel spectra of $\text{SnO}_2 + 5 \text{ wt. \% Au}$ (bottom) and $\text{SnO}_2 + 5 \text{ wt. \% Pt}$ (top) powder mixtures at four different temperatures (200, 250, 300 & 350 °C) recorded in the presence of synthetic air (left) and 250 ppm carbon monoxide (right).

by a perturbation of the detector. In the region below 2000 cm^{-1} an agglomeration of different peaks makes it quite a bit more difficult to distinguish between different species; While at around 1550 to 1650 cm^{-1} it is supposed to find molecular water [Dav03; Jon72], the entire range from 1600 to 1000 cm^{-1} corresponds to carboxylates and carbonates, which are to be assumed as the main intermediates in the carbon monoxide reaction on the SnO_2 surface [Koz06]. Since the actual profile of the detector shows a non-linear behavior in this region, it is, accordingly, difficult to get a meaningful interpretation of the surface components at a first glance. When restricting the analysis of the spectra to the shift in the actual baseline at the different measured gas compositions, it is evident that in the case of platinum addition much less displacement is observable than in the case of gold, the latter also showing strong temperature dependency. In simple terms, the higher the temperature of the $\text{SnO}_2 + 5 \text{ wt. \% Au}$ sample, the larger the baseline shift when applying a certain concentration of carbon monoxide.

The single channel spectra reported above have been further processed to obtain the

absorbance spectra. Figure 5.20 shows the absorbance spectra of the two measured powders ($\text{SnO}_2 + 5 \text{ wt. } \% \text{ Au}$ & $\text{SnO}_2 + 5 \text{ wt. } \% \text{ Pt}$) at the different measured temperatures (200, 250, 300 and 350 °C). Evaluating in this way - by calculating the absorbance spectra out of the single channel spectrum upon exposure to synthetic air and the single channel spectrum upon exposure to 250 ppm carbon monoxide - it is possible to gain information about reaction of carbon monoxide, the formation of potential intermediates or the impact on other surface species. Since the aim was to find out whether the contacting point between the two different noble metals and tin oxide is influencing the carbon monoxide reaction in particular, the region between 2500 and 800 cm^{-1} is plotted, where it is assumed to find the intermediates of the carbon monoxide reaction, as well as the gaseous carbon monoxide (2143 cm^{-1}) and carbon dioxide (2370 cm^{-1}) [43].

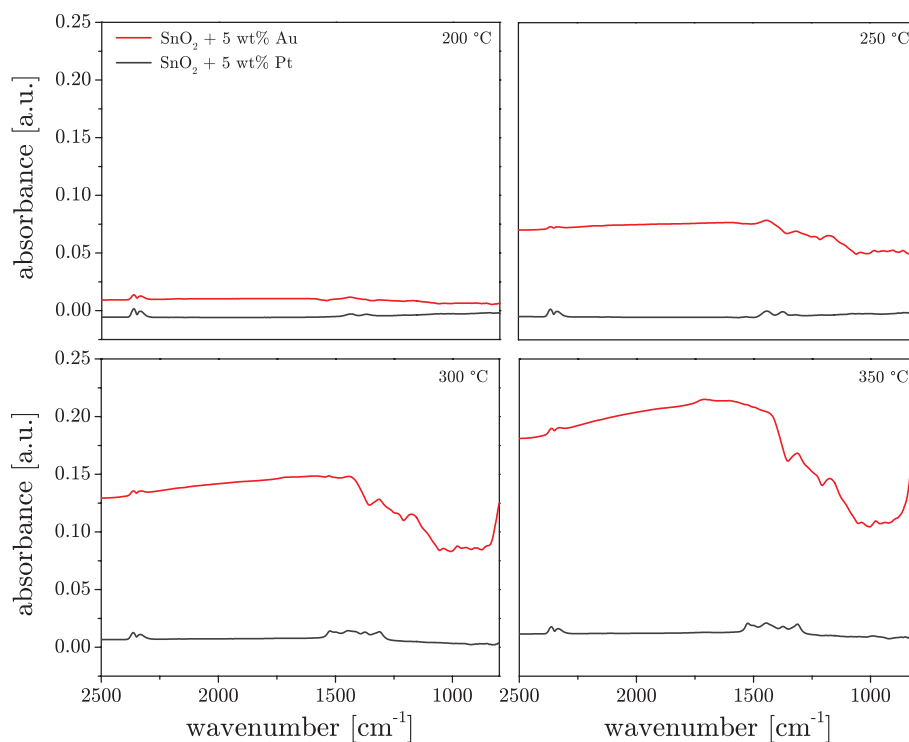


Figure 5.20: DRIFT spectra of the two different powder mixtures in the presence of 250 ppm carbon monoxide at 200 °C (top left), 250 °C (top right), 300 °C (bottom left) and 350 °C (bottom right). As reference the spectrum in dry synthetic air at the corresponding temperature was taken.

One clearly observes that the temperature dependent difference in the baseline upon exposure to carbon monoxide is seen as a shifted baseline due to the method of spectra calculation. The $\text{SnO}_2 + 5 \text{ wt. } \% \text{ Pt}$ doesn't show a large baseline shift in comparison to the $\text{SnO}_2 + 5 \text{ wt. } \% \text{ Au}$. By having a closer look at the

interpretable peaks the following observations can be made: For each sample and temperature an obvious peak is observable at 2350 cm^{-1} , which corresponds to the formation of carbon dioxide and validates the reaction of carbon monoxide with oxygen; independent of temperature, the platinum containing sample shows the highest CO_2 peaks in every case, which can be interpreted or quantified as a high turnover rate and therefore corresponds with the previously described assumptions on the catalytic conversion measurements; in the region below 1600 cm^{-1} multiple peaks are visible for both types of samples. Unfortunately, in the case of $\text{SnO}_2 + 5\text{ wt. \% Au}$, the peaks are pretty much blurred by the distorted baseline, so that a differentiation of a certain peak is impossible.

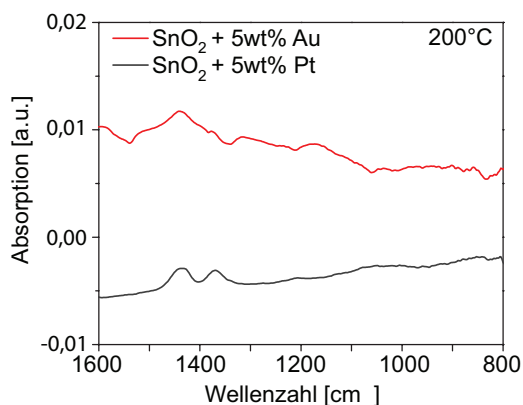
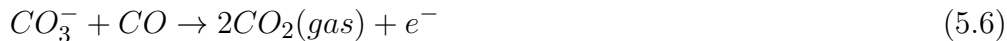


Figure 5.21: Carbonate and carboxylate range ($1600 - 800\text{ cm}^{-1}$) of the two different powder samples at 200 °C exposed to 250 ppm carbon monoxide. As reference the spectrum in dry synthetic air was taken.

Figure 5.21 shows a zoom-in of the measurement at 200 °C . By looking on these depictions, one can notice the differences in the case of the platinum powder. At lower temperatures - 200 and 250 °C (which is not shown here), to be precise - two peaks dominate; one at 1440 cm^{-1} and another at 1375 cm^{-1} . At elevated temperatures more distinguishable peaks are present. On the other hand, in the case of the gold containing samples it might be assumed that already at 200 °C more than two peaks can be read. However, any such questionable statements must be considered along with the knowledge that the baseline shift cause serious disturbance. Considering the reaction of CO with oxygen, it must be recalled that several forms of ionosorbed oxygen are possible. Hence, depending on the configuration of the ionosorbed oxygen, different intermediates are conceivable. Further, this may influence the position and shape of the miscellaneous bands compared to general IR studies on metal oxides, where an ordinary oxygen atom is assumed to be the reaction partner. The

reaction of CO with different ionosorbed oxygen species on tin oxide and the resultant formation of intermediates can be summarized as follows [Koz06]:



Important and considerable efforts have been made by Koziej et al. to acquire factual knowledge about the reaction pathway including the interpretation of infrared measurements in the case of carbon monoxide reaction on tin oxide based gas sensors [Koz06]. The IR bands shown in the upper graphs correspond to the different intermediates described in Equation (5.5) - Equation (5.11). In the case of SnO₂ + 5 wt. % Pt at 200 °C the two notable bands (1440 & 1375 cm⁻¹) are assigned to the asymmetric and symmetric vibrations of monodentate carbonates (CO₃⁻).

Table 5.2: Type of vibrations and the corresponding range of wavenumbers of different intermediates of the carbon monoxide reaction

	carboxylate	bidentate	monodentate	Non-coordinated
Wavenumber [cm ⁻¹]	1530	1545	1440	1495
/	$\nu_{as} COO^-$	$\nu C=O$	$\nu_{as} COO^-$	$\nu_{as} CO_3^{2-}$
type of vibration	1320	1330	1372	
	$\nu_s COO^-$	$\nu_{as} COO^-$	$\nu_s COO^-$	

The additional bands which can be seen at higher temperatures are interpretable as carboxylates ($\nu_{as}(COO^-) = 1523 \text{ cm}^{-1}$ & $\nu_s(COO^-) = 1320 \text{ cm}^{-1}$) and non-coordinated carbonates ($\nu_{as}(CO_3^{2-}) = 1500 \text{ cm}^{-1}$). A detailed assignment of the

different peaks is listed in Table 5.2 and extensively described in [Koz06] & [Dav03]. Due to the heavily distorted spectra in the case of $\text{SnO}_2 + 5 \text{ wt. } \% \text{ Au}$, a full characterization of the bands would reach the limit of reliability and therefore cannot be commented upon.

5.6.2 Discussion & Summary

Despite the fact that the recorded DRIFT spectra in the preceding section clearly indicate unambiguous differences between gold and platinum containing tin oxide powders, it is not possible to go much beyond. The explicit identification of the intermediates is impossible since numerous influences place the usability of the evaluable region ($1600 - 1000 \text{ cm}^{-1}$) in question. The bands in the case of $\text{SnO}_2 + 5 \text{ wt. } \% \text{ Pt}$ can be identified and these results are also reliable, nevertheless the principal interpretation of the intermediates on a single sample has been done in other surveys and do not come under the current scope of work. The priority was rather to analyze and compare the differences between two different admixtures in tin oxide powders respectively two different electrode materials. The fact that the spectra show such different general properties had prevented this step. The shift of the baseline is driven primarily by the free charge carrier absorption. Other basic parameters like reflectance of the gold and platinum particles are likely to be entirely different and can influence the signal intensity in an unpredictable way. Based on this consideration, and taking into account that the initial purpose of measuring powders was the increase of spectral information by using samples in a higher volume, it can be therefore concluded that also the undesired content increased. Naturally, there are different ways to diminish the unwanted features in DRIFT spectroscopy and also here attempts were made to reduce the baseline shift by applying a baseline correction (using a software feature in BRUKER OPUS©). But since the origin of the baseline shift is not entirely clear and the region of interest in the spectra is in a very unfavorable region anyway - considering the strong slope of the detector profile, the gained results are even more doubtful due to the manipulation of the spectra.

In relation to the previous discussion about the differences in spectra between $\text{SnO}_2 + 5 \text{ wt. } \% \text{ Au}$ and $\text{SnO}_2 + 5 \text{ wt. } \% \text{ Pt}$ at $200 \text{ }^\circ\text{C}$ it may be assumed that the abundance of peaks already visible at $200 \text{ }^\circ\text{C}$ only in the case of $\text{SnO}_2 + 5 \text{ wt. } \% \text{ Au}$ is a direct aftermath of an enhanced activation of oxygen adsorption on the Au/SnO_2 interface at lower working temperatures and, as consequence, a higher number of potential reaction partners for carbon monoxide. Without going into this matter

any further at this point, other interesting features have been discovered during the evaluation process. Figure 5.22 displays the region between 4000 and 3000 cm^{-1} , a section which features the hydroxyl groups on the tin oxide surface, for both types of material at a temperature of 200 °C.

Also in this region both spectra suffer from the baseline shift as can be seen in

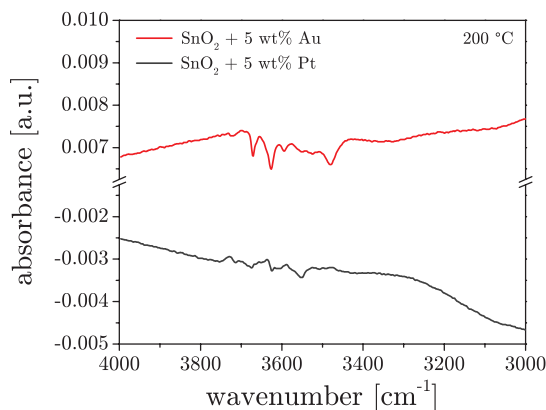


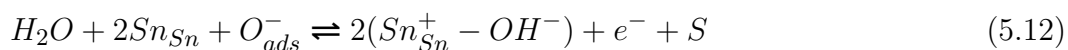
Figure 5.22: Hydroxyl range (4000 - 3000 cm^{-1}) of the two different powder samples at 200 °C exposed to 250 ppm carbon monoxide. As reference the spectrum in dry synthetic air was taken.

the very different values for the absorbance. However, the linear baseline which one can observe in this region makes the obtained signals much more suitable for interpretation as in the case of the carbonate- & carboxylate intermediates. Without going too much in details about the different peaks in this section, a clear distinction can be made for the different materials. Each individual distinguishable peak in the spectrum of the SnO₂ + 5 wt. % Au mixture shows a quantitatively enhanced signal in comparison to the spectra of the SnO₂ + 5 wt. % Pt mixture. In addition, in the lower region, at around 3470 cm^{-1} a further band can be observed for the gold containing sample, which is not present in the other spectrum.

Although no useful differences could be observed in the region of the carbon monoxide reaction intermediates, significant variations can be found for hydroxyl groups on the tin oxide surface being in contact with either gold or platinum. Another conclusion is the fact that measuring powders will not improve matters as expected, but on contrary will confuse things even further since there is no possibility to gain an insight into phenomenological information such as changes in conductivity in order to understand the quality of the baseline shift. Printing the powder mixtures on substrates, as it was done already for the electrical measurements in Section 5.4 is the next logical step.

5.7 DRFITS measurements II

On the basis of the previous observations of an apparent difference in the hydroxyl region depending on the electrode material the next investigation focus on how the quantity and type of hydroxyl groups is affected by a potentially varying availability of adsorbed oxygen or by side-reactions with reducing gases. In an investigation about the surface species of tin oxide based gas sensors, Koziej et al. were able to demonstrate the interplay between gaseous water and pre-adsorbed oxygen on the basis of spectroscopic results [Koz06]. More than that, the formation of hydroxyl groups through this reaction is heavily depending on the availability of pre-adsorbed oxygen. The results lead to the assumption of a continuous dynamic equilibrium of an ongoing hydroxylation and de-hydroxylation (Equation (5.12)) [Koz06].



By increasing or decreasing the amount of adsorbed oxygen on the tin oxide surface the equilibrium can easily be shifted. Reducing gases like carbon monoxide or hydrogen are competing with water for the available pre-adsorbed oxygen. These reactions (Equation (5.13) & Equation (5.14)) decrease the amount of oxygen which is available for the reaction with water and shift the equilibrium to the left side [Gro12a].



On the other hand, an increase of pre-adsorbed oxygen concentration can be achieved by simply increasing the oxygen concentration in the surrounding atmosphere or by a "catalytic activation" of the oxygen adsorption, such as discussed for the spillover effect on gold. Hence, the chance of a formation of a hydroxyl group would increase by the presence of more oxygen on the surface.

5.7.1 Results

In order to exploit the benefits of an increased SnO₂ - noble metal interface provided by powder mixtures without distancing too far from the classical sensor system, the mixtures of the same type as used in the conversion experiments and in the previous DRIFTS measurements have been printed on the alumina substrates. By this, not

only the typical system geometry is maintained, it further allows to measure the resistance in parallel in order to gather additional electrical data and get a far more complete picture linking phenomenological and spectroscopic information. According to the estimations presented in the experimental chapter, the amount of platinum respectively gold in the mixtures is about 5 wt. % and is representing the electrode / sensitive layer interface but in a more distributed manner. The mixtures are printed on alumina substrates with either gold or platinum electrodes; two different types of samples were used, first, $\text{SnO}_2 + 5 \text{ wt. } \% \text{ Au}$ on an alumina substrate with gold electrodes, second, $\text{SnO}_2 + 5 \text{ wt. } \% \text{ Pt}$ on an alumina substrate with platinum electrodes. Both samples were measured in a sequence of different gaseous ambiants at four different temperatures (200, 250, 300 and 350 °C). Each experiment started

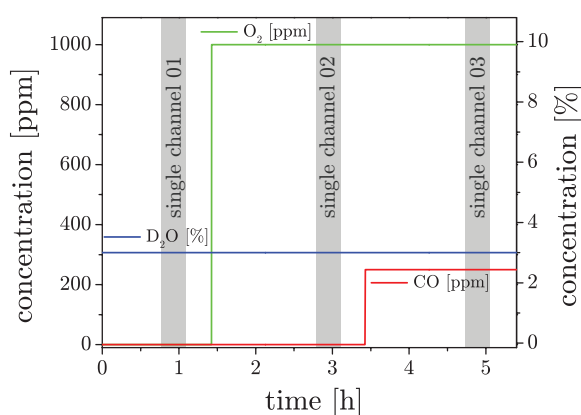


Figure 5.23: Given gas concentration plotted as a function of time. The grey shaded areas indicate the time when the single channels were recorded, which were then used for the calculation of the absorbance spectra.

with several hours' exposure to "pure" nitrogen (N_2 6.0 Westfalen Gas) and 3 % D_2O in order to reach an equilibrium. The actual oxygen contamination amounts to around 25 ppm. Due to the parallel resistance measurement it was possible to estimate that the time which was needed to reach the equilibrium is comparable to the initial electrical measurements. In a subsequent step 1000 ppm O_2 were added for two hours; finally 250 ppm carbon monoxide were added for additional two hours. The use of deuterated water instead of H_2O provides some benefits. It was shown that depending on the synthesis and the fabrication process the quantity of hydroxyl groups can differ quite a lot [Gro12b]. In IR spectra, these surface species appears in the region between around 3800 and 3400 cm^{-1} . Deuterated species (OD - groups) on the other side are shifted to lower wavenumbers. In this region they are not interfering with the initial hydroxyl groups; additionally this region is much less

affected by the free charge carrier absorption which greatly facilitates the evaluation and interpretation. The whole protocol of gas exposure is displayed in Figure 5.23. In addition, the graph indicates the time of recording the single channel spectra which have been used for the evaluation process.

Similar to the previous DRIFTS experiments, single channel spectra were recorded each 15 minutes out of 1024 scans with a resolution of 4 cm^{-1} . The second last single channel spectra before a change in the gas atmosphere was taken into consideration for the further evaluation steps as it is indicated in Figure 5.23.

Measurements at 200 °C - Out of the considered single channels the respective absorbance spectra were calculated. Figure 5.24 shows the absorbance spectra for $\text{SnO}_2 + 5 \text{ wt. } \% \text{ Au}$ and $\text{SnO}_2 + 5 \text{ wt. } \% \text{ Pt}$ at 200 °C, on the one hand in event of a change from $\text{N}_2 + 3 \% \text{ D}_2\text{O}$ to $\text{N}_2 + 3 \% \text{ D}_2\text{O} + 1000 \text{ ppm O}_2$ (a) and on the other hand in event of a change from $\text{N}_2 + 3 \% \text{ D}_2\text{O} + 1000 \text{ ppm O}_2$ to $\text{N}_2 + 3 \% \text{ D}_2\text{O} + 1000 \text{ ppm O}_2 + 250 \text{ ppm CO}$ (b). According to Equation (5.15) the formation

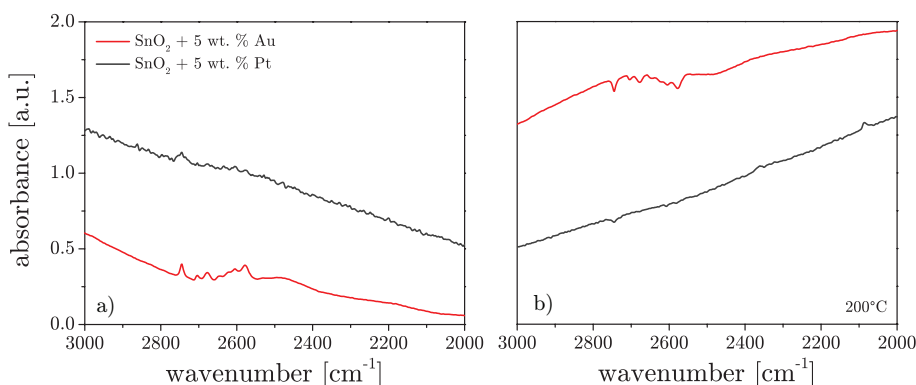
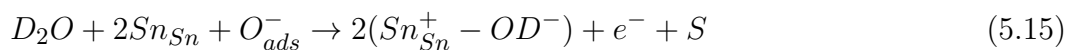


Figure 5.24: DRIFT spectra of two different mixtures screen-printed on alumina substrates ($\text{SnO}_2 + 5 \text{ wt. } \% \text{ Au}$ on substrates with Au electrodes & $\text{SnO}_2 + 5 \text{ wt. } \% \text{ Pt}$ on substrates with Pt electrodes) at 200 °C upon exposure to a) 1000 ppm O_2 (Reference: $\text{N}_2 + 3 \% \text{ D}_2\text{O}$) and b) 1000 ppm $\text{O}_2 + 250 \text{ ppm CO}$ (Reference: $\text{N}_2 + 3 \% \text{ D}_2\text{O} + 1000 \text{ ppm O}$) in a background of $\text{N}_2 + 3 \% \text{ D}_2\text{O}$

of OD groups is expected under exposure to 1000 ppm oxygen in a background of nitrogen and 3 % D_2O , which is shown in Figure 5.24 a).



Indeed, both samples show a peak at 2744 cm^{-1} , which indicates a formation of a terminal OD group. In the case of the gold containing sample four additional peaks are clearly visible ($2703, 2678, 2605 \text{ \& } 2576 \text{ cm}^{-1}$). In literature peaks originating

from OD-groups - or rather OH-groups - which are shifted to lower wavenumbers are described as interacting OD-groups [Dav03], hence, one can assume a higher number of neighboring and interacting OD-groups in the case of $\text{SnO}_2 + 5 \text{ wt. } \% \text{ Au}$. The second step, displayed in Figure 5.24 b), the addition of 250 ppm carbon monoxide should cause a disturbance in the equilibrium (Equation (5.15)) due to the reaction of carbon monoxide with adsorbed oxygen (Equation (5.16)). This would lead to a decrease of the previously formed OD groups.



As expected, in Figure 5.24 b) a decrease of the OD groups is observable. The peak positions are equivalent to case a), which means that exactly those species which have been created before are affected now in this phase. Another important implication is the appearance of a peak at 2087 cm^{-1} , which is related to adsorbed carbon monoxide on platinum [Ras03], it reinforces the assumption of direct combustion. In the case of $\text{SnO}_2 + 5 \text{ wt. } \% \text{ Pt}$ the doublet peak at 2348 cm^{-1} indicates the production of carbon dioxide. Even if this peak is not visible for the $\text{SnO}_2 + 5 \text{ wt. } \% \text{ Au}$ sample, simultaneous recorded mass spectrometer data indicates a conversion from CO to CO_2 also in this case, but to a much lower extent (Figure 5.25).

As indicated above, measuring the resistance of the samples in parallel can bring

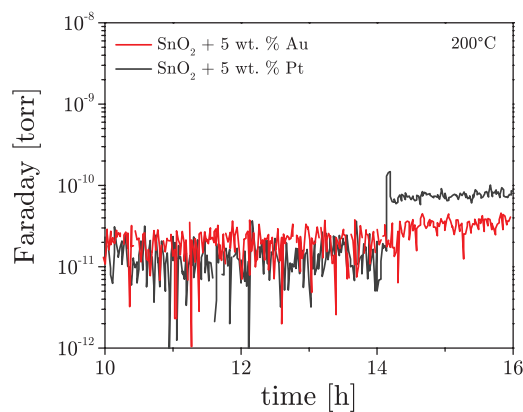


Figure 5.25: Mass spectrometer data recorded for the respective DRIFTS measurement at $200 \text{ }^\circ\text{C}$. Gas atmosphere during hour (10 - 12): $\text{N}_2 + 3 \text{ } \% \text{ D}_2\text{O}$ - (12 - 14): $\text{N}_2 + 3 \text{ } \% \text{ D}_2\text{O} + 1000 \text{ ppm O}_2$ - (14 - 16): $\text{N}_2 + 3 \text{ } \% \text{ D}_2\text{O} + 1000 \text{ ppm O}_2 + 250 \text{ ppm CO}$

considerable benefits. Figure 5.26 shows the electrical measurement of both samples for the discussed scenario.

At first glance, the absolute difference in resistance of both samples independent of the sequential gas composition is noticeable. The general difference between gold

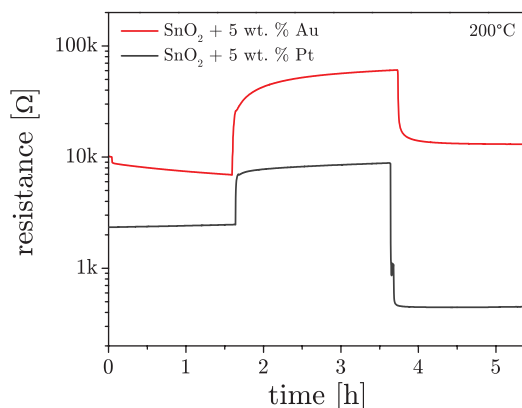


Figure 5.26: Time-dependent resistance measurement of the two different mixtures printed on substrates for the respective DRIFTS measurements at 200 °C. Gas atmosphere during hour (10 - 12): $N_2 + 3\% D_2O$ - (12 - 14): $N_2 + 3\% D_2O + 1000\text{ ppm } O_2$ - (14 - 16): $N_2 + 3\% D_2O + 1000\text{ ppm } O_2 + 250\text{ ppm } CO$

& platinum containing samples has been discussed in Section 5.4; however, in this case it can be linked to the recorded spectra in order to explain - at least partially - the baseline shift which is assumed to be a consequence of the free charge carrier absorption. In case a) - the change from $N_2 + 3\% D_2O$ to $N_2 + 3\% D_2O + 1000\text{ ppm } O_2$ - the absolute difference in resistance is somewhat lower than in case b) - change from $N_2 + 3\% D_2O + 1000\text{ ppm } O_2$ to $N_2 + 3\% D_2O + 1000\text{ ppm } O_2 + 250\text{ ppm } CO$. This trend is repeated in the baseline of the respective spectra. A higher resistance at a certain temperature means less free charge carriers and consequently less free charge carrier absorption and a lower baseline in the spectrum. The first section in the resistance measurement shows a higher absolute resistance for the gold containing sample, which can be attributed to the rather oxygen lean conditions than oxygen free conditions (oxygen impurities of around 25 ppm are measurable), a phenomena which appeared in the previous electrical measurements as well. Therein, the enhanced oxygen adsorption (spill-over effect) of gold was proposed to be responsible. The relative change in resistance upon exposure to 1000 ppm oxygen reveals a comparable situation as indicated for the electrical measurements in Section 5.4 as well. The combination of SnO_2 and gold on gold electrodes exhibits a higher sensor signal ($S = 16.20$) than the platinum containing sample ($S = 3.70$), putting the response behavior upon oxygen exposure significantly higher for $SnO_2 + Au$ and underlining the theory of an enhanced oxygen adsorption. Subsequently, the sensors were exposed to 250 ppm carbon monoxide. The calculated sensor signals are $S = 5.20$ for the $SnO_2 + Au$ mixture and $S = 11.07$ for the $SnO_2 + Pt$. These

results are a clear contradiction to the response behavior of the two sensor types (Au-electrode & Pt-electrode) at 200 °C. A detailed discussion about this phenomenon will follow at the end of this section after discussing the results at the higher temperatures.

Measurements at 250 °C - Figure 5.27 depicts the spectra of both samples measured at 250 °C in the same way as discussed before. The first observation is that the baseline of all spectra is moved closer together. Following the change from N₂ + 3 % D₂O to N₂ + 3 % D₂O + 1000 ppm O₂ (a) the following observations can be made: First, the peak at 2744 cm⁻¹ appears with an increased intensity for both samples in comparison to the measurement at 200 °C. This indicates a higher number of isolated OD groups on the surface of SnO₂. Second, the variation of peaks between 2703 and 2576 cm⁻¹ started to develop also for the platinum containing sample, although the intensity in the case of SnO₂ + 5 wt. % Au is still slightly higher. With the introduction of 250 ppm carbon monoxide is creating the same situation as before. The reaction of CO with adsorbed oxygen disturbs the mentioned equilibrium in such a way, that a reduction of the OD groups, which have been formed in the previous step, is clearly visible. While the formation of carbon monoxide is still apparent in the case of SnO₂ + 5 wt. % Pt - with a higher intensity - the direct adsorption of CO on platinum is missing. This could be related to the fact that, at elevated temperatures, the reaction rate is dramatically increased and the dwelling time of carbon monoxide on platinum is too short to be resolved in the spectrum. Also at this temperature

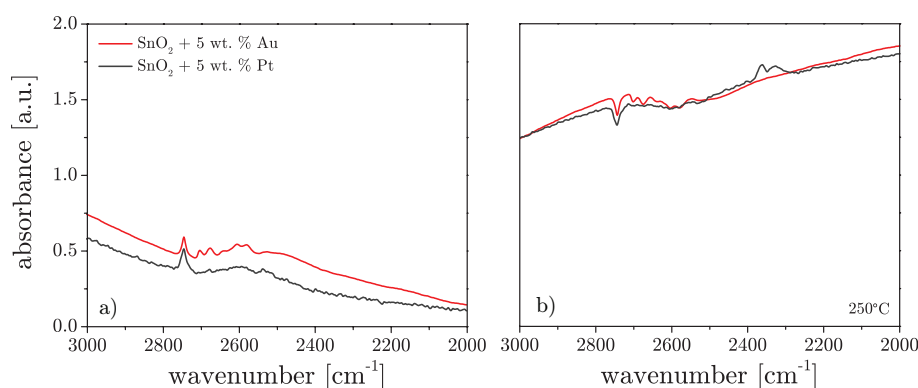


Figure 5.27: DRIFT spectra of the two different samples at 250 °C upon exposure to a) 1000 ppm O₂ (Reference: N₂ + 3 % D₂O) and b) 1000 ppm O₂ + 250 ppm CO (Reference: N₂ + 3 % D₂O + 1000 ppm O₂) in a background of N₂ + 3 % D₂O

the recorded mass spectrometer data (Figure 5.28) underscores the difference in the carbon monoxide turnover rate between gold and platinum containing samples. In relative terms, SnO₂ + 5 wt. % Pt has an increased combustion of carbon monoxide.

In Figure 5.29 the resistance measurement is plotted for both samples measured at

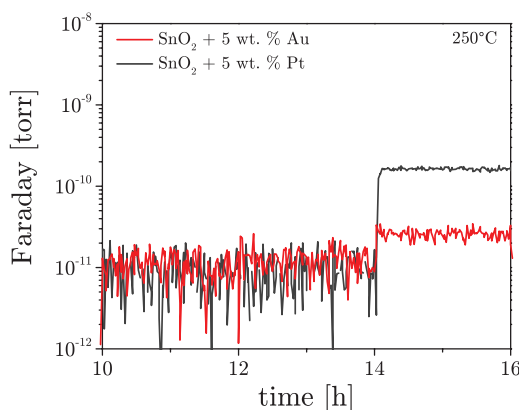


Figure 5.28: Mass spectrometer data recorded for the respective DRIFTS measurement at 250 °C. Gas atmosphere during hour (10 - 12): $N_2 + 3\% D_2O$ - (12 - 14): $N_2 + 3\% D_2O + 1000\text{ ppm } O_2$ - (14 - 16): $N_2 + 3\% D_2O + 1000\text{ ppm } O_2 + 250\text{ ppm } CO$

250 °C. As already mentioned, the baselines of the DRIFT spectra are closer at this temperature; an observation which can be made for the resistance values as well. In

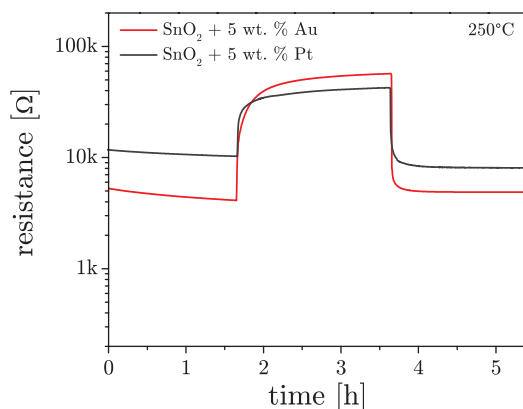


Figure 5.29: Time-dependent resistance measurement of the two different mixtures printed on substrates for the respective DRIFTS measurements at 250 °C. Gas atmosphere during hour (10 - 12): $N_2 + 3\% D_2O$ - (12 - 14): $N_2 + 3\% D_2O + 1000\text{ ppm } O_2$ - (14 - 16): $N_2 + 3\% D_2O + 1000\text{ ppm } O_2 + 250\text{ ppm } CO$

the absence of oxygen (or strictly speaking in oxygen lean conditions) the difference between $SnO_2 + 5\text{ wt. \% } Au$ and $SnO_2 + 5\text{ wt. \% }$ is still visible. The change to 1000 ppm oxygen is increasing the resistance as expected in both cases. For $SnO_2 + 5\text{ wt. \% } Au$ the relative change is higher than for $SnO_2 + 5\text{ wt. \% } Pt$. A sensor signal of 15.48 is obtained for the gold containing sample, while the platinum one gives a sensor signal of 6.18. In the case of carbon monoxide exposure the signals are $S = 15.05$ for $SnO_2 + 5\text{ wt. \% } Au$ and $S = 5.40$ for $SnO_2 + 5\text{ wt. \% }$. Here, the response is higher for $SnO_2 + Au$, which corresponds to the observations made in

the initial electrical measurements.

Measurements at 300 °C - In a further step the measurement sequence has been applied on the both samples heated up to 300 °C. Figure 5.30 shows the respective spectra corresponding to a change from $N_2 + 3\% D_2O$ to $N_2 + 3\% D_2O + 1000$ ppm O_2 (a) and to a change from $N_2 + 3\% D_2O + 1000$ ppm O_2 to $N_2 + 3\% D_2O + 1000$ ppm $O_2 + 250$ ppm CO (b).

The peak at 2744 cm^{-1} is the one with the highest intensity, which leads to the

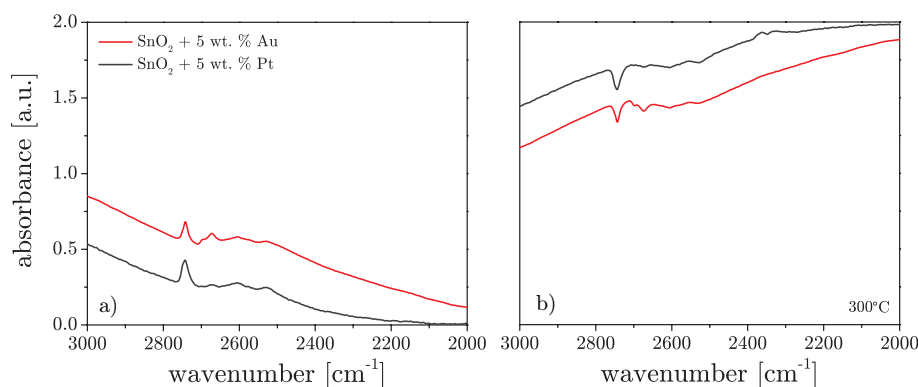


Figure 5.30: DRIFT spectra of the two different samples at 300 °C upon exposure to a) 1000 ppm O_2 (Reference: $N_2 + 3\% D_2O$) and b) 1000 ppm $O_2 + 250$ ppm CO (Reference: $N_2 + 3\% D_2O + 1000$ ppm O_2) in a background of $N_2 + 3\% D_2O$

conclusion that the terminal OD group is still the dominating species on the SnO_2 surface. Regarding the multiple peaks between 2703 and 2576 cm^{-1} one can assume certain similarity for both types of samples. In comparison to the measurement at 250 °C, those peaks became a little faint and blurry due to a natural broadening, which can be explained by the elevated temperature and the resulting shortened lifetime of the excited states. Therefore, it seems that all of them have lost in intensity. Also at this temperature, the introduction of 250 ppm carbon monoxide leads again to the expected observations. All species which have been built up in the former step are influenced by the carbon monoxide reaction and therefore decrease in the spectra. The MS data indicated that at the elevated temperature the carbon monoxide conversion increase, which correlates with the results gained in the conversion experiments.

The electrical measurement, which is shown in Figure 5.32, demonstrates once more the dependency of the actual resistance, in terms of free charge carrier concentration and the baseline shift in the DRFIT spectra. The difference in resistance upon exposure to certain gas compositions can be linked to the difference of the general

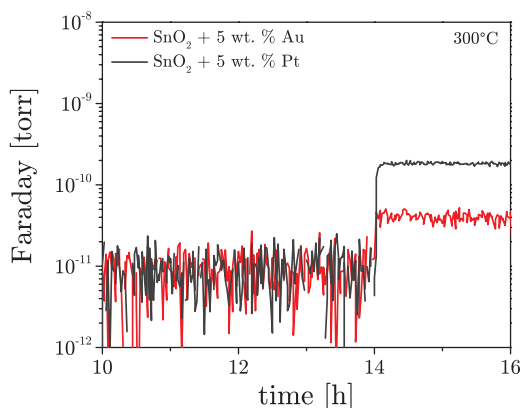


Figure 5.31: Mass spectrometer data recorded for the respective DRIFTS measurement at 300 °C. Gas atmosphere during hour (10 - 12): $N_2 + 3\% D_2O$ - (12 - 14): $N_2 + 3\% D_2O + 1000\text{ ppm } O_2$ - (14 - 16): $N_2 + 3\% D_2O + 1000\text{ ppm } O_2 + 250\text{ ppm } CO$

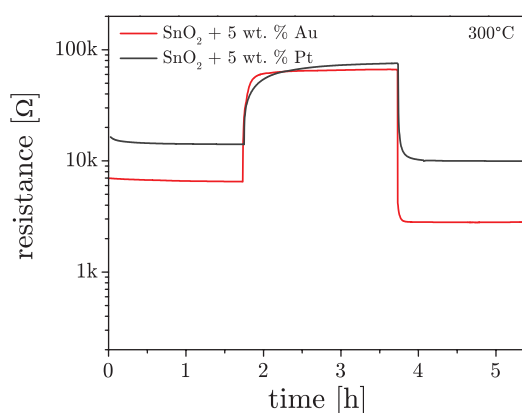


Figure 5.32: Time-dependent resistance measurement of the two different mixtures printed on substrates for the respective DRIFTS measurements at 300 °C. Gas atmosphere during hour (10 - 12): $N_2 + 3\% D_2O$ - (12 - 14): $N_2 + 3\% D_2O + 1000\text{ ppm } O_2$ - (14 - 16): $N_2 + 3\% D_2O + 1000\text{ ppm } O_2 + 250\text{ ppm } CO$

baseline in the absorbance spectra. The calculated sensor signals that corresponds to the introduction of 1000 ppm oxygen are 6.06 for $SnO_2 + 5\text{ wt. } \% Au$ and 7.32 for $SnO_2 + 5\text{ wt. } \% Pt$. This parity is in line with the observations made in Section 5.4. In Figure 5.15 the sensor signals upon exposure to different levels of oxygen are higher for the gold mixture up to a temperature of 250 °C. The "changing point" - the working temperature of the sensor at which the dominating effect of the sensors with gold electrode is no longer apparent - could be situated at around 300 °C.

Measurements at 350 °C - Finally, like in all previous experiments, both samples have been measured at 350 °C. Figure 5.33 shows the spectra for event a) (introduction of 1000 ppm oxygen) as well as event b) (introduction of 250 ppm carbon monoxide).

The distinguishable peak at 2703 cm^{-1} now has the same intensity as the peak at

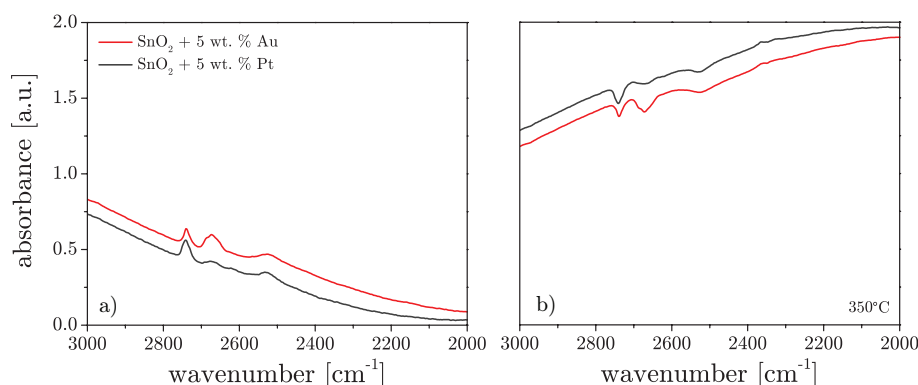


Figure 5.33: DRIFT spectra of the two different samples at $350\text{ }^{\circ}\text{C}$ upon exposure to a) 1000 ppm O_2 (Reference: $\text{N}_2 + 3\% \text{ D}_2\text{O}$) and b) $1000\text{ ppm O}_2 + 250\text{ ppm CO}$ (Reference: $\text{N}_2 + 3\% \text{ D}_2\text{O} + 1000\text{ ppm O}_2$) in a background of $\text{N}_2 + 3\% \text{ D}_2\text{O}$

2744 cm^{-1} . While the peaks at 2678 and 2605 cm^{-1} are no longer visible the peak at 2576 cm^{-1} becomes extremely broad and lost in intensity. Summarizing, it can be said, that the higher the temperature the more dominating the peaks at higher wavenumbers, while peaks at lower wavenumbers decreased or almost disappeared.

The data gathered from the MS measurement indicates the highest CO conversion

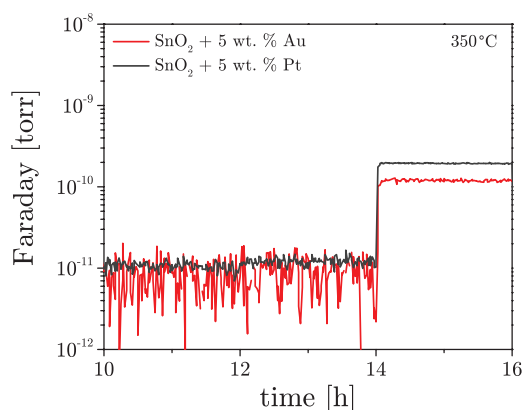


Figure 5.34: Mass spectrometer data recorded for the respective DRIFTS measurement at $350\text{ }^{\circ}\text{C}$. Gas atmosphere during hour (10 - 12): $\text{N}_2 + 3\% \text{ D}_2\text{O}$ - (12 - 14): $\text{N}_2 + 3\% \text{ D}_2\text{O} + 1000\text{ ppm O}_2$ - (14 - 16): $\text{N}_2 + 3\% \text{ D}_2\text{O} + 1000\text{ ppm O}_2 + 250\text{ ppm CO}$

at $350\text{ }^{\circ}\text{C}$, although this does not mean that this results in a higher change in conductance. A significant amount might be consumed directly on the noble metal and therefore has not any influence on the free charge carrier concentration in the metal oxide.

The change in resistance upon exposure to oxygen can be expressed as sensor signal with a value of 5.5 for the platinum containing sample and with a value of

3.33 for the gold containing one.

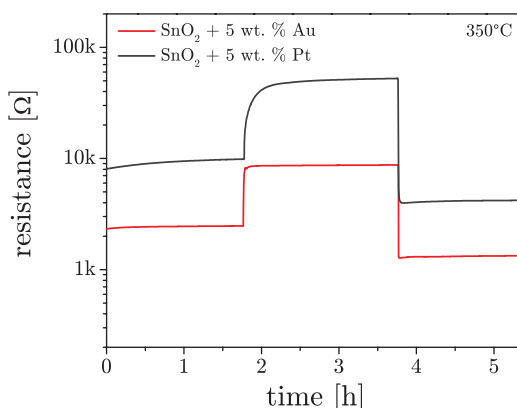


Figure 5.35: Time-dependent resistance measurement of the two different mixtures printed on substrates for the respective DRIFTS measurements at 350 °C. Gas atmosphere during hour (10 - 12): N₂ + 3 % D₂O - (12 - 14): N₂ + 3 % D₂O + 1000 ppm O₂ - (14 - 16): N₂ + 3 % D₂O + 1000 ppm O₂ + 250 ppm CO

5.7.2 Discussion & Summary

The present results strongly confirm a difference in surface chemistry at the lowest working temperature (200 °C); with increasing the temperature the spectra become similar. The main difference can be found in the region of the OD groups, where certain species are more pronounced in the case of SnO₂ + 5 wt. % Au at lower temperature. To understand the differences, a discussion about the different OD groups is necessary. In IR spectra, OD groups are simply mirroring OH groups, but due to a replacement of the hydrogen atom with a deuterium atom and the resulting increase in the reduced mass, the bands are shifted towards lower wavenumbers. Calculations give a value of 0,703 for this shift [Gro12a]. For this reasons, the discussion about the different OD groups can be held on the basis of OH groups respectively.

It is assumed that the reaction of water with pre-adsorbed oxygen to terminal OH-groups is the principal reaction [Sch91]. The relative wide broadening or multiple various peaks in case of better resolved spectra can be attributed to a variety of factors, including a highly distorted surface with steps, edges, nooks and other irregularities such as a variable amount of vacancies, which can dramatically change the situation, especially when it comes to an interaction between hydroxyl groups. Further, on neighboring, sterically favored OH groups, H-bonding between those groups is perfectly possible to achieve. All these variations result in a wide range of different peaks.

Basically, a distinction can be made between resonances in the higher wavenumber range ($> 3600 \text{ cm}^{-1}$) and resonances in the lower wavenumber range ($3200 - 3600 \text{ cm}^{-1}$). Many authors have attributed the higher wavenumbers to the isolated terminal OH groups and the lower wavenumbers to the ones which interact via H-bonds [AP01; Jon71; Pri71]. In general, the OH stretching vibration of a hydroxyl group appears at lower wavenumbers and is broadened in case of H-bond interactions [Dav03]. These assumptions are supported by the observations made in outgassing experiments (Figure 5.36). With increasing the temperature, a broadened band with a maximum at around 3200 cm^{-1} is decreasing. This band is assumed to originate from OH groups bond to each other by hydrogen bridges and therefore more suitable for removal from the surface as water [Ser02]. Since pre-adsorbed oxygen plays a key

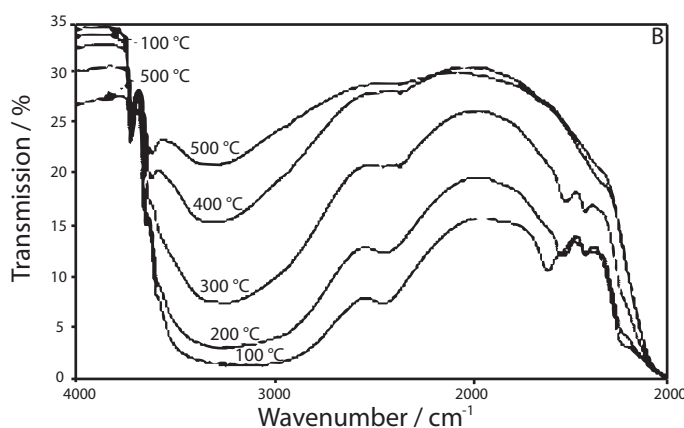


Figure 5.36: FTIR spectra of a SnO_2 sample showing temperature dependent intensities of bands ($3000 - 3500 \text{ cm}^{-1}$) which can be ascribed to H-bonded hydroxyl groups. For more details see [Ser02].

role for the formation of OH groups (see Section 2.2.3), the existence of such species can be a decisive factor for the formation of multiple hydroxyl-groups on the tin oxide surface. It is presumed that the gold particles in the sample as well as the gold electrode enhance or activate the oxygen adsorption. Hence, more oxygen is available on the surface and therefore an increased number of potential reaction partners for gaseous water. From a statistical point of view the formation of neighboring OH-groups is far more likely. Platinum, on the other hand, is not prominent for such an effect. Nevertheless, SnO_2 -sensors with platinum electrodes or rather $\text{SnO}_2 + \text{Pt}$ mixtures respond to an oxygen increase in electrical measurements at $200 \text{ }^\circ\text{C}$, even if only with reduced intensity. Thus, the disparity in the DRIFTS spectra can be explained: In the case of $\text{SnO}_2 + 5 \text{ wt. } \% \text{ Pt}$ terminal OD groups are dominant in the spectrum (2744 cm^{-1}), but fairly low activity in the range of 2500 and 2700

cm^{-1} ; while the spectrum of the gold containing sample obviously shows peaks with higher intensities at lower wavenumbers (multiple peaks in the region between 2500 and 2700 cm^{-1}). Therefore, one can assume a larger amount of OD groups in the case of $\text{SnO}_2 + 5 \text{ wt. } \% \text{ Au}$.

A temperature increase lowers the significance of the spill-over effect. The thermal energy becomes sufficiently high to adsorb a proper amount of oxygen directly on the metal oxide surface and therefore enables the formation of a similar amount of OD groups in both cases. This explains the alignment of the spectra in the specific region (2500 - 2700 cm^{-1}). At 300 °C both spectra have more or less the same characteristics. A second effect of increasing the temperature is the earlier discussed removal of H-bonded OH groups as water. Also this effect can be observed in the present results for both types of samples, where bands in between 2500 - 2700 cm^{-1} are losing in overall intensity with increasing the temperature.

Table 5.3: Overview of the calculated sensors signals for the different gas exposures within the DRIFTS experiments at 200, 250, 300 % 350 °C

	CO [ppm]	O ₂ [ppm]	D ₂ O [% r.H.]	Sensor Signal (SnO ₂ + Au)	Sensor Signal (SnO ₂ + Pt)
200 °C	0	0	3		
	0	1000	3	16.20	3.70
	250	1000	3	5.20	11.07
250 °C	0	0	3		
	0	1000	3	15.48	6.18
	250	1000	3	15.05	5.40
300 °C	0	0	3		
	0	1000	3	6.06	7.32
	250	1000	3	20.52	7.90
350 °C	0	0	3		
	0	1000	3	3.33	5.50
	250	1000	3	5.47	19.73

As observed in the evaluation of the measurement at 200 °C, the sensor signal for the carbon monoxide exposure revealed a disagreement with the observations made in the experiments shown in Section 5.2. Table 5.3 provides an overview

of all calculated sensor signals for the different gas exposures within the DRIFTS experiments. It is clearly visible that a clear trend can be identified, whereupon an increase in the oxygen concentration delivers the higher sensor signals for $\text{SnO}_2 + \text{Au}$ at 200 °C and 250 °C. In principle, an analogous tendency for the carbon monoxide exposure is visible starting from 250 °C. The only exception is the measurement at 200 °C. Electrical measurement upon exposure to carbon monoxide in lean oxygen background can shed light on this feature. Therefore, the electrical response of a set of sensors (SnO_2 at Au-electrodes & SnO_2 at Pt-electrodes) have been measured upon exposure to 200 ppm carbon monoxide in a background of 100 ppm oxygen and 500 ppm oxygen (Figure 5.37). At 200 °C the sensor signal for both types of sensors is similarly high when exposing them to carbon monoxide in 100 ppm O_2 . By increasing the oxygen concentration up to 500 ppm, the sensor signal of the sensor with platinum electrodes stays at a similar value as calculated in a background of 100 ppm, while the sensor signal of the sensor equipped with gold electrodes is decreasing. At 250 °C the sensor signals captured at a background of 500 ppm oxygen are smaller for both types of sensors, but with the addition of a higher signal for the sensor with gold electrodes. At 300 °C, the difference in oxygen concentration still affects the sensor signal: In low oxygen concentrations the sensor signals are larger than in higher oxygen concentrations, but interestingly the signal for the platinum electrode sensors exceeds once again the gold electrode sensor signal, which refers to the aforementioned "changing point". Hübner et al. stated in their work about the reaction mechanism of reducing gases in absence of oxygen that carbon monoxide reacts mainly by creating donor states on the surface as long as the concentration of oxygen will not exceed the concentration of carbon monoxide [Hue11a]. The latter measurements have been performed in 100 ppm oxygen and in 500 ppm oxygen. Considering the work of Hübner et al. the reaction of 200 ppm carbon monoxide in these measurements will follow the "donor-state"-reaction mechanism, while at 500 ppm oxygen carbon monoxide will react with the ionosorbed oxygen to carbon dioxide. The higher sensor signals - for 200 ppm carbon monoxide in 100 ppm oxygen - are a clear evidence for this consideration. This holds true as long as the available oxygen in the atmosphere is really ionosorbed on the tin oxide surface. Within this work, it could be considerably demonstrated that the amount of ionosorbed oxygen on SnO_2 (in contact with Pt) is not as high as on SnO_2 (in contact with Au) at 200 °C. With a high probability, at 200 °C and a given oxygen concentration of 500 ppm but also at a oxygen concentration of 1000 ppm (as measured in the latter DRIFTS

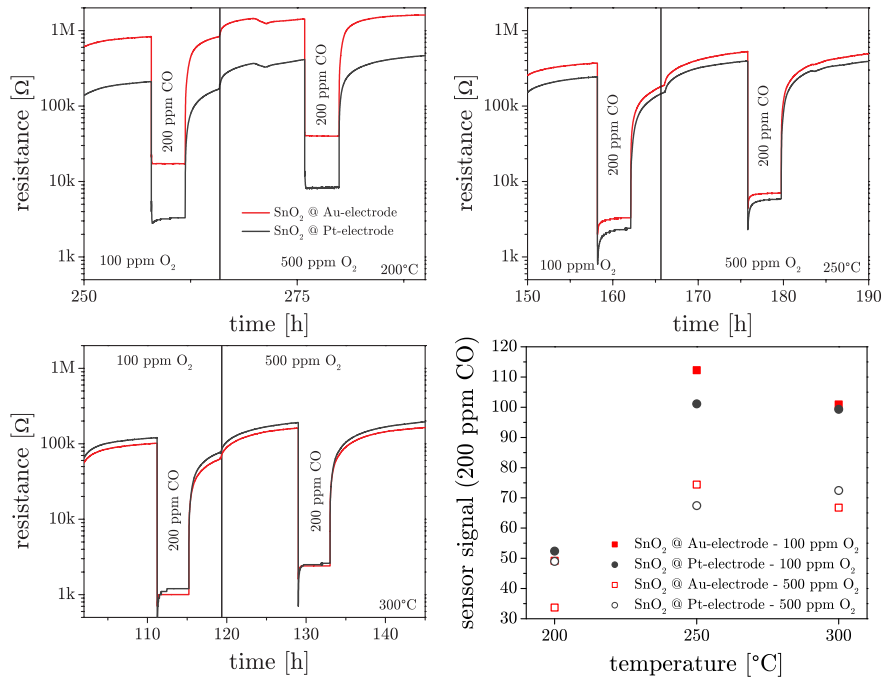


Figure 5.37: Electrical Measurement of SnO₂ thick film sensors with gold electrodes and platinum electrodes at 200, 250 and 300 °C. Measurements performed in nitrogen with different levels of oxygen background concentration (100 & 200 ppm). The sensors were exposed to a pulse of 200 ppm of carbon monoxide at each oxygen background condition.

measurements), the amount of ionosorbed oxygen on the SnO₂ + Pt samples is effectively smaller than the amount of carbon monoxide and the reaction mechanism is going into the direction of the donor-state scenario resulting in a higher sensor signal; while in the case of gold containing samples the spill-over effect is providing enough ionosorbed oxygen to have the ordinary reaction mechanism. Especially the similarity of the sensor signals (for carbon monoxide) for sensors equipped with platinum electrodes measured at 200 °C in 100 ppm and 500 ppm oxygen emphasizes this theory. With increasing the temperature, the spill-over effect is no longer the crucial factor for the oxygen ionosorption, which results in the expected behavior of gold-electrode and platinum-electrode sensors when exposing them to carbon monoxide.

CHAPTER 6

Summary

Increasingly scarce resources and the stringent rules and regulations of most governments make it necessary to gain a fundamental understanding of different material parameters opening the possibility for alternatives. A generally applicable comprehension of such parameters can be used not only for a better understanding of certain results in basic research, but also for application oriented R&D. Thus, the dissertation aims at assessing the influence of the nature of the electrode on the performance of SnO₂ thick film gas sensors.

For SnO₂ thick film gas sensors, as discussed within this work, the electrical influence of the electrode contact is negligible and the sensor performance differences, which depend on the temperature and the material of the electrode, seem to be linked to the three phase boundary impact on the surface chemistry. Extensive electrical measurements provided meaningful data, indicating a significant increase of the sensor performance at lower temperatures by using gold electrodes. With knowledge of the reaction mechanism of target gases like hydrogen and carbon monoxide, it was demonstrated that the sensing process is not only influenced by the reaction of the specific target gas, but also by the availability of the reaction partner, which is ionosorbed oxygen. Considering the sensing of a reducing gas molecule as a two-step process, the crucial and limiting factor in this regard is then the first step - the ionosorption of oxygen. Indeed, DC resistance measurements at different levels of oxygen corroborated the trend that, especially at lower temperatures, sensors with gold electrodes are showing a better response towards oxygen. This clearly underlines the ideas about enhanced oxygen activation on metallic gold at the three-phase boundary (spill-over effect).

Further, the catalytic conversion of carbon monoxide was significantly increased for

powder mixtures of SnO₂ and gold, whereas for pure SnO₂ or pure gold this couldn't be observed, which is in turn another indication for a synergy effect between gold and SnO₂. Finally, spectroscopic measurements brought the proof, albeit indirectly, that at lower temperatures, gold supports or rather activates the adsorption of oxygen on the metal oxide surface and therefore increases the number of potential reaction partners for certain gases like carbon monoxide, hydrogen or rather water. The presence of certain surface species detected for gold containing samples, can be explained only by the increased concentration of ionosorbed oxygen. Figure 6.1

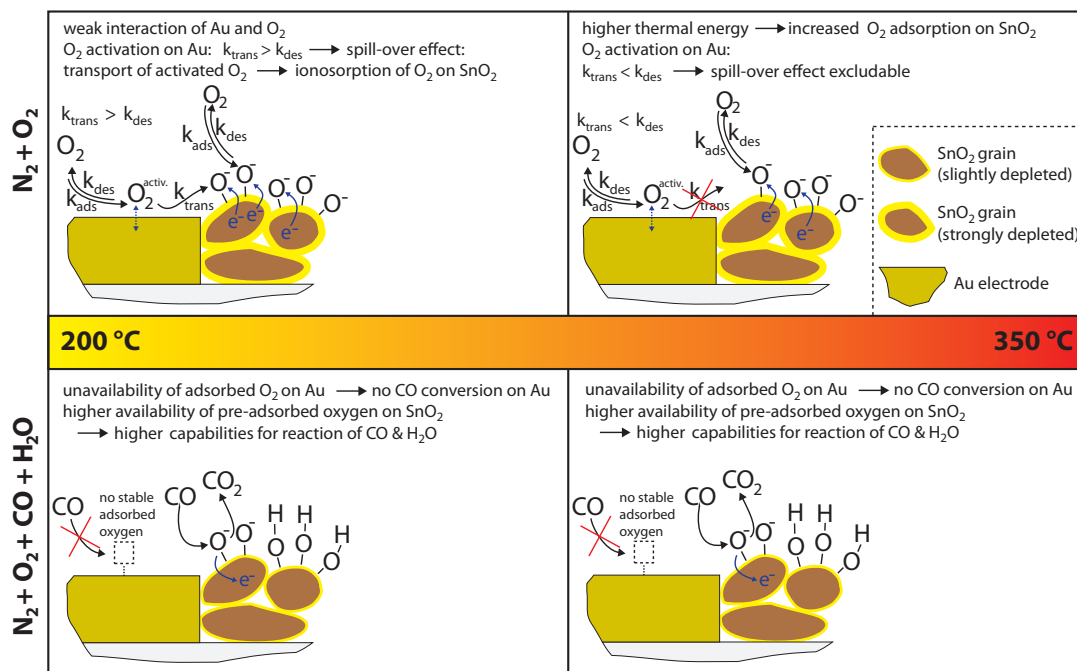


Figure 6.1: Summary of findings and assumed activities on the three phase boundary in the case of gold electrodes.

presents a model illustration of the expected processes at the three phase boundary and summarizes them by the example of N₂ and O₂ as well as N₂, O₂, CO and H₂O exposure at different working temperatures of a SnO₂ thick film sensor. In the presence of N₂ and O₂ at the lowest temperature around 200 °C, one can expect a weak interaction of gold and oxygen. Still, oxygen is activated on gold and further transported to a neighboring SnO₂ grain, where it gets ionosorbed and is increasing the depletion layer (Figure 6.1 - top left). Due to the enhanced availability of ionosorbed oxygen on SnO₂ and no adsorbed oxygen on the metallic gold, carbon monoxide dominantly reacts with the ionosorbed oxygen by releasing electrons and decreasing the depletion layer, while water forms hydroxyl groups (Figure 6.1 - bottom left). At higher temperatures the desorption of the activated oxygen species

on gold has a higher probability than a further transport to the SnO_2 grain. This reduces the probability of a spill-over effect. Anyhow, one can expect an increased direct ionosorption of oxygen on SnO_2 due to the higher thermal energy (Figure 6.1 - top right). In the presence of carbon monoxide and water the situation is comparable to the one described before. While CO consumes the ionosorbed oxygen and releasing the captured electrons, water forms hydroxyl groups with the oxygen species on the SnO_2 surface (Figure 6.1 - bottom right).

A negative aspect is that sensors with platinum electrodes have shown lower signals at lower working temperatures. Catalytic conversion measurements confirmed the assumption that a significant amount of the target gas is consumed by the noble metal electrodes. The platinum was especially active, as it has been demonstrated by spectroscopic measurements. In this case, the consumption of the target gas will not influence the electrical properties of the metal oxide which correspondingly leads to a smaller signal. Figure 6.2 summarizes the findings for the Pt / SnO_2 interface. The

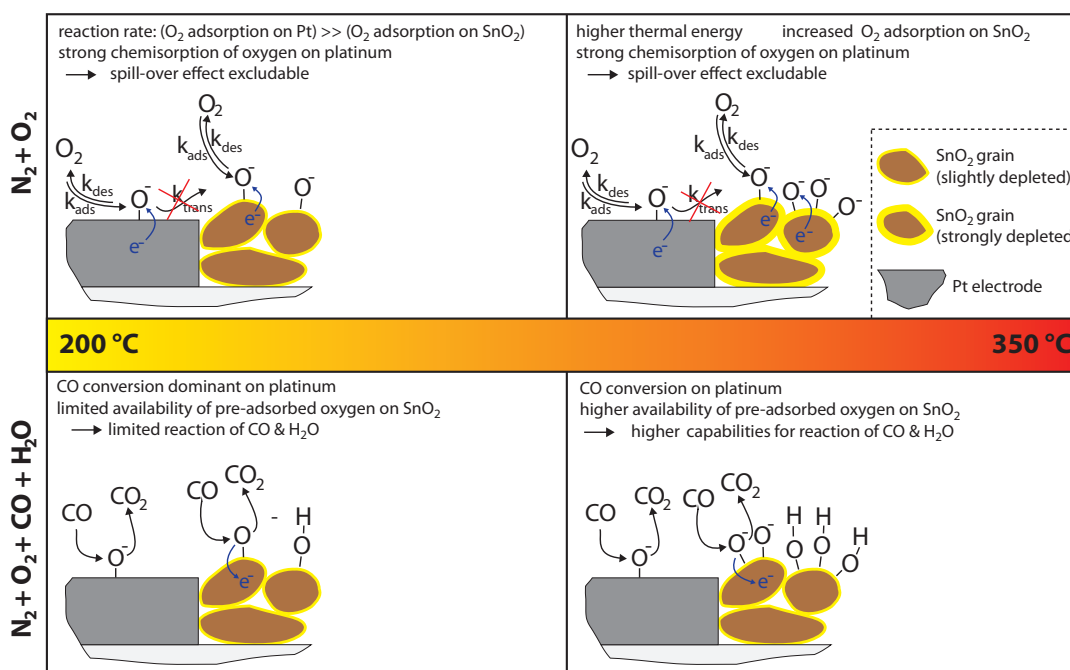


Figure 6.2: Summary of findings and assumed activities on the three phase boundary in the case of platinum electrodes.

strong chemisorption of oxygen on platinum excludes a spill-over effect. Thus, the amount of ionosorbed oxygen on SnO_2 and the resulting influence on the depletion layer is not as large as in the case of the Au / SnO_2 interface (Figure 6.2 - top left). When exposed to carbon monoxide and water, the direct CO conversion on platinum is the dominant route, while only limited capabilities in terms of adsorbed

oxygen on SnO_2 are available for the reaction of CO and the formation of hydroxyl groups on SnO_2 (Figure 6.2 - bottom left). At a higher temperature (≥ 300 °C) an absorption of oxygen on platinum is still possible, but in addition a higher thermal energy enables the direct ionosorption of oxygen on SnO_2 . Thus, the amount of ionosorbed oxygen on SnO_2 is no longer dependent on the spill-over effect (Figure 6.2 - top right). In the presence of CO and H_2O enough ionosorbed oxygen is available for a reaction of carbon monoxide on the SnO_2 and for the formation of hydroxyl groups. Still, the direct conversion of CO on platinum plays a major role (Figure 6.2 - bottom right).

To conclude the beneficial effect of gold electrodes seems to be valid only for lower working temperatures. At higher temperatures, the demonstrated spill-over effect is no longer relevant. Both in electrical and in spectroscopic measurements, the results of both materials have converged. An increased thermal energy, which is given to the system facilitates the direct adsorption of oxygen on the metal oxide and diminishes the role of the three-phase boundary.

CHAPTER 7

Outlook

Although the main reasons for different sensor performance with different electrode materials is elucidated, it is worth to note that certain aspects have not been truly clarified and it is still a long way for a full understanding or quantification of the implied mechanisms. Activated states of the adsorbates, respectively intermediates which are responsible for the charge transfer couldn't be ascertained up to now.

Especially the activation of oxygen, which is ascribed to the gold electrode or metallic gold in general within this work, is and will be the subject of current research and scientific discussion - but not only in the metal oxide sensor community. Unfortunately, the identification of the activated oxygen species could not be achieved, as the methods for investigating adsorbed oxygen which are applicable on a working sensor system are rather limited, as described in the previous chapters. However, approaches can be applied which narrow down the possible bonding capacities of the oxygen molecule on gold respectively SnO₂. First of all, in order to cause an electrical effect on a sensor, the ionosorption - that means the transfer of an electron into the adsorbed species - has to take place on the SnO₂. Apart from that, a direct oxidation of the gold itself is extremely unlikely; this fact is well supported by numerous surveys and considerations according to which an oxidation of gold is very much depending on the size of the gold cluster and has been indicated only on very small nano-particles so far [Bok09]. This excludes a Fermi control mechanism, where an electron from the gold is trapped by the adsorbed oxygen and further compensated by an interchange with SnO₂. As previously mentioned, there is a limitation of a strong interaction between metallic gold and oxygen. For the standard enthalpy of formation $d_f H_{298}^\circ$, values between -13 [Ash72] and 81 *kJ/mol* have been reported [Got03]. To adopt an initial, spontaneous interaction or activation of oxygen on the gold surface ($dG < 0$)

anyway, high entropy based on a high mobility of the weakly-bond oxygen must be presumed. The increased mobility of activated oxygen on the metallic gold would be a further indication for the assumed spillover effect. The activation of oxygen could be described on the basis of a temporary back donation of electrons from the gold to a pi^* antibonding orbital of the oxygen [Bak11]. In that case the O-O bond is weakened while a formed Au-O₂ bond would be strengthened by the back donation. Generally, the interaction between an adsorbate and a metallic surface can be described in a two-step process [Kol12]. In a first step an adsorbate orbital interacts with the s band of the metal, which is usually very broad. According to the Anderson-Grimley-Newns approach, this leads to an interaction of the weak chemisorption type [And61; Gri76; New69], but since the bonding level lies below the Fermi-level in the case of Au, the interaction is appealing. In the next step, the newly created bonding level interacts with the narrow d -band of the metal, which leads to the formation of a bonding and an antibonding state. However, due to the unfavorable position of the d -band in Au, which is below the Fermi-level, the antibonding state is fully occupied and neutralize the intensified interaction from step one (Figure 7.1) [Kol12].

This discussion is only a very early step to enter into a debate on the matter.

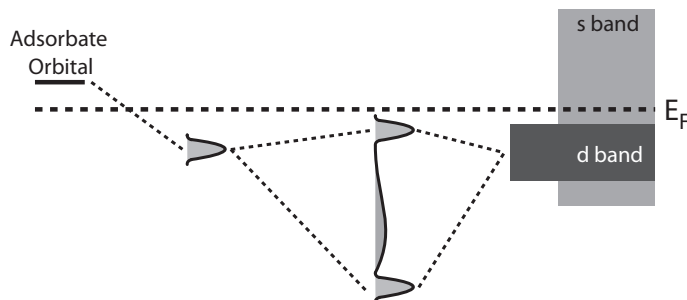


Figure 7.1: Chemisorption of adsorbents on metal surfaces as a two-step process. After [Kol12].

Hence, the research on activated states on metal oxide and noble metals surfaces must be investigated further. In general, there are some additional methods which are capable of determining surface species or give information about the chemical state of the adsorbent:

- Raman-spectroscopy could round-up the informations gathered by DRIFTS spectroscopy. In particular, it would be possible to investigate the adsorbed oxygen species
- EXAFS (Extended X-ray Adsorption Fine Structure) and XANES (X-ray

Absorption Near Edge Structure) measurement are one possible way to get an idea about the chemical state of the noble metal, dependent on the gas atmosphere

In any case, the most important thing of all additional techniques is - and will remain - the feasibility of operando measurements.

Bibliography

- [AP01] D. AMALRIC-POPESCU and F. BOZON-VERDURAZ: ‘Infrared studies on SnO₂ and Pd/SnO₂’. In *Catalysis Today* (Oct. 2001), vol. 70(1-3): pp. 139–154 (cit. on p. 107).
- [And61] P. ANDERSON: ‘Localized Magnetic States in Metals’. In *Physical Review* (Oct. 1961), vol. 124(1): pp. 41–53 (cit. on p. 116).
- [Ash72] S. J. ASHCROFT and E. SCHWARZMANN: ‘Standard enthalpy of formation of crystalline gold (III) oxide’. In *Journal of the Chemical Society, Faraday Transactions 1: Physical Chemistry in Condensed Phases* (1972), vol. 68(0): pp. 1360–1361 (cit. on p. 115).
- [Atk06] PETER ATKINS and J. DE PAULA: ‘Atkins Physical Chemistry 2002’. In *Oxford University Press, New York* (2006), vol. (cit. on pp. 23, 55).
- [Bak11] THOMAS BAKER, XIAOYING LIU, and CYNTHIA M. FRIEND: ‘The mystery of gold’s chemical activity: local bonding, morphology and reactivity of atomic oxygen.’ In *Physical chemistry chemical physics : PCCP* (Jan. 2011), vol. 13(1): pp. 34–46 (cit. on p. 116).
- [Bar02] M.-I. BARATON, L. MERHARI, H. FERKEL, and J.-F. CASTAGNET: ‘Comparison of the gas sensing properties of tin, indium and tungsten oxides nanopowders: carbon monoxide and oxygen detection’. In *Materials Science and Engineering: C* (Jan. 2002), vol. 19(1-2): pp. 315–321 (cit. on p. 28).
- [Bar11] NICOLAE BARSAN, MICHAEL HÜBNER, and UDO WEIMAR: ‘Conduction mechanisms in SnO₂ based polycrystalline thick film gas sensors exposed to CO and H₂ in different oxygen backgrounds’. In *Sensors and Actuators B: Chemical* (Oct. 2011), vol. 157(2): pp. 510–517 (cit. on p. 69).

- [Bar01] NICOLAE BARSAN and UDO WEIMAR: ‘Conduction model of metal oxide gas sensors’. In *Journal of Electroceramics* (2001), vol. 7(3): pp. 143–167 (cit. on pp. 25, 28, 29, 35, 36).
- [Bar99] NICOLAE BARSAN, MARKUS SCHWEIZER-BERBERICH, and WOLFGANG GÖPEL: ‘Fundamental and practical aspects in the design of nanoscaled SnO₂ gas sensors: a status report’. In *Fresenius’ journal of ...* (1999), vol. (June): pp. 287–304 (cit. on pp. 8, 9, 27, 28, 68, 70).
- [Bar07] NICOLAE BARSAN, DOROTA KOZIEJ, and UDO WEIMAR: ‘Metal oxide-based gas sensor research: How to?’ In *Sensors and Actuators B: Chemical* (Jan. 2007), vol. 121(1): pp. 18–35 (cit. on pp. 53, 61, 88).
- [Bar03] NICOLAE BARSAN and UDO WEIMAR: ‘Understanding the fundamental principles of metal oxide based gas sensors; the example of CO sensing with SnO₂ sensors in the presence of humidity’. In *Journal of Physics: Condensed Matter* (May 2003), vol. 15(20): R813–R839 (cit. on pp. 50, 78).
- [Bat05] M. BATZILL and ULRIKE DIEBOLD: ‘The surface and materials science of tin oxide’. In *Progress in Surface Science* (2005), vol. 79(2-4): pp. 47–154 (cit. on pp. 25, 69).
- [Ber96] F. BERGER, E. BECHE, R. BERJOAN, D. KLEIN, and A. CHAMBAUDET: ‘An XPS and FTIR study of SO₂ adsorption on SnO₂ surfaces’. In *Applied Surface Science* (Jan. 1996), vol. 93(1): pp. 9–16 (cit. on p. 27).
- [Ber81] STEVEN L. BERNASEK and STEPHEN R. LEONE: ‘Direct detection of vibrational excitation in the CO₂ product of the oxidation of CO on a platinum surface’. In *Chemical Physics Letters* (Dec. 1981), vol. 84(2): pp. 401–404 (cit. on p. 84).
- [Bie57] A. BIELANSKI, J. DEREN, and J. HABER: ‘Electric conductivity and catalytic activity of semiconducting oxide catalysts’. In *Nature* (Mar. 1957), vol. 179(4561): pp. 668–669 (cit. on p. 5).
- [Bla06] M. BLASCHKE, T. TILLE, P. ROBERTSON, S. MAIR, UDO WEIMAR, and HEIKO ULMER: ‘MEMS Gas-Sensor Array for Monitoring the Perceived Car-Cabin Air Quality’. In *IEEE Sensors Journal* (Oct. 2006), vol. 6(5): pp. 1298–1308 (cit. on p. 9).

- [Bok09] JEROEN A. van BOKHOVEN: *Catalysis by Gold: Why Size Matters*. 2009 (cit. on p. 115).
- [Bok06] JEROEN A. van BOKHOVEN, CATHERINE LOUIS, JEFFREY T. MILLER, MONIEK TROMP, OLGA V. SAFONOVA, and PIETER GLATZEL: ‘Activation of oxygen on gold/alumina catalysts: in situ high-energy-resolution fluorescence and time-resolved X-ray spectroscopy.’ In *Angewandte Chemie (International ed. in English)* (2006), vol. 45: pp. 4651–4654 (cit. on p. 71).
- [Boy77] J. F. BOYLE and K. A. JONES: ‘The effects of CO, water vapor and surface temperature on the conductivity of a SnO₂ gas sensor’. In *Journal of Electronic Materials* (Nov. 1977), vol. 6(6): pp. 717–733 (cit. on p. 28).
- [Bra53] WALTER H. BRATTAIN and JOHN BARDEEN: ‘Surface Properties of Germanium’. In *Bell System Technical Journal* (1953), vol. 32(1): pp. 1–41 (cit. on p. 5).
- [Bri13] D. BRIAND and J. COURBAT: ‘Micromachined semiconductor gas sensors’. In *Semiconductor gas sensors*. Woodhead Publishing Limited, 2013: pp. 220–258 (cit. on p. 9).
- [Cam80] C. T. CAMPBELL, G. ERTL, H. KUIPERS, and J. SEGNER: ‘A molecular beam study of the catalytic oxidation of CO on a Pt(111) surface’. In *The Journal of Chemical Physics* (1980), vol. 73(11): p. 5862 (cit. on p. 84).
- [Cap06] SIMONETTA CAPONE, MAURO EPIFANI, LUCA FRANCIOSO, SAULIUS KACIULIS, ALESSIO MEZZI, PIETRO SICILIANO, and ANTONELLA M. TAURINO: ‘Influence of electrodes ageing on the properties of the gas sensors based on SnO₂’. In *Sensors and Actuators B: Chemical* (May 2006), vol. 115(1): pp. 396–402 (cit. on p. 37).
- [Cap01] SIMONETTA CAPONE, PIETRO SICILIANO, F. QUARANTA, R. RELLA, MAURO EPIFANI, and L. VASANELLI: ‘Moisture influence and geometry effect of Au and Pt electrodes on CO sensing response of SnO₂ microsensors based on sol-gel thin film’. In *Sensors and Actuators B: Chemical* (June 2001), vol. 77(1-2): pp. 503–511 (cit. on pp. 37, 39, 40).
- [Cav95] R. E. CAVICCHI, J. S. SUEHLE, K. G. KREIDER, M. GAITAN, and P. CHAPARALA: ‘Fast temperature programmed sensing for micro-hotplate gas sensors’. In *IEEE Electron Device Letters* (June 1995), vol. 16(6): pp. 286–288 (cit. on p. 9).

- [Cha80] SHIH–CHIA CHANG: ‘Oxygen chemisorption on tin oxide: Correlation between electrical conductivity and EPR measurements’. In *Journal of Vacuum Science and Technology* (Jan. 1980), vol. 17(1): p. 366 (cit. on pp. 25, 70).
- [Chi92] AKIRA CHIBA: ‘Development of the TGS Gas Sensor’. In *Chemical Sensor Technology*. Ed. by S YAMAUCHI. Bd. 4. Elsevier Science, 1992 (cit. on pp. 7, 33).
- [Com06] ELISABETTA COMINI: ‘Metal oxide nano-crystals for gas sensing.’ In *Analytica chimica acta* (May 2006), vol. 568(1-2): pp. 28–40 (cit. on p. 15).
- [Cou91] GEORGE W. COULSTON and GARY L. HALLER: ‘The dynamics of CO oxidation on Pd, Rh, and Pt studied by high-resolution infrared chemiluminescence spectroscopy’. In *The Journal of Chemical Physics* (1991), vol. 95(9): p. 6932 (cit. on p. 84).
- [Cou12] J. COURBAT, D. BRIAND, L. YUE, S. RAIBLE, and N. F. de ROOIJ: ‘Drop-coated metal-oxide gas sensor on polyimide foil with reduced power consumption for wireless applications’. In *Sensors and Actuators B: Chemical* (Jan. 2012), vol. 161(1): pp. 862–868 (cit. on p. 9).
- [Cox83] P. A. COX, F. W. H. DEAN, and A. A. WILLIAMS: ‘Electrostatic models for surfaces of ionic crystals’. In *Vacuum* (Oct. 1983), vol. 33(10-12): pp. 839–841 (cit. on p. 22).
- [Dav03] ANATOLI DAVYDOV: *Molecular Spectroscopy of Oxide Catalyst Surfaces*. Chichester, UK: John Wiley & Sons, Ltd, Apr. 2003: p. 690 (cit. on pp. 27, 88–90, 94, 99, 107).
- [De 94] P. DE PADOVA, M. FANFONI, R. LARCIPRETE, M. MANGIANTINI, S. PRIORI, and P. PERFETTI: ‘A synchrotron radiation photoemission study of the oxidation of tin’. In *Surface Science* (July 1994), vol. 313(3): pp. 379–391 (cit. on p. 19).
- [Dem88] V. DEMARNE and A. GRISEL: ‘An integrated low-power thin-film CO gas sensor on silicon’. In *Sensors and Actuators* (Apr. 1988), vol. 13(4): pp. 301–313 (cit. on p. 8).

- [Dje09] IGOR DJERDJ, ALEXANDER HAENSCH, DOROTA KOZIEJ, SUMAN POKHREL, NICOLAE BARSAN, UDO WEIMAR, and MARKUS NIEDERBERGER: ‘Neodymium Dioxide Carbonate as a Sensing Layer for Chemoresistive CO₂ Sensing’. In *Chemistry of Materials* (Nov. 2009), vol. 21(22): pp. 5375–5381 (cit. on p. 5).
- [Dur06] S. M. DURRANI: ‘The influence of electrode metals and its configuration on the response of tin oxide thin film CO sensor.’ In *Talanta* (Feb. 2006), vol. 68(5): pp. 1732–5 (cit. on p. 37).
- [Dut92] PASCALE DUTRONC, BERTRAND CARBONNE, FRANCIS MENIL, and CLAUDE LUCAT: ‘Influence of the nature of the screen-printed electrode metal on the transport and detection properties of thick-film semiconductor gas sensors’. In *Sensors and Actuators B: Chemical* (Jan. 1992), vol. 6(1-3): pp. 279–284 (cit. on p. 39).
- [Ega81] MAKOTO EGASHIRA, MASAYO NAKASHIMA, and SHOHACHI KAWASUMI: ‘Change of thermal desorption behaviour of adsorbed oxygen with water coadsorption on Ag² - doped tin (IV) oxide’. In *Journal of the Chemical Society, Chemical Communications* (1981), vol. (20): p. 1047 (cit. on p. 27).
- [Eic00] A. EICHLER, F. MITTENDORFER, and J. HAFNER: ‘Precursor-mediated adsorption of oxygen on the (111) surfaces of platinum-group metals’. In *Physical Review B* (Aug. 2000), vol. 62(7): pp. 4744–4755 (cit. on p. 81).
- [Elo12] SOFIA ELOUALI, LEANNE G BLOOR, RUSSELL BINIONS, IVAN P. PARKIN, CLAIRE J. CARMALT, and JAWWAD A DARR: ‘Gas sensing with nano-indium oxides (In₂O₃) prepared via continuous hydrothermal flow synthesis.’ In *Langmuir : the ACS journal of surfaces and colloids* (Jan. 2012), vol. 28(3): pp. 1879–85 (cit. on p. 5).
- [Emi01] S. EMIROGLU, NICOLAE BARSAN, UDO WEIMAR, and V. HOFFMANN: ‘In situ diffuse reflectance infrared spectroscopy study of CO adsorption on SnO₂’. In *Thin Solid Films* (July 2001), vol. 391(2): pp. 176–185 (cit. on p. 88).
- [EPA] EPA: <http://www.epa.gov/air/criteria.html> - 2014.06.01 (cit. on pp. 12, 13).

- [Eri] ERIC EDWARDS: <http://england.prm.ox.ac.uk/englishness-Miners-lamp.html> - 2014.06.01 (cit. on p. 4).
- [Fag98] GUIDO FAGLIA, ELISABETTA COMINI, G. SBERVEGLIERI, R. RELLA, PIETRO SICILIANO, and L. VASANELLI: ‘Square and collinear four probe array and Hall measurements on metal oxide thin film gas sensors’. In *Sensors and Actuators B: Chemical* (Nov. 1998), vol. 53(1-2): pp. 69–75 (cit. on p. 38).
- [Fag99] GUIDO FAGLIA, ELISABETTA COMINI, A. CRISTALLI, G. SBERVEGLIERI, and L. DORI: ‘Very low power consumption micromachined CO sensors’. In *Sensors and Actuators B: Chemical* (May 1999), vol. 55(2-3): pp. 140–146 (cit. on p. 9).
- [Gal02] K. GALATSI, Y. X. LI, W. WLODARSKI, ELISABETTA COMINI, G. SBERVEGLIERI, C. CANTALINI, S. SANTUCCI, and M. PASSACANTANDO: ‘Comparison of single and binary oxide MoO₃, TiO₂ and WO₃ sol–gel gas sensors’. In *Sensors and Actuators B: Chemical* (Mar. 2002), vol. 83(1-3): pp. 276–280 (cit. on p. 5).
- [Gar91] JULIAN W. GARDNER: ‘Detection of vapours and odours from a multi-sensor array using pattern recognition Part 1. Principal component and cluster analysis’. In *Sensors and Actuators B: Chemical* (May 1991), vol. 4(1-2): pp. 109–115 (cit. on p. 6).
- [Gar92] JULIAN W. GARDNER, E. L. HINES, and H. C. TANG: ‘Detection of vapours and odours from a multisensor array using pattern-recognition techniques Part 2. Artificial neural networks’. In *Sensors and Actuators B: Chemical* (July 1992), vol. 9(1): pp. 9–15 (cit. on p. 6).
- [Gar95] JULIAN W. GARDNER and A. PIKE: ‘Integrated array sensor for detecting organic solvents’. In *Sensors and Actuators B . . .* (Jan. 1995), vol. 26(1-3): pp. 135–139 (cit. on p. 9).
- [Gen86] S. J. GENTRY and T. A. JONES: ‘The role of catalysis in solid-state gas sensors’. In *Sensors and Actuators* (Sept. 1986), vol. 10(1-2): pp. 141–163 (cit. on p. 28).
- [Gen84] S. J. GENTRY and S. R. HOWARTH: ‘The use of charcoal and carbon cloth for the poison-protection of catalytic gas sensors’. In *Sensors and Actuators* (July 1984), vol. 5(4): pp. 265–273 (cit. on p. 6).

- [Ger03] M. GERLICH, S. KORNELY, MAXIMILIAN FLEISCHER, H. MEIXNER, and R. KASSING: ‘Selectivity enhancement of a WO_3/TiO_2 gas sensor by the use of a four-point electrode structure’. In *Sensors and Actuators B: Chemical* (Aug. 2003), vol. 93(1-3): pp. 503–508 (cit. on p. 38).
- [Gil76] B. GILLOT, C. FEY, and D. DELAFOSSE: ‘Surface properties of tin (IV) oxide depending upon the mode of preparation’. In *Journal of Chemical Physics* (1976), vol. 73(19) (cit. on pp. 25, 70).
- [Goe91] WOLFGANG GOEPEL and KLAUS-DIETER SCHIERBAUM: ‘Sensors Set: A Comprehensive Survey’. In *Sensors Set: A Comprehensive Survey*. Wiley-VCH Verlag GmbH, 1991 (cit. on p. 3).
- [Goe95] WOLFGANG GOEPEL and KLAUS-DIETER SCHIERBAUM: ‘ SnO_2 sensors: current status and future prospects’. In *Sensors and Actuators B: Chemical* (Jan. 1995), vol. 26(1-3): pp. 1–12 (cit. on pp. 1, 33, 34).
- [Goe94] WOLFGANG GOEPEL and CHRISTIANE ZIEGLER: *Struktur der Materie: Grundlagen, Mikroskopie und Spektroskopie*. Vol. 98. 12. Stuttgart Leipzig: Teubner Verlag, Dec. 1994: p. 668 (cit. on p. 22).
- [Gol94] L. J. GOLONKA, J. KOZOWSKI, and B. W. LICZNERSKI: ‘The influence of the electrode material on the sensitivity of an SnO_2 thick-film gas sensor’. In *Sensors and Actuators B: Chemical* (Apr. 1994), vol. 19(1-3): pp. 453–456 (cit. on pp. 38, 39).
- [Got03] J. M. GOTTFRIED: ‘CO Oxidation over Gold’. PhD Thesis. Freie Universität Berlin, 2003 (cit. on p. 115).
- [Gou99] H. GOURARI, M. LUMBRERAS, R. VAN LANDSCHOOT, and J. SCHOONMAN: ‘Electrode nature effects on stannic oxide type layers prepared by electrostatic spray deposition’. In *Sensors and Actuators B: Chemical* (Sept. 1999), vol. 58(1-3): pp. 365–369 (cit. on p. 39).
- [Gri76] T B GRIMLEY: ‘Chemisorption Theory, Electronic Structure, and Reactivity of Metal Surfaces’. English. In *Electronic Structure and Reactivity of Metal Surfaces SE - 5*. Ed. by E G DEROUANE and A A LUCAS. Vol. 16. NATO Advanced Study Institutes Series. Springer US, 1976: pp. 113–162 (cit. on p. 116).

- [Gro12a] KATHARINA GROSSMANN: ‘Detection mechanism of reducing gases and influence of water on tin dioxide based gas sensors - differences in surface chemistry between undoped and platinum doped materials’. PhD. 2012: p. 106 (cit. on pp. 26, 29, 42, 96, 106).
- [Gro12b] KATHARINA GROSSMANN, ROMAN G. PAVELKO, NICOLAE BARSAN, and UDO WEIMAR: ‘Interplay of H₂, water vapor and oxygen at the surface of SnO₂ based gas sensors – An operando investigation utilizing deuterated gases’. In *Sensors and Actuators B: Chemical* (May 2012), vol. 166-167: pp. 787–793 (cit. on p. 97).
- [Gru99] JAN-DIERK GRUNWALDT: ‘Comparative Study of Au/TiO₂ and Au/ZrO₂ Catalysts for Low-Temperature CO Oxidation’. In *Journal of Catalysis* (Sept. 1999), vol. 186(2): pp. 458–469 (cit. on p. 71).
- [Gue85] A. GUEST: ‘PhD Thesis’. PhD. University of Nottingham, 1985 (cit. on p. 27).
- [Gur06] ALEXSANDER GURLO: ‘Interplay between O₂ and SnO₂: oxygen ionosorption and spectroscopic evidence for adsorbed oxygen.’ In *Chemphyschem: a European journal of chemical physics and physical chemistry* (Oct. 2006), vol. 7(10): pp. 2041–52 (cit. on pp. 25, 69).
- [Gur07] ALEXSANDER GURLO and RALF RIEDEL: ‘In situ and operando spectroscopy for assessing mechanisms of gas sensing’. In *Angewandte Chemie International Edition* (Jan. 2007), vol. 46(21): pp. 3826–48 (cit. on p. 53).
- [Hah02] SIMONE HAHN: ‘SnO₂ thick film sensors at ultimate limits: Performance at low O₂ and H₂O concentrations-Size reduction by CMOS technology’. PhD. 2002 (cit. on p. 42).
- [Hah03] SIMONE HAHN, NICOLAE BARSAN, UDO WEIMAR, S. G. EJAKOV, J. H. VISSER, and R. E. SOLTIS: ‘CO sensing with SnO₂ thick film sensors: role of oxygen and water vapour’. In *Thin Solid Films* (July 2003), vol. 436(1): pp. 17–24 (cit. on pp. 28, 57).
- [Har05] S. HARBECK: ‘Characterisation and functionality of SnO₂ gas sensors using vibrational spectroscopy’. PhD. University of Tübingen, 2005 (cit. on p. 88).

- [Har03] SERPIL HARBECK, A. SZATVANYI, NICOLAE BARSAN, UDO WEIMAR, and V. HOFFMANN: ‘DRIFT studies of thick film un-doped and Pd-doped SnO₂ sensors: temperature changes effect and CO detection mechanism in the presence of water vapour’. In *Thin Solid Films* (July 2003), vol. 436(1): pp. 76–83 (cit. on pp. 25, 28).
- [Hei57] G. HEILAND: ‘Zum Einfluss von Wasserstoff auf die elektrische Leitfähigkeit an der Oberfläche von Zinkoxydkristallen’. In *Zeitschrift für Physik* (Feb. 1957), vol. 148(1): pp. 15–27 (cit. on p. 5).
- [Hei88] G. HEILAND and DIETER KOHL: *Chemical Sensor Technology*. Elsevier, 1988: pp. 15–38 (cit. on p. 26).
- [Hei97] ARNDT HEILIG, NICOLAE BARSAN, UDO WEIMAR, MARKUS SCHWEIZER-BERBERICH, JULIAN W. GARDNER, and WOLFGANG GOEPEL: ‘Gas identification by modulating temperatures of SnO₂-based thick film sensors’. In *Sensors and Actuators B: Chemical* (Sept. 1997), vol. 43(1-3): pp. 45–51 (cit. on p. 9).
- [Hen94] VICTOR E. HENRICH and P. A. COX: *The Surface Science of Metal Oxides*. Cambridge University Press, 1994: p. 480 (cit. on pp. 26, 28).
- [HR09] FRANCISCO HERNANDEZ-RAMIREZ, J. DANIEL PRADES, ROMAN JIMENEZ-DIAZ, THOMAS FISCHER, ALBERT ROMANO-RODRIGUEZ, SANJAY MATHUR, and JOAN R. MORANTE: ‘On the role of individual metal oxide nanowires in the scaling down of chemical sensors’. In *Physical Chemistry Chemical Physics* (2009), vol. 11(33): p. 7105 (cit. on p. 15).
- [Hoe95] ULRICH HOEFER, KLAUS STEINER, and ELMAR WAGNER: ‘Contact and sheet resistance of SnO₂ thin films from transmission-line model measurements’. In *Sensors and Actuators B: Chemical* (Jan. 1995), vol. 26(1-3): pp. 59–63 (cit. on p. 37).
- [Hoe01] ULRICH HOEFER, JOACHIM FRANK, and MAXIMILIAN FLEISCHER: ‘High temperature Ga₂O₃-gas sensors and SnO₂-gas sensors: a comparison’. In *Sensors and Actuators B: Chemical* (Aug. 2001), vol. 78(1-3): pp. 6–11 (cit. on p. 5).
- [Hoe98] ULRICH HOEFER, H. BÖTTNER, ELMAR WAGNER, and C. D. KOHL: ‘Highly sensitive NO₂ sensor device featuring a JFET-like transducer

- mechanism'. In *Sensors and Actuators B: Chemical* (Apr. 1998), vol. 47(1-3): pp. 213–217 (cit. on p. 37).
- [Hö8] MICHAEL HÜBNER: 'Leitfähigkeitsmessungen an SnO₂-Gassensoren in sauerstofffreier Atmosphäre: Aufbau und Messung'. Diploma Thesis. University of Tuebingen, 2008: pp. 1–56 (cit. on p. 74).
- [H11] MICHAEL HÜBNER, ROMAN G. PAVELKO, NICOLAE BARSAN, and UDO WEIMAR: 'Influence of oxygen backgrounds on hydrogen sensing with SnO₂ nanomaterials'. In *Sensors and Actuators B: Chemical* (June 2011), vol. 154(2): pp. 264–269 (cit. on p. 69).
- [Hue11a] MICHAEL HUEBNER: 'New Approaches for the Basic Understanding of Semiconducting Metal Oxide Based Gas Sensors: Sensing , Transduction and Appropriate Modeling'. PhD. University of Tuebingen, 2011 (cit. on pp. 21, 31, 42, 109).
- [Hue12] MICHAEL HUEBNER, DOROTA KOZIEJ, JAN-DIERK GRUNWALDT, UDO WEIMAR, and NICOLAE BARSAN: 'An Au clusters related spill-over sensitization mechanism in SnO₂-based gas sensors identified by operando HERFD-XAS, work function changes, DC resistance and catalytic conversion studies.' In *Physical chemistry chemical physics : PCCP* (Oct. 2012), vol. 14(38): pp. 13249–54 (cit. on p. 71).
- [Hue11b] MICHAEL HUEBNER, DOROTA KOZIEJ, MATTHIAS BAUER, NICOLAE BARSAN, KRISTINA KVASHNINA, MARTA D. ROSSELL, UDO WEIMAR, and JAN-DIERK GRUNWALDT: 'The structure and behavior of platinum in SnO₂-based sensors under working conditions.' In *Angewandte Chemie (International ed. in English)* (Mar. 2011), vol. 50(12): pp. 2841–4 (cit. on pp. 7, 42).
- [Hug00] O. HUGON, M. SAUVAN, P. BENECH, CHRISTOPHE PIJOLAT, and F. LEFEBVRE: 'Gas separation with a zeolite filter, application to the selectivity enhancement of chemical sensors'. In *Sensors and Actuators B: Chemical* (Sept. 2000), vol. 67(3): pp. 235–243 (cit. on p. 6).
- [Hul91] ADAM HULANICKI, STANISLAW GLAB, and FOLKE INGMAN: 'Chemical Sensors Definitions and Classification'. In *Pure & Appl. Chem.* (1991), vol. 63(9): pp. 1247–1250 (cit. on p. 2).

- [Iho94] KOUSUKE IHOKURA and JOSEPH WATSON: *The Stannic Oxide Gas Sensor Principles and Applications*. 1994: p. 208 (cit. on p. 1).
- [J. 98] MARTIN J. WILLETT, VASILIS N. BURGANOS, CHRISTOS D. TSAKIROGLOU, and ALKIVIADES C. PAYATAKES: ‘Gas sensing and structural properties of variously pretreated nanopowder tin (IV) oxide samples’. In *Sensors and Actuators B: Chemical* (Nov. 1998), vol. 53(1-2): pp. 76–90 (cit. on p. 28).
- [Jai90] UMA JAIN, A. H. HARKER, A. M. STONEHAM, and DAVID E. WILLIAMS: ‘Effect of electrode geometry on sensor response’. In *Sensors and Actuators B: Chemical* (May 1990), vol. 2(2): pp. 111–114 (cit. on p. 37).
- [Jan89] J. JANATA: *Principles of chemical sensors*. 1989 (cit. on p. 3).
- [Jar76] Z. M. JARZEBSKI: ‘Physical Properties of SnO₂ Materials’. In *Journal of The Electrochemical Society* (1976), vol. 123(7): p. 199C (cit. on p. 18).
- [Jia00] LI JIANPING, WANG YUE, GAO XIAO GUANG, MA QING, WANG LI, and HAN JINGHONG: ‘H₂S sensing properties of the SnO₂-based thin films’. In *Sensors and Actuators B: Chemical* (June 2000), vol. 65(1-3): pp. 111–113 (cit. on p. 5).
- [Jim04] I. JIMENEZ, M. A. CENTENO, and R. SCOTTI: ‘NH₃ interaction with chromium-doped WO₃ nanocrystalline powders for gas sensing applications’. In *Journal of materials . . .* (2004), vol. (cit. on p. 5).
- [Jol86] J. P. JOLY, L. GONZALES-CRUZ, and Y. ARNAUD: ‘Desorption a temperature programme de l’oxygene labile de SnO₂’. fre. In *Bulletin de la Société chimique de France* (1986), vol. (1): pp. 11–17 (cit. on pp. 19, 25, 70).
- [Jon71] P. JONES and J. A. HOCKEY: ‘Infra-red studies of rutile surfaces. Part 1’. In *Transactions of the Faraday Society* (1971), vol. 67: p. 2669 (cit. on p. 107).
- [Jon72] P. JONES and J. A. HOCKEY: ‘Infra-red studies of rutile surfaces. Part 3. Adsorption of water and dehydroxylation of rutile’. In *Journal of the Chemical Society, Faraday Transactions 1* (1972), vol. 68(1): p. 907 (cit. on p. 90).

- [Kap01a] JUERGEN KAPPLER, A. TOMESCU, NICOLAE BARSAN, and UDO WEIMAR: ‘CO consumption of Pd doped SnO₂ based sensors’. In *Thin Solid Films* (July 2001), vol. 391(2): pp. 186–191 (cit. on pp. 41, 82, 84).
- [Kap01b] JÜRGEN KAPPLER: ‘Characterisation of high-performance SnO₂ gas sensors for CO detection by in situ techniques’. PhD. University of Tuebingen, 2001 (cit. on pp. 42, 45, 47–50).
- [Kem13a] JENS A. KEMMLER, SUMAN POKHREL, LUTZ MÄDLER, UDO WEIMAR, and NICOLAE BARSAN: ‘Flame spray pyrolysis for sensing at the nanoscale.’ In *Nanotechnology* (Nov. 2013), vol. 24(44): p. 442001 (cit. on p. 15).
- [Kem13b] JENS A. KEMMLER, SVEN SCHOPF, LUTZ MÄDLER, NICOLAE BARSAN, and UDO WEIMAR: ‘Laminiertes Zinndioxid - Restrukturierte FSP Schichten für Sensoranwendungen’. In *11. Dresdner Sensor Symposium*. 2013: pp. 355–359 (cit. on p. 15).
- [Kem12] JENS A. KEMMLER, SUMAN POKHREL, JOHANNES BIRKENSTOCK, MARCO SCHOWALTER, ANDREAS ROSENAUER, NICOLAE BARSAN, UDO WEIMAR, and LUTZ MÄDLER: ‘Quenched, nanocrystalline In₄Sn₃O₁₂ high temperature phase for gas sensing applications’. In *Sensors and Actuators B: Chemical* (Jan. 2012), vol. 161(1): pp. 740–747 (cit. on p. 5).
- [Kim11] HAE-RYONG KIM, ALEXANDER HAENSCH, IL-DOO KIM, NICOLAE BARSAN, UDO WEIMAR, and JONG-HEUN LEE: ‘The Role of NiO Doping in Reducing the Impact of Humidity on the Performance of SnO₂-Based Gas Sensors: Synthesis Strategies, and Phenomenological and Spectroscopic Studies’. In *Advanced Functional Materials* (Dec. 2011), vol. 21(23): pp. 4456–4463 (cit. on p. 15).
- [Koh92] DIETER KOHL: ‘Oxidic Semiconductor Gas Sensors’. In *Gas Sensors*. Ed. by G. SBERVEGLIERI. Springer Netherlands, 1992: pp. 43–88 (cit. on p. 27).
- [Koh90] DIETER KOHL: ‘The role of noble metals in the chemistry of solid-state gas sensors’. In *Sensors and Actuators B: Chemical* (Jan. 1990), vol. 1(1-6): pp. 158–165 (cit. on p. 7).
- [Kol12] K. K. KOLASINSKI: *Surface Science: Foundations of Catalysis and Nanoscience*. Wiley, 2012 (cit. on p. 116).

- [Kor11] GHENADII KOROTCENKOV: *Chemical Sensors Comprehensive Sensor Technologies: Solid State Sensors*. Ed. by GHENADII KOROTCENKOV. Momentum Press, 2011 (cit. on pp. 10, 11).
- [K95] L. KÖVÉR: ‘High resolution photoemission and Auger parameter studies of electronic structure of tin oxides’. In *Journal of Vacuum Science & Technology A: Vacuum, Surfaces, and Films* (May 1995), vol. 13(3): p. 1382 (cit. on p. 19).
- [Koz06] DOROTA KOZIEJ: ‘Phenomenological and Spectroscopic Studies on Gas Detection Mechanism of Selected Gases with Tin Dioxide Based Sensors’. PhD. 2006 (cit. on pp. 26, 27, 42, 61, 88, 90, 93, 94, 96).
- [Koz09] DOROTA KOZIEJ, MICHAEL HUEBNER, NICOLAE BARSAN, UDO WEIMAR, MARCIN SIKORA, and JAN-DIERK GRUNWALDT: ‘Operando X-ray absorption spectroscopy studies on Pd-SnO₂ based sensors.’ In *Physical chemistry chemical physics : PCCP* (Oct. 2009), vol. 11(38): pp. 8620–5 (cit. on pp. 7, 42).
- [Kro56] F. A. KROEGER and H. J. VINK: ‘Relations between the Concentrations of Imperfections in Crystalline Solids’. In *Solid State Physics*. Ed. by FREDERICK SEITZ and DAVID TURNBULL. 1956. Chap. 9: pp. 307–435 (cit. on p. 69).
- [Kub31] PAUL KUBELKA and FRANZ MUNK: ‘Ein Beitrag zur Optik der Farbanstriche’. In *Zeitschrift fuer technische Physik* (1931), vol. 12: pp. 593–601 (cit. on p. 57).
- [Lal84] R. LALAUZE, N. BUI, and CHRISTOPHE PIJOLAT: ‘Interpretation of the electrical properties of a SnO₂ gas sensor after treatment with sulfur dioxide’. In *Sensors and Actuators* (Oct. 1984), vol. 6(2): pp. 119–125 (cit. on pp. 38, 39).
- [Len95] S. LENAERTS, J. ROGGEN, and G. MAES: ‘FT-IR characterization of tin dioxide gas sensor materials under working conditions’. In *Spectrochimica Acta Part A: Molecular and Biomolecular Spectroscopy* (May 1995), vol. 51(5): pp. 883–894 (cit. on pp. 25, 27, 28, 70).
- [Lew68] R. LEWIS and R. GOMER: ‘Adsorption of oxygen on platinum’. In *Surface Science* (Oct. 1968), vol. 12(2): pp. 157–176 (cit. on p. 81).

- [Llo02] EDUARD LLOBET, JESÚS BREZMES, RADU IONESCU, XAVIER VILANOVA, SHERZAD AL-KHALIFA, JULIAN W. GARDNER, NICOLAE BARSAN, and XAVIER CORREIG: ‘Wavelet transform and fuzzy ARTMAP-based pattern recognition for fast gas identification using a micro-hotplate gas sensor’. In *Sensors and Actuators B: Chemical* (Mar. 2002), vol. 83(1-3): pp. 238–244 (cit. on p. 9).
- [Lop04] N. LOPEZ: ‘The adhesion and shape of nanosized Au particles in a Au/TiO₂ catalyst’. In *Journal of Catalysis* (July 2004), vol. 225(1): pp. 86–94 (cit. on p. 71).
- [Mad89] MARC J. MADOU and S. ROY MORRISON: *Chemical Sensing with Solid State Devices*. Elsevier Inc., 1989 (cit. on pp. 3, 70).
- [Mar04] R. MARTINS, E. FORTUNATO, P. NUNES, I. FERREIRA, A. MARQUES, M. BENDER, N. KATSARAKIS, V. CIMALLA, and G. KIRIAKIDIS: ‘Zinc oxide as an ozone sensor’. In *Journal of Applied Physics* (2004), vol. 96(3): p. 1398 (cit. on p. 5).
- [McA88] JEROME F. MCALEER, PATRICK T. MOSELEY, JOHN O. W. NORRIS, DAVID E. WILLIAMS, and BRUCE C. TOFIELD: ‘Tin dioxide gas sensors. Part 2. - The role of surface additives’. In *Journal of the Chemical Society, Faraday Transactions 1* (1988), vol. 84(2): p. 441 (cit. on p. 41).
- [Mic77] HERBERT B. MICHAELSON: ‘The work function of the elements and its periodicity’. In *Journal of Applied Physics* (1977), vol. 48(11): p. 4729 (cit. on p. 35).
- [Mil06] JEFFREY T. MILLER, A. J. KROPF, Y. ZHA, J. R. REGALBUTO, L. DELANNOY, CATHERINE LOUIS, E. BUS, and JEROEN A. van BOKHOVEN: ‘The effect of gold particle size on Au-Au bond length and reactivity toward oxygen in supported catalysts’. In *J. Catal.* (2006), vol. 240(2): pp. 222–234 (cit. on p. 71).
- [Mis94] V. N. MISHRA and R. P. AGARWAL: ‘Effect of electrode material on sensor response’. In *Sensors and Actuators B: Chemical* (Nov. 1994), vol. 22(2): pp. 121–125 (cit. on p. 39).
- [Mit07] J. MITROVICS, F. RÖCK, and U. WEIMAR: ‘Elektronische Nase und Signalgewinnung’. In *Technisches Messen* (2007), vol. 74: pp. 157–165 (cit. on p. 7).

- [Mit98] J. MITROVICS, H. ULMER, U. WEIMAR, and W. GÖPEL: ‘Modular Sensor Systems for Gas Sensing and Odor Monitoring: The MOSES Concept’. In *ACS Symposium Series: "Chemical Sensors and Interfacial Design"* (1998), vol. 31: pp. 307–315 (cit. on p. 3).
- [Mon03] PIERRE MONTMEAT, JEAN-CLAUDE MARCHAND, RENÉ LALAUZE, JEAN-PAUL VIRICELLE, GUY TOURNIER, and CHRISTOPHE PIJOLAT: ‘Physico-chemical contribution of gold metallic particles to the action of oxygen on tin dioxide sensors’. In *Sensors and Actuators B: Chemical* (Oct. 2003), vol. 95(1-3): pp. 83–89 (cit. on pp. 41, 71).
- [Mon02] PIERRE MONTMEAT, CHRISTOPHE PIJOLAT, GUY TOURNIER, and JEAN-PAUL VIRICELLE: ‘The influence of a platinum membrane on the sensing properties of a tin dioxide thin film’. In *Sensors and Actuators B: Chemical* (May 2002), vol. 84(2-3): pp. 148–159 (cit. on p. 41).
- [Mor80] KUNIMISTU MORISHIGE, SHIGEHARU KITAKA, and TETSUO MORIMOTO: ‘The thermal desorption of surface hydroxyls on tin (IV) oxide.’ In *Bulletin of the Chemical Society of Japan* (1980), vol. 53(8): pp. 2128–2132 (cit. on p. 27).
- [Mor77a] S. ROY MORRISON: ‘Surface Sites in Heterogeneous Catalysis’. English. In *The Chemical Physics of Surfaces SE - 10*. Springer US, 1977: pp. 327–362 (cit. on p. 69).
- [Mor77b] S. ROY MORRISON: *The chemical physics of surfaces*. Plenum Press, 1977 (cit. on pp. 22, 70).
- [Mos87] PATRICK T. MOSELEY and BRUCE C. TOFIELD: *Solid state gas sensors*. Adam Hilger series on sensors. A. Hilger, 1987 (cit. on pp. 3, 25).
- [Mun83] S. MUNNIX and M. SCHMEITS: ‘Electronic structure of tin dioxide surfaces’. In *Physical Review B* (June 1983), vol. 27(12): pp. 7624–7635 (cit. on pp. 20, 22).
- [Nag02] YATSUHISA NAGANO: ‘Standard enthalpy of formation of platinum hydrous oxide’. English. In *Journal of Thermal Analysis and Calorimetry* (2002), vol. 69(3): pp. 831–839 (cit. on p. 81).
- [Nak12] SHINJI NAKAGOMI, TSUBASA SAI, and YOSHIHIRO KOKUBUN: ‘Hydrogen Gas Sensor Based on β -Ga₂O₃ Thin Film with a Function of Self Temperature Compensation’. In (2012), vol.: pp. 750–753 (cit. on p. 5).

- [Nao72] TAGUCHI NAOYOSHI: *Gas detecting device US 3695848 A*. Oct. 1972 (cit. on pp. 5, 7).
- [New69] D. M. NEWS: ‘Self-Consistent Model of Hydrogen Chemisorption’. In *Physical Review* (Feb. 1969), vol. 178(3): pp. 1123–1135 (cit. on p. 116).
- [Onl] WALLSTREET ONLINE: http://www.wallstreet-online.de/_print/nachricht/6288107-gas-analyzer-market-worth-3-2-billion-by-2018-2014.06.01 (cit. on p. 10).
- [Our03] K. OURA, A. SARANIN, V. G. LIFSHITS, A. V. ZOTOV, and M. KATAYAMA: *Surface Science - An Introduction*. Ed. by K. OURA. Springer, 2003: p. 440 (cit. on p. 22).
- [Pin80] H. PINK, L. TREITINGER, and L. VITÉ: ‘Preparation of fast detecting SnO₂ gas sensors’. In *Jpn. J. Appl. Phys* (1980), vol. (cit. on p. 8).
- [Pra03] A. K. PRASAD and P. I. GOUMA: ‘MoO₃ and WO₃ based thin film conductimetric sensors for automotive applications’. In *Journal of materials science* (2003), vol. 8: pp. 4347–4352 (cit. on p. 5).
- [Pra10] RAVI M. PRASAD, ALEXSANDER GURLO, RALF RIEDEL, MICHAEL HÜBNER, NICOLAE BARSAN, and UDO WEIMAR: ‘Microporous ceramic coated SnO₂ sensors for hydrogen and carbon monoxide sensing in harsh reducing conditions’. In *Sensors and Actuators B . . .* (Aug. 2010), vol. 149(1): pp. 105–109 (cit. on p. 6).
- [Pri71] MICHEL PRIMET, PIERRE PICHAT, and MICHEL V. MATHIEU: ‘Infrared study of the surface of titanium dioxides. I. Hydroxyl groups’. In *The Journal of Physical Chemistry* (Apr. 1971), vol. 75(9): pp. 1216–1220 (cit. on p. 107).
- [Ran09] SVEN RANK: ‘Untersuchung der Reaktionsmechanismen von Kohlenmonoxid und Wasserstoff an SnO₂-Sensoren in sauerstofffreier Atmosphäre - Umsatz- und Widerstandsmessungen’. Diploma. University of Tuebingen, Mar. 2009: p. 74 (cit. on p. 69).
- [Ras03] J RASKÓ: ‘CO-induced surface structural changes of Pt on oxide-supported Pt catalysts studied by DRIFTS’. In *Journal of Catalysis* (May 2003), vol. 217: pp. 478–486 (cit. on p. 99).
- [Roe09] FRANK ROECK: ‘System-Based Selectivity Improvements of Gas Sensor Arrays’. PhD. University of Tuebingen, 2009: p. 170 (cit. on p. 74).

- [Rum97] M. N. RUMYANTSEVA and M. LABEAU: ‘Copper and nickel doping effect on interaction of SnO₂-films with H₂S’. In *J. Mater. Chem.* (1997), vol. 7(9): pp. 1785–1790 (cit. on p. 5).
- [Sah05] THORSTEN SAHM, ALEXSANDER GURLO, NICOLAE BARSAN, UDO WEIMAR, and LUTZ MÄDLER: ‘Fundamental studies on SnO₂ by means of simultaneous work function change and conduction measurements’. In *Thin Solid Films* (Oct. 2005), vol. 490(1): pp. 43–47 (cit. on p. 28).
- [Sam73] S. SAMSON: ‘Defect structure and electronic donor levels in stannic oxide crystals’. In *Journal of Applied Physics* (1973), vol. 44(10): p. 4618 (cit. on p. 21).
- [Sau03] S. SAUKKO and V. LANTTO: ‘Influence of electrode material on properties of SnO₂-based gas sensor’. In *Thin Solid Films* (July 2003), vol. 436(1): pp. 137–140 (cit. on pp. 38, 39).
- [Sch91] K.D. SCHIERBAUM, U WEIMAR, W. GÖPEL, and R. KOWALKOWSKI: ‘Conductance, work function and catalytic activity of SnO₂-based gas sensors’. In *Sensors and Actuators B: Chemical* (Mar. 1991), vol. 3(3): pp. 205–214 (cit. on p. 106).
- [SB98] MARKUS SCHWEIZER-BERBERICH: ‘Gas sensors based on stannic oxide’. PhD. Univeristy of Tuebingen, 1998 (cit. on pp. 42, 61).
- [SB97] MARKUS SCHWEIZER-BERBERICH, NICOLAE BARSAN, UDO WEIMAR, JOAN R. MORANTE, and WOLFGANG GOEPEL: ‘Electrode effects on gas sensing properties of nanocrystalline SnO₂ gas sensors’. In *Proceedings of the 11th European Conference on Solid State Transducers*. 1997: pp. 1377–1380 (cit. on pp. 38, 39).
- [Sei62] TETSURO SEIYAMA, A. KATO, K. FUJIISHI, and M. NAGATANI: ‘A New Detector for Gaseous Components Using Semiconductive Thin Films.’ In *Analytical Chemistry* (1962), vol.: pp. 5–6 (cit. on p. 5).
- [Sei72] TETSURO SEIYAMA, H. FUTATA, F. ERA, and N. YAMAZOE: ‘Gas detection by activated semi-conductive sensor’. In *Denki Kagaku*. Vol. 40. 1972: pp. 244–249 (cit. on p. 7).

- [Sem01] S. SEMANCIK, R. E. CAVICCHI, M. C. WHEELER, J. E. TIFFANY, G. E. POIRIER, R. M. WALTON, J. S. SUEHLE, B. PANCHAPAKESAN, and D. L. DEVOE: ‘Microhotplate platforms for chemical sensor research’. In *Sensors and Actuators B: Chemical* (June 2001), vol. 77(1-2): pp. 579–591 (cit. on p. 9).
- [Sen] APPLIED SENSOR: <https://www.appliedsensor.com/> - 2014.06.01 (cit. on p. 9).
- [Ser02] NICOLAS SERGENT, P. GELIN, and L. PERIER-CAMBY: ‘Preparation and characterisation of high surface area stannic oxides: structural, textural and semiconducting properties’. In *Sensors and Actuators B ...* (2002), vol. 84: pp. 176–188 (cit. on p. 107).
- [Sim01] ISOLDE SIMON, NICOLAE BARSAN, MICHAEL BAUER, and UDO WEIMAR: ‘Micromachined metal oxide gas sensors: opportunities to improve sensor performance’. In *Sensors and Actuators B: ...* (2001), vol. 73 (cit. on p. 9).
- [Ste03] JOSEPH R. STETTER, WILLIAM R. PENROSE, and SHENG YAO: ‘Sensors, Chemical Sensors, Electrochemical Sensors, and ECS’. In *Journal of The Electrochemical Society* (2003), vol. 150(2): S11 (cit. on p. 3).
- [Tam02] JUN TAMAKI and CHIZUKO NARUO: ‘Sensing properties to dilute chlorine gas of indium oxide based thin film sensors prepared by electron beam evaporation’. In *Sensors and Actuators B: ...* (2002), vol. 83: pp. 190–194 (cit. on p. 5).
- [Tay96] R. F. TAYLOR: ‘Chemical and biological sensors: Markets and commercialization’. In *Handbook of Chemical Sensors and Biosensors*. Ed. by TAYLOR R.F. and SCHULTZ. Bristol and Philadelphia: CRC Press, 1996. Chap. 23 (cit. on p. 10).
- [The92] JEAN-MARC THEMLIN, MOHAMMED CHTAÏB, LUC HENRARD, PHILIPPE LAMBIN, JACQUES DARVILLE, and JEAN-MARIE GILLES: ‘Characterization of tin oxides by x-ray-photoemission spectroscopy’. In *Physical Review B* (July 1992), vol. 46(4): pp. 2460–2466 (cit. on p. 19).
- [Tho75] EDWARD W. THORNTON and PHILIP G. HARRISON: ‘Tin oxide surfaces. Part 1.-Surface hydroxyl groups and the chemisorption of carbon dioxide and carbon monoxide on tin (IV) oxide’. In *Journal of the Chemical*

- Society, Faraday Transactions 1: Physical Chemistry in Condensed Phases* (1975), vol. 71: p. 461 (cit. on pp. 27, 28).
- [Van58] L. J. VAN DER PAUW: 'A method of measuring specific resistivity and Hall effect of discs of arbitrary shape'. In *Philips research ...* (1958), vol. 13(1): pp. 1–9 (cit. on p. 38).
- [Var98] O. K. VARGHESE and L. K. MALHOTRA: 'Electrode-sample capacitance effect on Ethanol sensitivity of nano-grained SnO₂ thin films'. In *Sensors and Actuators B: Chemical* (1998), vol. 53: pp. 19–23 (cit. on pp. 39, 40).
- [Vas98] R. B. VASILIEV, M. N. RUMYANTSEVA, N. V. YAKOVLEV, and A. M. GASKOV: 'CuO/SnO₂ thin film heterostructures as chemical sensors to H₂S'. In *Sensors and Actuators B: Chemical* (Aug. 1998), vol. 50(3): pp. 186–193 (cit. on p. 5).
- [Vil98] X. VILANOVA, EDUARD LLOBET, J. BREZMES, J. CALDERER, and X. CORREIG: 'Numerical simulation of the electrode geometry and position effects on semiconductor gas sensor response'. In *Sensors and Actuators B: Chemical* (May 1998), vol. 48(1-3): pp. 425–431 (cit. on p. 37).
- [Voe01] HANS G. VOELZ: *Industrielle Farbpruefung*. Weinheim, Germany: Wiley-VCH Verlag GmbH & Co. KGaA, Aug. 2001 (cit. on p. 57).
- [Vol81] A. M. VOLODIN and A. E. CHERKASHIN: 'Observation conditions and thermal stability of O²⁻ on SnO₂'. In *Reaction Kinetics and Catalysis Letters* (Oct. 1981), vol. 17(3-4): pp. 329–332 (cit. on pp. 25, 70).
- [Wat84] JOSEPH WATSON: 'The tin oxide gas sensor and its applications'. In *Sensors and Actuators* (Jan. 1984), vol. 5(1): pp. 29–42 (cit. on p. 1).
- [Wei01] UDO WEIMAR: 'Gas sensing with tin oxide: elementary steps and signal transduction'. Habilitation. University of Tuebingen, 2001 (cit. on pp. 8, 17, 42, 45, 47, 48, 68).
- [Wei95] UDO WEIMAR and WOLFGANG GOEPEL: 'A.c. measurements on tin oxide sensors to improve selectivities and sensitivities'. In *Sensors and Actuators B: Chemical* (Jan. 1995), vol. 26(1-3): pp. 13–18 (cit. on p. 38).
- [Wei09] UDO WEIMAR et al.: 'Microsystem Technology for Ambient Assisted Living (AAL)'. In *Procedia Chemistry* (Sept. 2009), vol. 1(1): pp. 710–713 (cit. on p. 14).

- [Wei90] UDO WEIMAR, KLAUS-DIETER SCHIERBAUM, WOLFGANG GÖPEL, and R. KOWALKOWSKI: ‘Pattern recognition methods for gas mixture analysis: Application to sensor arrays based upon SnO₂’. In *Sensors and Actuators B: Chemical* (Jan. 1990), vol. 1(1-6): pp. 93–96 (cit. on p. 6).
- [WHOa] WHO: http://whqlibdoc.who.int/hq/2006/WHO_SDE_PHE_OEH_06.02_eng.pdf - 2014.06.01 (cit. on pp. 12, 14).
- [WHO] WHO: <http://www.who.int/ceh/risks/cehair/en/> - 2014.06.01 (cit. on p. 12).
- [WHOb] WHO: <http://www.who.int/indoorair/info/briefing2.pdf> - 2014.06.01 (cit. on p. 12).
- [Wika] WIKIPEDIA: http://en.wikipedia.org/wiki/Carbon_monoxide - 2014.06.01 (cit. on p. 27).
- [Wikb] WIKIPEDIA: <http://en.wikipedia.org/wiki/Sensor> - 2014.06.01 (cit. on p. 2).
- [Wil99] DAVID E. WILLIAMS: ‘Semiconducting oxides as gas-sensitive resistors’. In *Sensors and Actuators B: Chemical* (1999), vol. 57(January): pp. 1–16 (cit. on p. 1).
- [Wil91] DAVID E. WILLIAMS and PATRICK T. MOSELEY: ‘Dopant effects on the response of gas-sensitive resistors utilising semiconducting oxides’. In *Journal of Materials Chemistry* (1991), vol. 1(5): p. 809 (cit. on p. 1).
- [Win79] HENRY WINDISCHMANN: ‘A Model for the Operation of a Thin-Film SnO_x Conductance-Modulation Carbon Monoxide Sensor’. In *Journal of The Electrochemical Society* (1979), vol. 126(4): p. 627 (cit. on p. 28).
- [Wö3] J. WÖLLENSTEIN, J.A. PLAZA, C. CANÉ, Y. MIN, H. BÖTTNER, and H.L. TULLER: ‘A novel single chip thin film metal oxide array’. In *Sensors and Actuators B: Chemical* (Aug. 2003), vol. 93(1-3): pp. 350–355 (cit. on p. 5).
- [Yam83] N. YAMAZOE, Y. KUROKAWA, and TETSURO SEIYAMA: ‘Effects of additives on semiconductor gas sensors’. In *Sensors and Actuators* (Jan. 1983), vol. 4: pp. 283–289 (cit. on p. 7).
- [Yam94] N. YAMAZOE and N. MIURA: ‘Environmental gas sensing’. In *Sensors and Actuators B: Chemical* (1994), vol. 20: pp. 95–102 (cit. on p. 5).

- [Yam91] NOBORU YAMAZOE: ‘New approaches for improving semiconductor gas sensors’. In *Sensors and Actuators B: Chemical* (Aug. 1991), vol. 5(1-4): pp. 7–19 (cit. on p. 41).
- [Yam79] NOBORU YAMAZOE, JUN FUCHIGAMI, MASATO KISHIKAWA, and TETSURO SEIYAMA: ‘Interactions of tin oxide surface with O₂, H₂O and H₂’. In *Surface Science* (July 1979), vol. 86: pp. 335–344 (cit. on pp. 25, 69, 70).
- [Yli93] A. YLINAMPA, V. LANTTO, and S. LEPPÄVUORI: ‘Some differences between Au and Pt electrodes in SnO₂ thick-film gas sensors’. In *Sensors and Actuators B: Chemical* (June 1993), vol. 14(1-3): pp. 602–604 (cit. on pp. 39, 40).
- [Zam97] T. ZAMBELLI, J. V. BARTH, J. WINTTERLIN, and G. ERTL: ‘Complex pathways in dissociative adsorption of oxygen on platinum’. In *Nature* (Dec. 1997), vol. 390(6659): pp. 495–497 (cit. on p. 81).

List of Figures

1.1	Sensing principle	2
1.2	Sensing and Transduction of a chemical gas sensor	3
1.3	Models for feature extraction and pattern recognition	7
2.1	Unit cell of SnO ₂ (rutile crystalline structure) with four O ²⁻ anions and two Sn ⁴⁺ cations. Each tin atom is sixfold coordinated, placed approximately at the corners of a regular slightly deformed octahedron, to threefold coordinated oxygen atoms.	19
2.2	Band diagram of SnO ₂ (left) and projection of the density of states (<i>DOS</i>) for the 1s states of SnO ₂ , Sn and O (right) [Jol86].	19
2.3	Band diagram (schematic) of SnO ₂ with a band gap (E_g) of 3.6 eV. Two donor levels (E_1 & E_2), which results out of the oxygen vacancies, are located 0.03 and 0.15 eV below the conduction band.	21
2.4	Ideal SnO ₂ [110] surface (left) & reduced SnO ₂ [110] surface (right) .	22
2.5	Energetically representation of Physisorption and Chemisorption . . .	23
2.6	Schematic energy band representation of oxygen interaction with the SnO ₂ surface. Acceptor levels are created in a first step, which are then filled with electrons form the conduction band. The resulting band bending (qVs) leads to a formation of a potential barrier at the grain-grain boundaries and thus to an increase in resistance.	24
2.7	Literature review of oxygen species at the SnO ₂ surface dependent on the temperature detected by the means of IR (Infrared) - spectroscopy, TPD (Temperature Programmed Desorption) and EPR (Electron Paramagnetic Resonance) after [Bar01]. For details see [Cha80; Gil76; Jol86; Len95; Vol81; Yam79]	25

2.8	Literature review of hydroxyl species at the SnO ₂ surface dependent on the temperature detected by the means of IR (Infrared) - spectroscopy and TPD (Temperature Programmed Desorption). For details see [Ber96; Ega81; Gue85; Koh92; Len95; Mor80; Tho75]	27
2.9	Literature review of CO reaction intermediates at the SnO ₂ surface dependent on the temperature detected by the means of IR (Infrared) - spectroscopy. For details see [Boy77; Gen86; J. 98; Len95; Tho75; Win79]	28
2.10	From the reaction of a gaseous species on the surface to the electrical signal - Schematic representation of the working principle of a n-type metal oxide gas sensor. Depending on the amount of chemisorbed oxygen a depletion layer is formed at the surface of each SnO ₂ grain. A reducing gas (e.g. carbon monoxide) use up the pre-adsorbed oxygen and thus the depletion layer or the potential barrier respectively is decreased, which finally results in a decrease in resistance.	30
3.1	Overview of typical electrode geometries. From the "classical" Taguchi type gas sensor to the "modern approach" of micro contacts. After [Goe95].	33
3.2	Three different cases describing the situation before (left) and after (right) contact between the electrode and the semiconductor. Case 1 & 2: In both cases the electronic affinity is assumed to be equal. After the contact between both materials the Fermi levels equilibrates, which results in a band bending independent of the initial band bending (before contact). Case 3: The electronic affinity is different compared to case 1 & 2, which results in a different barrier height after contact of the metal and the semiconductor. After [Bar01]	36
3.3	Potential of a single elementary charge (q ⁺) and a hydroxyl dipole (q ⁺ & q ⁻). The area shaded in grey is giving the potential of the thermal energy. q ⁺ is the origin of the x-axis, while the distance [m] is represented by r ₂ . For more details & explanations of calculations see [Bar01]	36
3.4	Ohmic behavior of the four-probe measurement readout of a SnO ₂ sensor at 200 °C in 50 % r.H. (left) non-ohmic behavior of the two-probe measurement readout of a SnO ₂ sensor at 200 °C at 50 % r.H. (right). For details see [Wei95]	38

3.5	Effect of noble metal additives at the surface of n-type metal oxide grains	41
3.6	Schematic layout of the typical "IPC" SnO ₂ sensor. The sensing layer is deposited via screen-printing on an alumina substrate. The interdigitated electrode structure beneath the sensing layer is out of platinum or gold. The heater structure on the backside is out of platinum or a palladium/silver-alloy.	43
3.7	Normalized measurement of the resistance of two different SnO ₂ sensors equipped with either platinum or gold electrodes at 250 °C and 350 °C under exposure to 25 ppm and 250 ppm carbon monoxide	43
4.1	Flowchart describing the SnO ₂ powder preparation and the sensor fabrication process	46
4.2	Average grain size of SnO ₂ (wet-chemistry synthesis) as a function of calcination temperature. Data determined by TEM in [Wei01]	48
4.3	XRD pattern of SnO ₂ calcinated for 8 hours at 1000 °C	49
4.4	Preparation of the SnO ₂ paste in a planetary ball mill. ZrO ₂ balls in the ZrO ₂ mug ensure an effective milling of the SnO ₂ + propylene glycol slurry. [Kap01b]	49
4.5	Fabrication of the sensors via screen printing. A rubber squeegee presses the viscous paste through the undeveloped part of the screen on the alumina substrate. By adjusting the speed, pressure and distance a defined and reproducible layer thickness is achievable. [Kap01b]	50
4.6	"IPC" sensor geometry from top view, bottom view, side view and cross section. [Bar03]	50
4.7	The "IPC" sensor device. SEM pictures (top - right) are showing a highly porous morphology of the SnO ₂ sensing layer which extends through the entire layer (FIB cut; top - left). The platinum electrode as well as the gold electrode is showing a comparable porous morphology (bottom)	51
4.8	Temperature calibration of the sensor device using an infrared pyrometer.	51
4.9	Overview of the different "operando" measurement approaches used at the Institute of Physical Chemistry at the University of Tuebingen. For more details see [Bar07]	53
4.10	Gas mixing system used in the laboratory at the University of Tuebingen	54

4.11	Experimental setup for electrical measurements. Gas mixtures are controlled via a computer controlled gas mixing system. Resistance readout of the heated sensors is performed via a digital multimeter.	55
4.12	Visualization of the variables used in Lamberts cosine law	56
4.13	Different shares of the incident beam (I_i). Specular reflectance (I_s) occurs on grains with a larger diameter than the wavelength. A special mirror alignment reduces the normal specular reflectance to a minimum and is mainly capturing the diffuse reflection (I_d).	57
4.14	Experimental setup for simultaneous DRIFTS and resistance measurements. Gas mixtures are controlled via a computer controlled gas mixing system. Resistance readout of the heated sensors is performed via a digital multimeter. Spectroscopic information is gathered via a FT-IR spectrometer equipped with a DRIFTS unit.	58
4.15	Experimental setup for catalytic conversion measurements. Gas mixtures are controlled via a computer controlled gas mixing system. The gas mixtures pass through a catalytic reactor which is heated via a tube furnace. The exhaust components are analyzed with a photo acoustic gas monitor.	59
5.1	Overview of investigated samples	62
5.2	Time-dependent measurement of the resistance for two different sensor types (SnO_2 on substrates with Au-Electrodes & SnO_2 on substrates with Pt-electrodes). Measurements performed in dry air and 50 % r.H. for pulsed, subsequent increasing concentrations of hydrogen (30, 50, 100, 200 ppm) and carbon monoxide (25, 75, 150, 250 ppm). The sensors were heated up to 200 °C (top left), 250 °C (top right), 300 °C (bottom left) and 350 °C (bottom right)	64
5.3	Sensor signal as a function of the hydrogen concentration for the different sensor types in dry air and 50 % r.H. at the four different temperatures	65
5.4	Sensor signal as a function of the carbon monoxide concentration for the different sensor types in dry air and 50 % r.H. at the four different temperatures	66

5.5	Sensor signal as a function of the working temperature of the different sensor types at 250 ppm carbon monoxide in dry air (top left), 250 ppm carbon monoxide in 50 % r.H. (top right), 200 ppm hydrogen in dry air (bottom left) and 200 ppm hydrogen in 50 % r.H. (bottom right).	67
5.6	Baseline resistance (R_0) - measured right before gas exposure - as a function of the working temperature of the different sensor types in dry air and at 50 % r.H.	67
5.7	Literature review of oxygen species at the SnO ₂ surface dependent on the temperature detected by the means of IR (Infrared) - spectroscopy, TPD (Temperature Programmed Desorption) and EPR (Electron Paramagnetic Resonance) [Bar99]. For details see [Cha80; Gil76; Jol86; Len95; Vol81; Yam79]	70
5.8	Time-dependent measurement of the resistance for two different sensor types (SnO ₂ on substrates with Au-Electrodes & SnO ₂ on substrates with Pt-electrodes). Measurements performed in nitrogen for subsequent increasing concentrations of oxygen (1, 2 %). The sensors were heated up to 200 °C (top left), 250 °C (top right), 300 °C (bottom left) and 350 °C (bottom right)	73
5.9	Sensor signal as a function of the working temperature of the different sensor types at 1 % oxygen in nitrogen (left) and 2 % oxygen in nitrogen (right)	74
5.10	Time-dependent measurement of the resistance for two different sensor types (SnO ₂ on substrates with Au-Electrodes & SnO ₂ on substrates with Pt-electrodes). Measurements performed in nitrogen for subsequent increasing concentrations of oxygen (200, 500 ppm). The sensors were heated up to 200 °C (top left), 250 °C (top right), 300 °C (bottom left) and 350 °C (bottom right). The actual oxygen concentration in the exhaust is monitored by an oxygen analyzer.	75
5.11	Sensor signal as a function of the working temperature of the different sensor types at 200 ppm oxygen in nitrogen (left) and 500 ppm oxygen in nitrogen (right).	76
5.12	Sensor signal as a function of the oxygen concentration for the different sensor types - SnO ₂ on substrates with Au electrodes (left) & SnO ₂ on substrates with Pt electrodes (right).	76

- 5.13 Schematic drawing of the sensor cross-section illustrating the area which might be affected by the spill-over effect on the electrode (top). An increased amount of metallic gold - distributed through the whole layer - would increase the affected area. 78
- 5.14 Time-dependent measurement of the resistance for two different mixtures printed on the regular substrates ($\text{SnO}_2 + 5 \text{ wt. } \% \text{ Au}$ on substrates with Au-Electrodes & $\text{SnO}_2 + 5 \text{ wt. } \% \text{ Pt}$ on substrates with Pt-electrodes). Measurements performed in nitrogen for subsequent increasing concentrations of oxygen (200, 500 ppm). The sensors were heated up to 200 °C (top left), 250 °C (top right), 300 °C (bottom left) and 350 °C (bottom right). The actual oxygen concentration in the exhaust is monitored by an oxygen analyzer. 79
- 5.15 Sensor signal as a function of the working temperature of the different samples at 200 ppm oxygen in nitrogen (left) and 500 ppm oxygen in nitrogen (right). 80
- 5.16 Actual measured resistance of SnO_2 sensors on substrates with platinum electrodes and a mixture of $\text{SnO}_2 + 5 \text{ wt. } \% \text{ Pt}$ on substrates with Pt electrodes upon exposure to nitrogen and 200 ppm oxygen as a function of temperature. 80
- 5.17 Time dependent measurement of the carbon dioxide concentration. A certain amount of the given carbon monoxide is converted by the powder samples. The amount of converted carbon dioxide is measured in the exhaust with a photo acoustic gas monitor. The depicted plots are showing the measured concentrations exemplary for measurements on four different powder samples (Au, Pt, $\text{SnO}_2 + \text{Au}$, $\text{SnO}_2 + \text{Pt}$) at 250 °C. 83
- 5.18 CO_2 turnover plotted as a function of temperature for the five different powder samples. The dashed lines are theoretical expected values for $\text{SnO}_2 + \text{Au}$ and $\text{SnO}_2 + \text{Pt}$ mixtures, calculated out of the values obtained for the "pure" samples. 84
- 5.19 Single channel spectra of $\text{SnO}_2 + 5 \text{ wt. } \% \text{ Au}$ (bottom) and $\text{SnO}_2 + 5 \text{ wt. } \% \text{ Pt}$ (top) powder mixtures at four different temperatures (200, 250, 300 & 350 °C) recorded in the presence of synthetic air (left) and 250 ppm carbon monoxide (right). 90

5.20	DRIFT spectra of the two different powder mixtures in the presence of 250 ppm carbon monoxide at 200 °C (top left), 250 °C (top right), 300 °C (bottom left) and 350 °C (bottom right). As reference the spectrum in dry synthetic air at the corresponding temperature was taken.	91
5.21	Carbonate and carboxylate range (1600 - 800 cm^{-1}) of the two different powder samples at 200 °C exposed to 250 ppm carbon monoxide. As reference the spectrum in dry synthetic air was taken.	92
5.22	Hydroxyl range (4000 - 3000 cm^{-1}) of the two different powder samples at 200 °C exposed to 250 ppm carbon monoxide. As reference the spectrum in dry synthetic air was taken.	95
5.23	Given gas concentration plotted as a function of time. The grey shaded areas indicate the time when the single channels were recorded, which were then used for the calculation of the absorbance spectra.	97
5.24	DRIFT spectra of two different mixtures screen-printed on alumina substrates ($\text{SnO}_2 + 5 \text{ wt. } \% \text{ Au}$ on substrates with Au electrodes & $\text{SnO}_2 + 5 \text{ wt. } \% \text{ Pt}$ on substrates with Pt electrodes) at 200 °C upon exposure to a) 1000 ppm O_2 (Reference: $\text{N}_2 + 3 \% \text{ D}_2\text{O}$) and b) 1000 ppm $\text{O}_2 + 250 \text{ ppm CO}$ (Reference: $\text{N}_2 + 3 \% \text{ D}_2\text{O} + 1000 \text{ ppm O}$) in a background of $\text{N}_2 + 3 \% \text{ D}_2\text{O}$	98
5.25	Mass spectrometer data recorded for the respective DRIFTS measurement at 200 °C. Gas atmosphere during hour (10 - 12): $\text{N}_2 + 3 \% \text{ D}_2\text{O}$ - (12 - 14): $\text{N}_2 + 3 \% \text{ D}_2\text{O} + 1000 \text{ ppm O}_2$ - (14 - 16): $\text{N}_2 + 3 \% \text{ D}_2\text{O} + 1000 \text{ ppm O}_2 + 250 \text{ ppm CO}$	99
5.26	Time-dependent resistance measurement of the two different mixtures printed on substrates for the respective DRIFTS measurements at 200 °C. Gas atmosphere during hour (10 - 12): $\text{N}_2 + 3 \% \text{ D}_2\text{O}$ - (12 - 14): $\text{N}_2 + 3 \% \text{ D}_2\text{O} + 1000 \text{ ppm O}_2$ - (14 - 16): $\text{N}_2 + 3 \% \text{ D}_2\text{O} + 1000 \text{ ppm O}_2 + 250 \text{ ppm CO}$	100
5.27	DRIFT spectra of the two different samples at 250 °C upon exposure to a) 1000 ppm O_2 (Reference: $\text{N}_2 + 3 \% \text{ D}_2\text{O}$) and b) 1000 ppm $\text{O}_2 + 250 \text{ ppm CO}$ (Reference: $\text{N}_2 + 3 \% \text{ D}_2\text{O} + 1000 \text{ ppm O}_2$) in a background of $\text{N}_2 + 3 \% \text{ D}_2\text{O}$	101

- 5.28 Mass spectrometer data recorded for the respective DRIFTS measurement at 250 °C. Gas atmosphere during hour (10 - 12): N₂ + 3 % D₂O - (12 - 14): N₂ + 3 % D₂O + 1000 ppm O₂ - (14 - 16): N₂ + 3 % D₂O + 1000 ppm O₂ + 250 ppm CO 102
- 5.29 Time-dependent resistance measurement of the two different mixtures printed on substrates for the respective DRIFTS measurements at 250 °C. Gas atmosphere during hour (10 - 12): N₂ + 3 % D₂O - (12 - 14): N₂ + 3 % D₂O + 1000 ppm O₂ - (14 - 16): N₂ + 3 % D₂O + 1000 ppm O₂ + 250 ppm CO 102
- 5.30 DRIFT spectra of the two different samples at 300 °C upon exposure to a) 1000 ppm O₂ (Reference: N₂ + 3 % D₂O) and b) 1000 ppm O₂ + 250 ppm CO (Reference: N₂ + 3 % D₂O + 1000 ppm O₂) in a background of N₂ + 3 % D₂O 103
- 5.31 Mass spectrometer data recorded for the respective DRIFTS measurement at 300 °C. Gas atmosphere during hour (10 - 12): N₂ + 3 % D₂O - (12 - 14): N₂ + 3 % D₂O + 1000 ppm O₂ - (14 - 16): N₂ + 3 % D₂O + 1000 ppm O₂ + 250 ppm CO 104
- 5.32 Time-dependent resistance measurement of the two different mixtures printed on substrates for the respective DRIFTS measurements at 300 °C. Gas atmosphere during hour (10 - 12): N₂ + 3 % D₂O - (12 - 14): N₂ + 3 % D₂O + 1000 ppm O₂ - (14 - 16): N₂ + 3 % D₂O + 1000 ppm O₂ + 250 ppm CO 104
- 5.33 DRIFT spectra of the two different samples at 350 °C upon exposure to a) 1000 ppm O₂ (Reference: N₂ + 3 % D₂O) and b) 1000 ppm O₂ + 250 ppm CO (Reference: N₂ + 3 % D₂O + 1000 ppm O₂) in a background of N₂ + 3 % D₂O 105
- 5.34 Mass spectrometer data recorded for the respective DRIFTS measurement at 350 °C. Gas atmosphere during hour (10 - 12): N₂ + 3 % D₂O - (12 - 14): N₂ + 3 % D₂O + 1000 ppm O₂ - (14 - 16): N₂ + 3 % D₂O + 1000 ppm O₂ + 250 ppm CO 105
- 5.35 Time-dependent resistance measurement of the two different mixtures printed on substrates for the respective DRIFTS measurements at 350 °C. Gas atmosphere during hour (10 - 12): N₂ + 3 % D₂O - (12 - 14): N₂ + 3 % D₂O + 1000 ppm O₂ - (14 - 16): N₂ + 3 % D₂O + 1000 ppm O₂ + 250 ppm CO 106

-
- 5.36 FTIR spectra of a SnO₂ sample showing temperature dependent intensities of bands (3000 - 3500 cm⁻¹) which can be ascribed to H-bonded hydroxyl groups. For more details see [Ser02]. 107
- 5.37 Electrical Measurement of SnO₂ thick film sensors with gold electrodes and platinum electrodes at 200, 250 and 300 °C. Measurements performed in nitrogen with different levels of oxygen background concentration (100 & 200 ppm). The sensors were exposed to a pulse of 200 ppm of carbon monoxide at each oxygen background condition. . 110
- 6.1 Summary of findings and assumed activities on the three phase boundary in the case of gold electrodes. 112
- 6.2 Summary of findings and assumed activities on the three phase boundary in the case of platinum electrodes. 113
- 7.1 Chemisorption of adsorbents on metal surfaces as a two-step process. After [Kol12]. 116

List of Tables

1.1 Overview of different types of chemical sensors	3
1.2 Metal oxide materials for gas detection	5
1.3 Deposition techniques for the preparation of MOX gas sensors. After [Bar99]	8
1.4 Market demands & potential fields of application for gas sensors. After [Kor11].	11
1.5 National Ambient Air Quality Standards (NAAQS) for six principal pollutants [EPA]	13
1.6 World Health Organization (WHO) principal pollution standards (2005) [WHOa]	14
3.1 Workfunction of metals in [eV] [Mic77]	35
3.2 Literature review on electrode effects	39
4.1 Surface area and particle size distribution for noble metal powders obtained from Ferro©	52
5.1 Turnover rate in percent for all measured samples at different temperatures	86
5.2 Type of vibrations and the corresponding range of wavenumbers of different intermediates of the carbon monoxide reaction	93
5.3 Overview of the calculated sensors signals for the different gas exposures within the DRIFTS experiments at 200, 250, 300 % 350 °C	108

Publications

1. **Sven Rank**, GEOFFROY GADACZ, NICOLAE BARSAN & UDO WEIMAR: ‘Perspektiven der Transduceroptimierung - Einfluss des Elektrodenmaterials bei verschiedenen Temperaturen auf SnO₂ Dickschicht Sensoren’. *10. Dresdner Sensor-Symposium*. G. Gerlach, A. Schütze, TUDpress, 42, **2011**, 253-256, Dresden.
2. **Sven Rank**, SVEN HAFNER, NICOLAE BARSAN & UDO WEIMAR: ‘The Impact of the Nature of the Electrode Material on SnO₂ Thick Film Sensor Performance: Influence on Oxygen Adsorption’. *Eurosensors XXVI*. 9-12 September, **2012**, Kraków, Poland.
3. **Sven Rank**, NICOLAE BARSAN & UDO WEIMAR: ‘Aktivierung der SnO₂-Oberfläche durch O₂-Spill-Over an Gold - Leistungsoptimierung des Sensors durch die Elektrode’. *11. Dresdner Sensor-Symposium*. **2013**, 22-27, Dresden.

Curriculum Vitae

Personalien

Name Sven Rank
geboren am 11.10.1982 in Bad Friedrichshall
verheiratet, zwei Kinder
deutsch

Schulbildung

1989 - 1993 Grundschule Erlenbach
1993 - 1999 Albert-Schweitzer-Gymnasium Neckarsulm
1999 - 2002 Abitur, Agrarwissenschaftliches Gymnasium Öhringen

Zivildienst

09/02 - 07/03 Klinikum Weissenhof, Weinsberg

Studium

10/03 - 08/05 Eberhard-Karls-Universität Tübingen, Grundstudium der Chemie
12.08.2005 Vordiplom
10/05 - 08/08 Eberhard-Karls-Universität Tübingen, Hauptstudium der Chemie
09/08 - 02/09 Schriftliche Ausarbeitung der Diplomarbeit 'Untersuchung der Reaktionsmechanismen von Kohlenmonoxid und Wasserstoff an SnO₂-Sensoren in sauerstofffreier Atmosphäre – Umsatz und Widerstandsmessungen', Institut für Physikalische und Theoretische Chemie Tübingen/ AK Weimar

Februar 2009 Diplom Chemie

Promotion

09/2009 - heute Wissenschaftlicher Mitarbeiter am Institut für Physikalische und
Theoretische Chemie Tübingen/ AK Weimar

Danksagung

Herrn Prof. Dr. Udo Weimar danke ich für die freundliche Aufnahme in die Arbeitsgruppe sowie die Bereitstellung des interessanten Themas meiner Dissertation. Zudem bin ich sehr dankbar für die Möglichkeiten neben der Doktorarbeit in vielen weiteren Bereichen zahlreiche Erfahrungen zu sammeln.

Dr. Nicolae Barsan danke ich für seine tolle Unterstützung meiner Arbeit und die stets kritischen aber auch oft humorvollen Diskussion.

Herrn Prof. Dr. Günter Gauglitz danke ich für die Übernahme des Co-Referats und zusammen mit Frau Prof. Dr. Huhn & Herrn Prof. Dr. Klaus Albert für die Bereitschaft, die Prüfungskommission bei der Verteidigung zu bilden.

Ein besonderer Dank richtet sich an Dr. Alexandu Oprea. Durch seine technische Expertise und vor allem durch seine Geduld konnte stets eine Lösung für jedes Problem gefunden werden.

Ute Harbusch, Diana Strauß & Egon Merz danke ich für die große Hilfsbereitschaft bei administrativen Tätigkeiten.

Alexander Haensch und André Sackmann, für eine sehr entspannte Büroatmosphäre, die Hilfsbereitschaft bei Computerproblemen und vor allem für die vielen tollen Jahre während des Studiums.

Thomas Heine und Peter Bonanati danke ich für die hervorragende Zusammenarbeit und die stets humorvolle und aufmunternde Stimmung wenn es mal stressiger zugeht.

Des Weiteren danke ich allen aktuellen & ehemaligen Mitarbeitern für das äußerst angenehme Arbeitsklima bei uns im "VG".

Ein großes Dankeschön an alle HiWis und Modulpraktikanten, welche mir über die gesamte Zeit viel Arbeit abgenommen haben und damit wesentlich zum Gelingen dieser Arbeit beigetragen haben.

Bei meinen Eltern bedanke ich mich für die Geduld, Unterstützung und Verständnis, welche sie über die Jahre aufgebracht haben.

Leah, Sophie und Miri. Ihr seid meine Kraft, mein Rückhalt, meine Familie, mein Leben! Danke! ♥

Meine akademischen Lehrer waren:

K. Albert, T. Chassé, D. Christen, H. Eckstein, O. Eibl, G. Gauglitz, N. Kuhn, M.E. Maier, H.A. Mayer, A. Meixner, H.J. Meyer, U. Nagel, H. Oberhammer, C. Ochsenfeld, H. Pommer, V. Schurig, E. Schweda, B. Speiser, J. Strähle, U. Weimar, L. Wesemann, K.P. Zeller, T. Ziegler

